ROMA TRE
UNIVERSITÀ DEGLI STUDI

***DOTTORATO DI RICERCA IN ELETTRONICA APPLICATA***

(XXXI Ciclo della formazione Dottorale)

# Design of scattering manipulating devices for novel antenna applications through metasurfaces

(Progetto di dispositivi per la manipolazione dello scattering in scenari d'antenna mediante metasuperfici)


Dottorando: *Dott. Stefano Vellucci*

Docenti-guida: *Prof. Filiberto Bilotti*

*Prof. Alessandro Toscano*

Coordinatore: *Prof. Enrico Silva*

*"Come sempre suole accadere in un lungo viaggio,*
*alle prime due o tre stazioni l'immaginazione resta ferma*
*nel luogo di dove sei partito, e poi d'un tratto,*
*col primo mattino incontrato per via, si volge verso la meta del viaggio*
*e ormai costruisce là i castelli dell'avvenire."*

Lev Nikolaevič Tolstoj

# Ringraziamenti

In questo percorso lungo tre anni sono state tante le persone che mi hanno aiutato a raggiungere questo traguardo e a superare i momenti difficili, anche solamente con piccoli gesti. Sarebbe dunque troppo lungo l'elenco di coloro che dovrei ringraziare, senza contare che colpevolmente me ne dimenticherei certamente alcuni. Doverosi ringraziamenti vanno però a coloro che più mi sono stati vicini e mi hanno sostenuto con più forza.

Innanzitutto, devo ringraziare i membri del Gruppo di Ricerca che mi ha accolto. Complessivamente è loro il merito della mia crescita professionale, personale e, più in generale, della meravigliosa esperienza.

Ringrazio in primis il Prof. Filiberto Bilotti, mentore accademico sin dai primi veri passi mossi nel mondo universitario. È indubbio che, senza il suo esempio e la sua passione, trasferitami, mai avrei intrapreso questi studi. Il suo apporto scientifico ha rappresentato, e rappresenta tuttora, una chiara guida da seguire e da cui costantemente apprendere.

Eguali ringraziamenti vanno al Prof. Alessandro Toscano, per la costante disponibilità e il sincero supporto. Lo ringrazio per tutte le opportunità offerte in questi anni, che hanno contribuito significativamente alla mia crescita. Il suo è un esempio di professionalità accademica che perseguirò.

Sincera gratitudine va al Dott. Ing. Alessio Monti, fonte di ispirazione e confronto più vicina. La sua presenza, sempre attenta, è stata l'elemento di sostegno più diretto. Lo ringrazio per l'essenziale supporto scientifico,

accademico ed umano. Ringrazio anche i Dott.ri Ing.ri Mirko Barbuto e Davide Ramaccia per i fondamentali momenti di confronto e i validi consigli.

Tutti e tre sono stati parte essenziale ed integrante del mio percorso e, ciascuno con le sue caratteristiche, spunto di continua e proficua ispirazione.

Ringrazio anche i miei compagni di viaggio, i Dott.ri Ing.ri Antonino Tobia e Angelica Viola Marini, per i momenti di vita quotidiana condivisi che hanno contribuito a rendere più piacevole le fatiche di ogni giorno.

Inoltre, devo ringraziare l'Università degli Studi ROMA TRE e, più nello specifico, i membri della Sezione di Elettronica Applicata per il gradevole ambiente di lavoro e le strutture offerte, che mi hanno consentito di rendere al meglio nel lavoro.

Tuttavia, i ringraziamenti più grandi vanno alla mia Famiglia.

Senza il loro supporto, pratico e morale, nulla di tutto questo sarebbe stato possibile. Rifugio quotidiano, luogo di confronto e di appoggio silente, mi hanno sempre saputo sorreggere con forza e convinzione ma, soprattutto, fiducia. Offrendo quel sostegno incondizionato ma vigile, di coloro che non hanno bisogno di chiedere.

Infine, ringrazio Flo, il regalo più prezioso colto durante questo percorso. A lei il merito di aver conferito una nuova e inaspettata luce a questa esperienza, trasferendogli il dolce ricordo delle cose inattese. Il suo instancabile sostegno, la sua impareggiabile pazienza, sono state essenziali, tanto da renderla parte integrante ed imprescindibile di questo viaggio.

# Contents

# Sommario (Italiano)

Si definiscono metamateriali quella classe di materiali artificiali ingegnerizzati che posseggono caratteristiche e proprietà che non si trovano nei materiali naturali [1],[2],[3],[4]. Storicamente, i primi studi sui metamateriali sono iniziati nell'ambito dell'elettromagnetismo sul finire degli anni '90, con lo scopo di realizzare materiali artificiali caratterizzati da una risposta alle frequenze delle microonde, tipica delle frequenze ottiche o dell'infrarosso [5],[6],[7], con i quali poter ottenere effetti anomali quali indice di rifrazione negativo [8],[9],[10]. Questi materiali artificiali sono caratterizzati da valori anomali della permeabilità e permittività tali per cui è possibile una interazione non convenzionale con i campi elettromagnetici esterni. Valori anomali di permeabilità e permittività sono generalmente realizzati inserendo in un materiale naturale delle inclusioni ingegnerizzate molto piccole rispetto alla lunghezza d'onda del campo interagente.

Negli ultimi decenni, in letteratura sono state proposte varie configurazioni e geometrie differenti per queste inclusioni, con le prime che furono chiaramente ispirate dai pioneristici studi sui mezzi chirali e bianisotropi. Tuttavia, la grande spinta alla diffusione dei metamateriali e all'utilizzo di queste inclusioni opportunamente ingegnerizzate è da attribuirsi ai lavori del prof. Pendry sugli *split-ring resonators* [9],[10], il quale utilizzando inclusioni piccole rispetto alla lunghezza d'onda in gioco, ha potuto ottenere una permeabilità negativa alle frequenze delle microonde.

Sebbene i primi studi sui metamateriali siano stati condotti all'interno della comunità di ingegneri e scienziati dell'elettromagnetismo operanti alle frequenze delle microonde, e successivamente si siano rapidamente estesi a lavori alle frequenze ottiche [11],[12],[13],[14],[15], oggi la comunità scientifica che lavora nell'ambito dei metamateriali si è espansa enormemente e include ormai settori della scienza quali l'acustica, la meccanica e la termodinamica [16],[17],[18].

Nonostante i vantaggi e le proprietà inusuali che i metamateriali possono offrire, questi presentano anche delle limitazioni intrinseche. Indipendentemente dal campo di applicazione, a causa di considerazioni energetiche, i metamateriali passivi devono essere necessariamente dei mezzi dispersivi [19], *i.e.*, essi posseggono caratteristiche non convenzionali solamente in una limitata banda di frequenze. Di conseguenza, le applicazioni basate sui metamateriali sono intrinsecamente a banda stretta. Inoltre, a causa delle loro natura dispersiva e alla relazione di causalità di Kramers-Kronig [20], i metamateriali sono necessariamente materiali con elevate perdite, e realizzabili con strutture volumetriche poiché devono essere descritti in termini elettromagnetici da una permittività efficace [19].

Negli ultimi anni, per cercare di ridurre gli effetti dovuti a queste limitazioni, sono notevolmente aumentati gli studi sulla controparte 2D dei metamateriali, *i.e.*, le metasuperfici [21],[22],[23].

Le metasuperfici sono strutture superficiali molto sottili che presentano dei motivi geometrici periodici sulla superficie stessa, con periodo molto piccolo rispetto alla lunghezza d'onda in gioco. Le metasuperfici sono dunque caratterizzate da basse perdite, peso ridotto, facilità di realizzazione e design generalmente conforme. Grazie agli evidenti vantaggi delle metasuperfici rispetto alla controparte 3D, la comunità scientifica si è ulteriormente interessata

alla realizzazione di applicazioni basate sui metamateriali/metasuperfcie, ottenendo significativi risultati negli ultimi decenni.

Tra le varie applicazioni dei metamateriali e delle metasuperfci, una delle più interessanti ed affascinanti è senza dubbio quella dell'occultamento elettromagnetico o invisibilità. La possibilità di ottenere effetti di invisibilità tramite l'utilizzo di metamateriali ha attratto grande attenzione da parte della comunità scientifica, oltre che dai media di informazione e settori dell'industria. Con il termine invisibilità elettromagnetica o *cloaking* ci si riferisce, in generale, all'effetto di riduzione del livello di visibilità di un oggetto o, i termini più rigorosi, alla capacità di minimizzare la segnatura radar dell'oggetto in uno specifico intervallo di frequenze tramite l'uso di opportuni dispositivi.

La riduzione della segnatura radar di un oggetto è un campo di ricerca che ha ricevuto grande interesse nel corso degli anni e può ritenersi nato con i primi studi sulla riduzione della *radar cross section* (RCS) di un oggetto attraverso l'uso di tecniche di ingegnerizzazione della forma dell'oggetto stesso, o di materiali radar-assorbenti [24]. Tuttavia, a differenza delle soluzioni canoniche sopra elencate, un dispositivo di cloaking mira ad una riduzione della *scattering cross section* totale di un oggetto, senza un incremento delle sue caratteristiche di assorbimento. Di conseguenza, un oggetto *cloaked* risulta essere sostanzialmente invisibile a qualsiasi sensore esterno che opera nella banda di funzionamento del dispositivo di cloaking.

Negli ultimi dieci anni, in letteratura sono state presentate e proposte differenti tecniche di cloaking [25],[26],[27],[28],[29],[30],[31]. Tra queste, una delle più promettenti e versatili è indubbiamente la cosiddetta tecnica del *mantle cloaking* [30]. Grazie all'utilizzo di metasuperfici e al possedere indubbi vantaggi in termini di facilità di fabbricazione, design, perdite, questa tecnica ha

dimostrato ripetutamente di essere dotata di un grande potenziale in termini di possibili applicazioni.

Il progetto di dispositivi di cloaking basati sulla tecnica del mantle cloaking è stato il principale oggetto delle ricerche del programma di dottorato. I risultati finali di queste ricerche sono riportati in questa tesi. In particolare, la tesi è organizzata come segue.

Nel Capitolo 1 si riporta una breve introduzione alle principali tecniche di invisibilità sviluppate in letteratura, con un confronto tra di esse e mettendo in luce i principali vantaggi e svantaggi di ciascuna tecnica. In particolare, vengono presentate le caratteristiche principali delle tecniche di cloaking che vanno sotto il nome di *transformation-optics*, *transmisison-line cloaking*, *scattering cancellation* e *mantle cloaking*. La tecnica del mantle cloaking viene poi ulteriormente approfondita poiché, utilizzando un simile approccio a quello utilizzato per affrontare il problema di invisibilità elettromagnetica, viene mostrato come tramite metasuperfici è possibile, non solo ottenere un effetto di cloaking, ma anche ottenere un più generale completo controllo delle caratteristiche di scattering di un oggetto. Più nello specifico, viene mostrato che tramite metasuperfici opportunamente ingegnerizzate è possibile ottenere effetti avanzati di manipolazione dello scattering, tali da riuscire ad ottenere effetti di *camouflage* o *illusion*. Partendo dalla classica teoria di Mie dello scattering prodotto da oggetti di forma cilindrica, viene inizialmente presentata la modalità di approccio teorica al problema della manipolazione delle proprietà di scattering di un oggetto e successivamente sono sviluppate le formule analitiche in forma chiusa della impedenza superficiale della metasuperfcie che consente di ottenere un effetto di camouflage o di cloaking. Infine, sono discussi i limiti di questo approccio in termini di banda di funzionato in frequenza.

Nel Capitolo 2 vengono discussi alcuni esempi significativi di applicazioni della tecnica di camouflage, tramite la progettazione di dispostivi di camuffamento. Nello specifico, vengono presentati diversi esempi sia analitici che numerici di applicazioni di camouflage, al fine di evidenziare la grande versatilità dell'approccio discusso nel Capitolo precedente. Inizialmente viene presentato il caso di un cilindro metallico avvolto da una metasuperfcie in grado di modificare le proprietà di scattering del cilindro in modo tale che questo possegga le stesse proprietà di scattering di un cilindro dielettrico equivalente. Questo caso è definito di *scattering reduction*. Successivamente, è discusso il caso di *scattering enhancement*, ossia il caso di aumento della segnatura radar di un oggetto di forma cilindrica e, infine, si dimostra come l'introduzione nella metasuperfcie di valori di perdita controllati consente di ottenere effetti di camouflage a larga banda.

Nel Capitolo 3, seguendo l'approccio alla manipolazione dello scattering discusso nei Capitoli precedenti, vengono presentate due differenti applicazioni del cloaking in scenari di antenna. La prima, si concentra sulla progettazione di dispositivi di cloaking per antenne in applicazioni satellitari. Nello specifico, sono evidenziati i vantaggi dell'utilizzo della tecnica di cloaking nel design di sistemi satellitari miniaturizzati ed in particolare del loro sistema d'antenna. A partire dal caso reale di un nanosatellite progettato per applicazioni metereologiche, è mostrato come l'effetto di interferenza sulle antenne montate a bordo, causato dalla presenza di dispositivi schierabili dopo il lancio in orbita, può essere eliminato attraverso la progettazione di opportuni dispositivi di cloaking, così da garantire una maggior stabilità di collegamento con le stazioni radio base di terra. Successivamente, vengono mostrate alcune nuove configurazioni dei sistemi di antenna montati sui nanosatelliti che possono essere progettate grazie a metasuperfici di cloaking, al fine di evidenziare i

vantaggi dovuti all'introduzione della tecnologia di cloaking in questo ambito. In particolare, sono progettati un nanosatellite estremamente miniaturizzato e un nanosatellite equipaggiato con antenne multifunzione. La seconda applicazione del cloaking in scenari di antenna riguarda il progetto di una metasuperfcie di cloaking *waveform-selctive* per antenne a filo, il cui effetto di invisibilità dipende dalla forma d'onda del segnale incidente. Più nello specifico, si introduce il concetto di waveform-selective cloak e si discute una sua possibile applicazione mostrando come è possibile ottenere questo effetto sfruttando metasuperfici caricate con elementi circuitali discreti. Successivamente, si mostra una possibile configurazione di un circuito che esibisce caratteristiche che dipendono dalla forma d'onda del segnale e se ne discutono le relative prestazioni. Infine, viene progettata la metasuperfcie di cloaking waveform-selective e le sue prestazioni sono analizzate una volta che questa è caricata con il circuito ad elementi discreti.

A concludere, nel Capitolo 4 vengono presentate le conclusioni tratte del lavoro di tesi.

All'inizio di ogni Capitolo è presente una breve introduzione agli argomenti trattati nel Capitolo e un sunto degli argomenti delle specifiche Sezioni. Inoltre, vengono discussi lo stato dell'arte attuale relativo agli argomenti in esame e, alla fine, è presente una lista dei contribuiti scientifici dell'autore di questa dissertazione relativi agli argomenti trattati.

# Introduction

Metamaterials are defined as a class of artificial material characterized by unusual properties and functionalities that cannot be realized in conventional materials and provided by engineered inclusions [1],[2],[3],[4]. Historically, the first studies on metamaterials begun in the field of electromagnetism in the late 90s, with the aim of creating artificial material at microwave and radio frequencies characterized by special properties usually found at optical frequencies [5],[6],[7], such as for example negative refraction index [8],[9]. These artificial materials were characterized by anomalous value of the permittivity and permeability such that an unusual interaction with an external electromagnetic filed was achieved. The anomalous values of the permittivity and permeability, were achieved synthetizing artificial mediums, starting from a natural host dielectric material loaded with properly engineered inclusions small compared to the wavelength of operation. In the last decades several different metamaterial inclusions with very different geometrical parameters, shapes and materials have been proposed in literature, with the first one inspired by the old studies on chiral and bianisotropic materials. However, the great impulse to the metamaterial filed can be assigned to the works by Pendry on the split-ring resonators [9],[10], *i.e.*, electrically small inclusions exhibiting an unusual negative permeability at microwave frequencies.

Although the first studies on metamaterials were developed by the electromagnetic community at microwave moving rapidly also to optics

[11],[12],[13],[14],[15], nowadays the metamaterial community has expanded tremendously compared to the beginning and includes by now many other areas of science, such as acoustics, mechanics and thermodynamics [16],[17],[18].

However, metamaterials are also characterized by intrinsic limitations. Independently by the field of applications, due to energy considerations, passive metamaterials are necessary dispersive medium [19], *i.e.*, they exhibit their unusual properties only in a narrow range of frequencies. Thus, metamaterials-based applications are usually characterized by a limited operational bandwidth. Moreover, due to their dispersive nature and Kramers-Kronig causality relationships [20], metamaterials are intrinsically lossy medium, and also usually bulky since they should exhibit an effective medium response [19].

In order to overcome or minimize these intrinsic limitations, in recent years studies on the 2D counterpart of metamaterials have rapidly grown. The so-called metasurfaces [21],[22],[23] are in fact artificial engineered thin surface, patterned on a small scale compared to the incident wavelength, characterized by low losses, straightforward of implementation, and minimal weight and conformal design. Due to their considerable advantages over their 3D counterpart, metasurfaces have attracted great attention by the scientific community and pushed further the rapid development of metamaterials/metasurfaces based applications.

Among the different applications enabled by metamaterials and metasurfaces, electromagnetic invisibility has caught great attention by the scientific community and has also given the greatest visibility by media and industry to the metamaterial's field, certainly. Electromagnetic invisibility or "cloaking" refers to the science of reduction of the visibility of an object or, in more rigorous terms, to the minimization of the scattering signature of the object in a specific range of frequencies exploiting properly designed covering devices.

The reduction of the scattering signature of an object is an old field of research, started with the first studies on the reduction of the radar cross section (RCS) of objects trough a shaping of the object itself or exploiting radar absorbing materials [24]. However, a cloaking device, unlike these canonical solutions, aims to a minimization of the total scattering cross section (SCS) of an object without enhancing its absorption characteristics. Thus, a cloaked object is substantially undetectable to any external detecting device or sensor operating within the band of operation of the cloaking device.

In the last decades several different techniques to achieve electromagnetic invisibility have been proposed in literature [25],[26],[27],[28],[29],[30],[31]. However, one of the most promising and undoubtedly most versatile is the so-called mantel cloaking technique [30]. Thanks to the use of metasurfaces and thus possessing all their advantages in term of fabrication, design and loss, the mantle cloaking technique has repletely proved to be of great potential and has enabled a great amount of interesting and novel applications.

The design of mantle cloaking devices to manipulate the scattering properties of objects coated by engineered metasurfaces it has been the main object of the researches of the three years doctoral school program, whose final results are collected in this thesis. The thesis is organized as follow.

In Chapter 1 a brief introduction to the invisibility techniques developed so far by the scientific community and a confront in term of their advantages and limitations is reported. The main characteristics of the transformation-optics technique, transmission-line cloaking technique, scattering cancellation approach and mantle cloaking technique are discussed, and the mantle cloaking technique is then further investigated, since its theoretical approach is then exploited to analytically demonstrate that properly designed metasurfaces can be used not only to achieve a cloaking effect but their use can be extend to

enable more general scattering manipulation capabilities. In particular, it is shown that metasurfaces can be designed to achieve advance scattering manipulation, enabling the possibility to achieve a camouflaging or illusion effect. Starting from the classical Mie scattering problem for object of cylindrical geometry, the theoretical basis of this scattering manipulation approach is developed and a closed form expression of the surface impedance of the coating metasurface required to achieve a camouflaging or cloaking effect is derived, and the limitations of this approach in term of frequency bandwidth are discussed.

Chapter 2 is focused on the development of some significant applications of the scattering manipulating approach discussed in the previous chapter, with the aim of designing devices able to achieve a camouflaging effect. Specifically, several different analytical and numerical examples showing the versatility of this scattering manipulation approach are discussed. First, the case of a metallic cylinder coated by a properly designed metasurface in order to achieve the same scattering level of a dielectric cylinder, *i.e.*, to induce a scattering reduction, is discussed. It is shown that a camouflaging effect can be achieved and that the cloaking effect is just a specific case of camouflaging. Then, the case of enhancement of the scattering signature of cylindrical objects is discussed with the aid of full-wave numerical simulations and, finally, it shown how the introduction of tunable and controllable losses into metasurfaces enable the possibility to achieve a broadband camouflaging effect.

Following the scattering manipulating approach developed in the previous chapters, in Chapter 3 two relevant applications of electromagnetic invisibility trough metasurfaces for antenna's scenarios are discussed. The first one focus on the design of cloaking devices for antenna's scenarios in satellite applications. In particular, the advantages and possibilities offered by cloaking in the design of

miniaturized satellites and their antenna subsystem are shown. Starting from the real scenario of a nanosatellite for weather measurement, it is shown that cloaking devices can be exploited in order to reduce the deteriorating effect on the antennas' performance mounted on board due to the deployable equipment. Then, to show the possibilities offered by the cloaking technology in satellite scenarios, some new configurations enabled by cloaking metasurfaces are discussed. The possibility of designing extremely compact nanosatellites and unprecedented miniaturized satellite equipped with multifunctional antennas is discussed with the aid of relevant examples. The second application in the antenna field of the cloaking approach, focus on the design of metasurface based cloaking devices for wire antennas whose functionality depends on the waveform of the impinging signal. In particular, the concept of waveform-selective cloaking is developed, and a possible application discussed showing how it is possible to achieve this effect exploiting metasurface loaded by lumped elements. Then, a possible lumped element circuit exhibiting waveform-selective characteristic is developed and its performance discussed, and, finally, the waveform-selective cloaking metasurface is designed and its performance analyzed once loaded with the lumped element circuit.

Finally, Chapter 4 focuses on the overall conclusions of this dissertation.

At the begging of all the Chapters, a short introduction to the arguments treated and a summary of the related Sections are reported. The state-of-the-art at the moment of writing this thesis on the topic of the chapter is discussed and, finally, a list of the specific contributions and findings as a result of the researches is reported.

# CHAPTER 1

# SCATTERING MANIPULATION AND CONTROL THROUGH METASURTFACES

In this Chapter the possibility of tailoring the scattering response of an object for achieving advanced scattering manipulation using metasurfaces is discussed. In particular, it is proposed a general methodology for transforming the scattering signature of an object in a desired way, exploiting properly designed metasurfaces.

This Chapter is organized as follow.

In Section 1.1 it is presented an overview of the main cloaking techniques proposed in literature for achieving scattering control with the aim of minimizing the scattering signature of an object.

In Section 1.2 it is presented a systematic analytical approach for the manipulation of the scattering characteristics on object, using metasurfaces, with the aim of achieving a more general scattering control, *i.e.*, to tailor the scattering characteristics of an object in a desired way to achieve unconventional effects, such as camouflage or illusion. As a significant example, the attention is focused on the cylindrical geometry and the analytical conditions needed to camouflage

the geometrical and electrical characteristics of dielectric and metallic cylinders coated with ideal metasurfaces are derived. A closed-form expression of the camouflaging metasurface depending on the cylinder's characteristics is derived, and, the frequency behavior of this technique is presented.
My contributions to this topic are available in the publications [J3],[J4],[C4],[C9].

## 1.1 Introduction to electromagnetic cloaking

The possibility to reduce the visibility of objects has always attracted great attention for its potential applications in particular in defence systems. In this field, in the last century, several different techniques have been proposed by the scientific and engineering communities to achieve this effect, *e.g.*, the use of active cancellation techniques, proper shaping of the object to hide, and the use of radar absorbing materials [24]. All these techniques aim to a reduction of the radar cross section (RCS) of the object to hide, where the RCS is defined as the physical quantity that describes an object visibility towards a radar system. In particular, following the formalism in [24], the RCS is defined as:

$$\sigma_{RCS} = \lim_{r\to\infty} 4\pi r^2 \frac{\left|\boldsymbol{E}^{scat}\right|^2}{\left|\boldsymbol{E}^{inc}\right|^2} \tag{1}$$

where $\boldsymbol{E}^{scat}$ and $\boldsymbol{E}^{inc}$ are the scattered and impinging electric fields evaluated in specific measurement point of space, and $r$ is the distance between the object and the measurement point. From Eq. (1) it is clear that the RCS is a quantity that depends on the direction of evaluation, *i.e.*, on the power scattered by the object in a specific direction.

Thus, it should be evident that all the techniques mentioned so far aim to a reduction of the visibility of an object only for a specific direction. This means

that the object could be still visible from other directions or, in more rigorous term, that its total scattering cross section (SCS) is not zero.

The SCS is a quantity strictly related to the RCS, and is defined as the integral over all spatial direction of the radar cross section:

$$\sigma_r = \frac{1}{4\pi}\int \sigma_{RCS} d\Omega \tag{2}$$

Analysing Eq. (1) and (2), it is evident that the RCS is a quantity that evaluate the scattering signature of an object in a specific direction only, while the SCS evaluate it for all the direction of observations. For these reasons, the techniques discussed so far for the reduction of the RCS cannot be considered electromagnetic invisibility techniques.

On the contrary, one of the most exciting and promising application enabled by metamaterials is represented by the invisibility cloaks [25],[27],[29],[30],[31], *i.e.*, devices able to reduce the overall electromagnetic visibility of an object by minimizing its total scattering cross section (SCS) in a given frequency range.

The effectiveness of electromagnetic cloaks has been experimentally proven in several scenarios [32],[33],[34] and for different fascinating applications, ranging from low observability in antennas and defence systems [35],[36],[37],[38],[39],[40] to non-invasive sensing [41],[42] at both radio and optical frequencies [43]. In all these cases, the cloaking effect is achieved through the use of covers that exploit the anomalous interaction between the electromagnetic wave and the metamaterial cloak, leading to an overall minimization of the scattering signature of the object.

Transformation-optics technique [25] is based on a transformation of the space surrounding the object enabled by inhomogeneous and anisotropic bulk metamaterials. Such a transformation is able to bend the incident

electromagnetic field around the object to hide, making the inner region of the cloak effectively invisible to any external excitations. Despite its theoretical impact, the stringent requirements of the metamaterial cover make the effective implementation of this technique very challenging for its extreme sensitivity to both fabrication imperfections and electromagnetic losses [29],[31]. Furthermore, the need of a superluminal propagation in the cloak limits the working bandwidth of this solution [27],[29],[30],[31],[44]. Finally, we also emphasize that this cloaking approach is impractical for sensing and antennas applications [41] due to the fact that the inner region of the cloak is electromagnetically isolated from the external perturbation.

Conceptually not too dissimilar, the transmission-line cloaking technique [27] uses transmission-line networks to hide objects from electromagnetic waves. In this case, the incident waves are convoyed into a transmission-line network that is tailored to exhibit very low scattering cross-section, *i.e.*, to be impedance-matched to free space. The main advantage of this approach is that a superluminal propagation is not required and, thus, it is inherently broadband. Moreover, the cloak design and manufacturing are quite straightforward. However, some important limitations for the shape of the cloaked object apply and, moreover, the corresponding cloak is a bulk and massive structure.

Conversely, the scattering cancellation method [29],[30] is based on a radically different approach that aims to cancel the dominant Mie scattering coefficients of the cloaked object. The invisibility effect is achieved when the induced dipole moments of the cloak and of the object to hide are equal in magnitude but out-of-phase. One important difference of this technique compared to the transformation-optics lies in the fact that the cloaked object is not isolated from the external field. This makes this technique suitable for antennas and sensor applications. Moreover, the design and the implementation

of the cloaks are quite straightforward since they can be realized using a single-layer of homogenous and isotropic materials [45]. As a disadvantage, the scattering cancellation method is not the best choice for objects that are large compared to the operative wavelength due to the increasing number of scattering terms that comes into play in the description of the scattering response of the object [46].

The implementation of the scattering cancellation method can be achieved using cloaks made of either bulk plasmonic metamaterials [29] or ultrathin coatings metasurfaces [30]. This latter approach, also known in literature as mantle cloaking, leads to lightweight, thin and conformal designs that can be easily implemented at RF, microwaves and even for acoustic waves [47],[48]. In these ranges of frequencies, in fact, a metasurface is implemented through a patterned metallic surface with subwavelength period that can be modelled using the homogenized physical quantity known as the average surface impedance Zs (Ω/sq), which is the ratio between the tangential component of the electric field and the surface current density. The surface impedance is a complex quantity described by a real and an imaginary part. The first one is due to the losses of the materials composing the metasurface while the second one describes the energy stored by the structure and, therefore, can assume negative (capacitive) or positive (inductive) values. For lossless structures, as we can safely assume for microwave metasurfaces due to the very high value of the metal conductivity at such frequencies, the surface impedance is a purely imaginary quantity and, therefore, it is described by its surface reactance Xs (Ω/sq).

So far, mantle cloaking has been demonstrated to be rather versatile and found many applications in the antenna field. However, the possibilities offered by the mantle cloaking approach, and, more in general, by metasurfaces go well

beyond the minimization of the overall scattered field. The invisibility effect, in fact, can be interpreted as a particular case of a more general manipulation of the scattering properties of a metasurface-coated object. The opportunity of a comprehensive control over the electromagnetic scattering properties of an object allows manipulating the scattering characteristics of an object transforming them into completely different ones (*e.g.*, making the object appearing as it was larger or thinner or made by a different material), leading to a camouflage or an illusion effect, *i.e.*, transforming the scattering properties of the object into the ones of another different object.

The possibility to achieve a camouflaging effect is highly desirable in several applications, such as defence security. In particular, it is possible to exploit this effect for inducing confusion in an observing radar through the camouflage of the observed target, even if with possible bandwidth limitations depending on the type of radar technique involved, as discussed later on. The same approach can be also useful in different applications where, for geometrical or structural reasons, it is not possible to reduce the dimensions of an object whose consequent level of scattering becomes incompatible with the electromagnetic functionalities owned by the object itself.

Recently, some studies based on the use of transformation optics and mantle cloaking to achieve an illusion effect have been developed [49],[50],[51],[52],[53],[54],[55]. In particular, in [53] it has been experimentally demonstrated that an ultrathin anisotropic metasurface can be used to transform the scattering response of a coated dielectric cylinder into the one of an uncoated conducting cylinder, and vice versa. In [54], a similar study has been proposed exploiting an active illusion/cloaking coat consisting of an array of magnetic monopoles. Despite these efforts, no closed-form design formulas are available and, moreover, the camouflage analysis is restricted to a single operative

frequency with a consequent limitation on the use of these approaches in real scenarios.

Inspired by these earlier works, in this paper, we propose a systematic analytical methodology for achieving advanced scattering manipulation. Starting from the well-known scattering problem by an infinite cylinder, we show that it is possible properly tailoring the value assumed by the surface impedance of the coating metasurface in order to achieve a desired level of scattering. Some theoretical and numerical examples are proposed to validate the proposed idea and, specifically, it is shown that the scattering response of a coated cylinder can be transformed and made equal to the one of a cylinder with different electrical and/or geometrical characteristics. An analysis of the frequency performances that can be theoretically achieved by the camouflage effect is carried out and some solutions to overcome the intrinsic narrow-band behaviour of the illusion effect are also proposed. Compared to the pioneering works about this topic [49],[50],[51],[52],[53],[54],[55], the results discussed here can be considered as an important step further toward the use of higher-performances camouflage device in realistic applications.

## 1.2 Analytical formulation of the scattering manipulation problem using metasurfaces

The basic principle of the camouflage effect we desire to achieve is depicted in Figure 1.1 for the case of a cylindrical geometry. In this case, the scattering signature of a cylindrical object (the grey cylinder) is transformed into the one of another cylinder (the azure cylinder) with different size and material properties through the use of metasurfaces (the red cover around the grey cylinder). In order to derive the analytical expression of the required camouflage surface

impedance, we need to equate the expressions of the scattering coefficients of the targeted object with the scattering coefficients of the covered object.

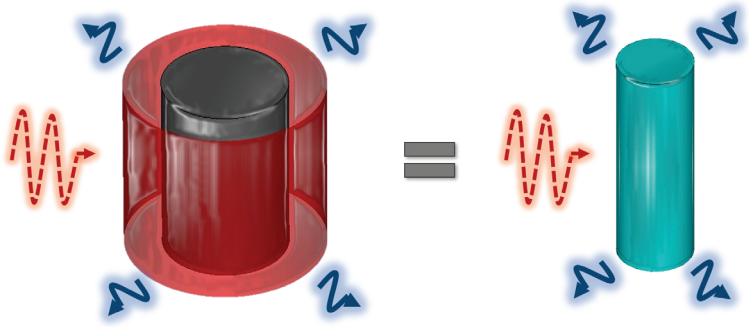

Figure 1.1 Sketch of the working principle of the camouflaging metasurface.

To do so, we have to first solve the well-known scattering problem by an infinite dielectric cylinder (hereinafter, the targeted cylinder) with radius $a_1$ and electromagnetic parameter $(\varepsilon_1, \mu_0)$ as sketched in Figure 1.2 (a). Then, we have to consider the scattering problem by another cylinder (coated cylinder) with radius $a_2$ and electromagnetic parameters $(\varepsilon_1, \mu_0)$ and surrounded by an ultrathin ideal metasurface with radius $a_c$ (Figure 1.2 (b)).

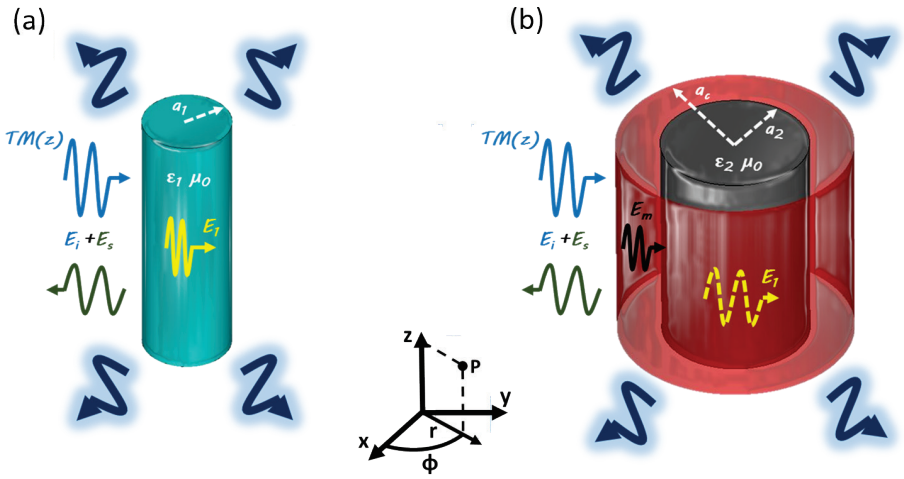


Figure 1.2 Geometry of the scattering problem by (a) a dielectric cylinder and (b) by a metasurface-coated dielectric cylinder.

We assume that the cylinders are illuminated by an external normally-incident plane wave with transverse-magnetic (TM) polarization (*i.e.*, with the electric field parallel to the cylinder axis). Using a cylindrical reference system $(r,\phi,z)$ and adopting a standard Mie expansion [56], we can write the incident electric field $(\boldsymbol{E}_i)$, the scattered electric field $(\boldsymbol{E}_s)$ and the electric field inside the dielectric cylinder $(\boldsymbol{E}_1)$ as:

$$\begin{aligned}
\boldsymbol{E}_i &= \sum_{n=-\infty}^{\infty} E_n \mathbf{N}_n^{(1)}(r,\phi,z), \\
\boldsymbol{E}_1 &= \sum_{n=-\infty}^{\infty} E_n \left[ c_n \mathbf{M}_n^{(1)} + d_n \mathbf{N}_n^{(1)} \right], \\
\boldsymbol{E}_s &= -\sum_{n=-\infty}^{\infty} E_n \left[ b_n \mathbf{N}_n^{(3)} + j\, a_n \mathbf{M}_n^{(3)} \right].
\end{aligned} \tag{3}$$

where the magnetic fields components can be derived as $\boldsymbol{H} = -j/\omega\mu_0 \, \nabla \times \boldsymbol{E}$ and the expression of $\mathbf{N}_n(r,\ \phi,\ z)$, $\mathbf{M}_n(r,\ \phi,\ z)$ can be found in [56]. In Eq. (3), the scattered field is conveniently expressed as the discrete sum of cylindrical harmonics with complex amplitudes $a_n$ and $b_n$ (with $n$ being an integer and $a_{-n} = -a_n$, $b_{-n} = -b_n$). Please note that, since these coefficients are the amplitude of the TE and of the TM cylindrical waves, they are also known in literature as $c_n^{TE}$ and $c_n^{TM}$ [29].

The coefficients $a_n$ and $b_n$ describing the electromagnetic field scattered by the cylinder are related to the total scattering efficiency of the object. In particular, the scattering cross section per unit length of an infinite cylinder can be expressed as [56]:

$$Q_{sca} = \frac{2}{x}\left[ |b_0|^2 + 2\sum_{n=1}^{\infty} (|b_n|^2 + |a_n|^2) \right] \tag{4}$$

where $x = ka_1$ and $k$ is the wave number. The total scattering efficiency $Q_{sca}$ is a sum of infinite terms. However, in the case of electrically small objects, the scattering coefficients above the fundamental order are negligible [56], *i.e.*, the scattered field is dominated by the first-order mode. The number $n$ of the terms that effectively contribute to the total efficiency usually increases with the physical or electrical size of the scatterer, and this is one of the reasons why larger objects generally scatter more.

To determine the analytical expressions of the scattering coefficients in the scenario depicted in Figure 1.2 (a), it is sufficient to enforce the boundary conditions for the tangential components of the electric and magnetic fields at the interface $r = a_1$ of the cylinder. In this way, it is possible to derive a compatible equations system whose analytical solution returns the unknown amplitude coefficients. In particular, for the case of normally-incidence TM-plane wave, the scattering coefficients $a_n$ are identically zero and, for electrically small cylinders, we can safely considerer only the first term of the scattering series ($b_0$). Moreover, the expression of the scattering coefficient available in literature [56] can be further simplified applying the asymptotic expansion of the Bessel functions for small arguments [57] obtaining, thus, the following expression:

$$\begin{aligned} b_0 &= \frac{J_0\left(a_1k_0\sqrt{\varepsilon_1}\right)J_1\left(a_1k_0\right)-\sqrt{\varepsilon_1}J_0\left(a_1k_0\right)J_1\left(a_1k_0\sqrt{\varepsilon_1}\right)}{J_0\left(a_1k_0\sqrt{\varepsilon_1}\right)H_1^{(1)}\left(a_1k_0\right)-\sqrt{\varepsilon_1}J_1\left(a_1k_0\sqrt{\varepsilon_1}\right)H_0^{(1)}\left(a_1k_0\right)} \cong \\ &\cong -\frac{j\ \pi a_1^2k_0^2\left(\varepsilon_1-1\right)}{2a_1^2k_0^2\varepsilon_1\ln\left(a_1k_0\right)+4} \end{aligned} \tag{5}$$

where $J_n\ \left(n=0,1\right)$ is the $n^{th}$-order cylindrical Bessel functions of the first kind, $H_n^{(1)}\ \left(n=0,1\right)$ is the $n^{th}$-order cylindrical Hankel function of the first kind and $k_0$ is the free space wave number.

In a similar way, it is possible to derive the expressions for a coated dielectric cylinder (see Figure 1.2 (b)). The analytical expressions of the incident, scattered and inner electric fields are the same as in Eq. (3) but, in this case, it is also present a field inside the shell between the surfaces of the inner cylinder and the outer metasurface $\left(\boldsymbol{E}_m\right)$:

$$\begin{aligned}
\boldsymbol{E}_i &= \sum_{n=-\infty}^{\infty} E_n \mathbf{N}_n^{(1)}\left(r,\phi,z\right), \\
\boldsymbol{E}_1 &= \sum_{n=-\infty}^{\infty} E_n \left[ c_n' \mathbf{M}_n^{(1)} + d_n' \mathbf{N}_n^{(1)} \right], \\
\boldsymbol{E}_m &= \sum_{n=-\infty}^{\infty} E_n \left[ j\, e_n' \mathbf{N}_n^{(3)} + j\, e_n'' \mathbf{N}_n^{(1)} - f_n' \mathbf{M}_n^{(3)} - f_n'' \mathbf{M}_n^{(1)} \right], \\
\boldsymbol{E}_s &= -\sum_{n=-\infty}^{\infty} E_n \left[ b_n' \mathbf{N}_n^{(3)} + j\, a_n' \mathbf{M}_n^{(3)} \right].
\end{aligned} \tag{6}$$

where $a_n', b_n', c_n', d_n', e_n', f_n', e_n'', f_n''$ are the new unknown amplitude coefficients. As for the previously analysed case of uncoated cylinder, the magnetic fields components of the incident, scattered and inner fields can be derived from the electric fields components reported in Eq. (6), using the relation $\boldsymbol{H}_{i|s|1|m} = -j/\omega\mu_0 \, \nabla \times \boldsymbol{E}_{i|s|1|m}$, where the expressions of $\mathbf{M}_n^{(1)}\left(r,\ \phi,\ z\right)$, $\mathbf{N}_n^{(1)}\left(r,\ \phi,\ z\right)$, $\mathbf{M}_n^{(3)}\left(r,\ \phi,\ z\right)$ and $\mathbf{N}_n^{(3)}\left(r,\ \phi,\ z\right)$ in Eq. (6) in cylindrical coordinate are:

$$\begin{aligned}
\mathbf{M}_n^{(1)} &= \sqrt{k^2-h^2}\left( jn\frac{Z_n^{(1)}(\rho)}{\rho}, -Z_n^{(1)'}(\rho), 0 \right) e^{j(n\phi+hz)}, \\
\mathbf{N}_n^{(1)} &= \frac{\sqrt{k^2-h^2}}{k}\left( jhZ_n^{(1)'}(\rho), -hn\frac{Z_n^{(1)}(\rho)}{\rho}, \sqrt{k^2-h^2}Z_n^{(1)}(\rho) \right) e^{j(n\phi+hz)}, \\
\mathbf{M}_n^{(3)} &= \sqrt{k^2-h^2}\left( jn\frac{Z_n^{(3)}(\rho)}{\rho}, -Z_n^{(3)'}(\rho), 0 \right) e^{j(n\phi+hz)}, \\
\mathbf{N}_n^{(3)} &= \frac{\sqrt{k^2-h^2}}{k}\left( jhZ_n^{(3)'}(\rho), -hn\frac{Z_n^{(3)}(\rho)}{\rho}, \sqrt{k^2-h^2}Z_n^{(3)}(\rho) \right) e^{j(n\phi+hz)}.
\end{aligned} \tag{7}$$

being $h=\cos\zeta$, $\zeta$ the angle of incidence (equal to $\pi/2$ for a normally-incidence TM-plane wave) and $Z_n$ a solution of the cylindrical Bessel equation $\rho\frac{d}{d\rho}\left(\rho\frac{d}{d\rho}Z_n\right)+\left(\rho^2-n^2\right)Z_n=0$. Thus, the analytical expressions of the electric fields can be written in the following form:

$$\begin{aligned}
&\boldsymbol{E}_i\,|_{\rho=k_0 r\sin\zeta}, \\
&\boldsymbol{E}_s\,|_{\rho=k_0 r\sin\zeta}, \\
&\boldsymbol{E}_1\,|_{\rho=k_0 r\sqrt{\varepsilon_2-\cos(\zeta)^2}}, \\
&\boldsymbol{E}_m\,|_{\rho=k_0 r\sin\zeta}.
\end{aligned} \tag{8}$$

By enforcing the continuity of the tangential components of the electric and magnetic fields at $r=a_2$ and the boundary condition of an ideal electrically-polarizable metasurface at the boundary $r=a_c$ [30], it is possible to derive the exact analytical expressions of the scattering coefficients $b_n'$. The boundary conditions to be applied at $r=a_2$ and at $r=a_c$ are, respectively:

$$\begin{aligned}
\boldsymbol{E}_1^{tan}|_{\rho=k_0a_2} &= \boldsymbol{E}_{\boldsymbol{m}}^{tan}|_{\rho=k_0a_2}, \\
\boldsymbol{H}_1^{tan}|_{\rho=k_0a_2} &= \boldsymbol{H}_{\boldsymbol{m}}^{tan}|_{\rho=k_0a_2}, \\
\boldsymbol{E}_{\boldsymbol{m}}^{tan}|_{\rho=k_0a_c} &= Z_S\,\hat{\boldsymbol{r}}\times\left[\left(\boldsymbol{H}_{\boldsymbol{i}}^{tan}|_{\rho=k_0a_c}+\boldsymbol{H}_{\boldsymbol{s}}^{tan}|_{\rho=k_0a_c}\right)-\boldsymbol{H}_{\boldsymbol{m}}^{tan}|_{\rho=k_0a_c}\right], \\
\boldsymbol{E}_{\boldsymbol{i}}^{tan}|_{\rho=k_0a_c}+\boldsymbol{E}_{\boldsymbol{s}}^{tan}|_{\rho=k_0a_c} &= Z_S\,\hat{\boldsymbol{r}}\times\left[\left(\boldsymbol{H}_{\boldsymbol{i}}^{tan}|_{\rho=k_0a_c}+\boldsymbol{H}_{\boldsymbol{s}}^{tan}|_{\rho=k_0a_c}\right)-\boldsymbol{H}_{\boldsymbol{m}}^{tan}|_{\rho=k_0a_c}\right].
\end{aligned} \tag{9}$$

Please note that, as for an uncoated dielectric cylinder [56], all the scattering coefficients $a_n'$ vanish when the impinging field is normal to the axis of the cylinder. Therefore, the series of the scattering coefficients $b_n'$ can be expressed in the convenient form $b_n' = \boldsymbol{N}/\boldsymbol{D}$ with:

$$\begin{aligned}
\boldsymbol{N}: & A_n\left[jK_nC_n\left(B_{n-1}C_{-n}+B_{1-n}C_n\right)+2Z_sB_{n-1}\right] \\
& +j\sqrt{\varepsilon_2}A_{n-1}\left[K_nC_n\left(B_{-n}C_n+B_nC_{-n}\right)+j2Z_sB_n\right] \\
\boldsymbol{D}: & \pi a_c[C_n\left(D_{n-1}A_n-\sqrt{\varepsilon_2}D_nA_{n-1}\right)\left(\mu_0\omega E_n-jk_0Z_sE_{n-1}\right) \\
& +E_nA_n\left(-\mu_0\omega B_{n-1}E_n+jk_0Z_sD_{n-1}C_{n-1}\right)+\sqrt{\varepsilon_2}E_nA_{n-1}\left(\mu_0\omega B_nE_n-jk_0Z_sD_nC_{n-1}\right)]
\end{aligned} \tag{10}$$

being $A_n = J_n\left(a_2k_0\sqrt{\varepsilon_2}\right)$, $B_n = J_n\left(a_2k_0\right)$, $C_n = J_n\left(a_ck_0\right)$, $D_n = H_n^{(1)}\left(a_2k_0\right)$, $E_n = H_n^{(1)}\left(a_ck_0\right)$, $K_n = \pi a_c\mu_0\omega\csc\left(n\pi\right)$ and $J_n(\cdot)$, $H_n^{(1)}(\cdot)$ the cylindrical Bessel and Hankel functions of the first kind, respectively.

As for the previously discussed case of uncoated cylinder, we assume that the coated cylinder is electrically small $\left(n\to 0\right)$, *i.e.*, $k_0a_c << 1$ and $k_ca_c << 1$ (where $k_0$ and $k_c$ are the wave numbers in free space and in the shell, respectively). Therefore, we can safely consider only the first term of the scattering series $\left(b_0'\right)$, *i.e.*, only the first- $\left(J_0(\cdot), H_0^{(1)}(\cdot)\right)$ and second-order $\left(J_1(\cdot), H_1^{(1)}(\cdot)\right)$ Bessel and Hankel functions give a significant contribution in Eq. (10). Thus, $b_0' = \boldsymbol{N}/\boldsymbol{D}$ assumes the following form:

$$\begin{aligned}
&\boldsymbol{N}:\left(2\sqrt{\varepsilon_2}B_0A_1-2B_1A_0\right)\left[2jC_0\left(\mu_0\omega E_0-jk_0Z_sE_1\right)-2k_0Z_sC_0E_0\right]\\
&\quad+2j\mu_0\omega C_0^2\left(2D_1A_0-2\sqrt{\varepsilon_2}D_0A_1\right)\\
&\boldsymbol{D}:A_0\left[-4j\mu_0\omega B_1E_0^2-2D_1E_0\left(-2k_0Z_sC_1-2j\mu_0\omega C_0\right)-4k_0Z_sD_1C_0E_1\right]\\
&\quad-4\sqrt{\varepsilon_2}A_1\left[\frac{1}{2}E_0\left(2k_0Z_sD_0C_1-2j\mu_0\omega B_0E_0\right)+D_0C_0\left(-k_0Z_sE_1+j\mu_0\omega E_0\right)\right]
\end{aligned} \tag{11}$$

Introducing again the following asymptotic expansion of the Bessel functions for small arguments [57]:

$$\begin{aligned}
A_n &\to \frac{1}{n!}\left(\frac{a_2k_0\sqrt{\varepsilon_2}}{2}\right)^n,\\
B_n &\to \frac{1}{n!}\left(\frac{a_2k_0}{2}\right)^n,\\
C_n &\to \frac{1}{n!}\left(\frac{a_ck_0}{2}\right)^n\\
D_0 &\to j\frac{2}{\pi}\ln\left(a_2k_0\right),\\
D_1 &\to -j\frac{1}{\pi}\left(\frac{a_2k_0}{2}\right)^{-1},\\
E_0 &\to j\frac{2}{\pi}\ln\left(a_ck_0\right),\\
E_1 &\to -j\frac{1}{\pi}\left(\frac{a_ck_0}{2}\right)^{-1}.
\end{aligned} \tag{12}$$

the expression of the fundamental order scattering coefficient of a coated cylinder, $b_0^{'}$, reduce from Eq. (11) to:

$$b_0^{'}\cong \frac{\pi\left\{a_2^2a_ck_0^2\mu_0\omega\left[\varepsilon_2 ln\left(\frac{a_2}{a_c}\right)+ln\left(a_ck_0\right)\right]-ja_2^2k_0^2Z_s\left(\varepsilon_2-1\right)+2a_c\mu_0\omega\right\}}{2a_2^2k_0^2\varepsilon_2 ln(a_2k_0)\left[Z_s+ja_c\mu_0\omega ln(a_ck_0)\right]+2a_c ln(a_ck_0)\left[-ja_2^2k_0^2\mu_0\omega(\varepsilon_2-1)ln(a_ck_0)+a_ck_0^2Z_s+2j\mu_0\omega\right]+4Z_s} \tag{13}$$

It is worth noticing that the scattering coefficient $b_0^{'}$ depends on the geometrical and electromagnetic parameters of the overall structure and on the surface

impedance $Z_s$. Once the analytical expression of the complex Mie scattering coefficients of the coated cylinder $b_0^{'}$ and the one of the targeted cylinder $b_0$ are found, it is possible to derive the analytical expression of the surface impedance needed to achieve the camouflage effect by equating the two scattering coefficients. In particular, the expression of $Z_s$ that allows making the two scattering coefficients equal in both imaginary and real part is:

$$Z_s \cong jX_s \cong$$
$$j\frac{2a_c\mu_0\omega\left\{a_1^2k_0^2\left[\varepsilon_1 ln\left(\frac{a_1}{a_c}\right)+ln\left(a_ck_0\right)\right]+2\right\}\left\{a_2^2k_0^2\left[\varepsilon_2 ln\left(\frac{a_2}{a_c}\right)+ln\left(a_ck_0\right)\right]+2\right\}}{k_0^2\left[a_2^2k_0^2 ln(a_ck_0)+2\right]\left\{a_1^2a_2^2k_0^2\left[\varepsilon_1\left(\varepsilon_2-1\right)ln\left(a_1k_0\right)-\varepsilon_2\left(\varepsilon_1-1\right)ln\left(a_2k_0\right)\right]+2\left[a_2^2\left(\varepsilon_2-1\right)-a_1^2\left(\varepsilon_1-1\right)\right]\right\}} \quad (14)$$

where $a_1$ and $\varepsilon_1$ are the geometrical and electrical parameters of the targeted cylinder, while $a_2$, $\varepsilon_2$ and $a_c$ are the parameters of the coated cylinder. It is interesting to note that the value of $Z_s$ is purely reactive and that if $\varepsilon_1 = \varepsilon_2$ and $a_1 = a_2$ (*i.e.*, the targeted cylinder and the coated are the same object) the surface impedance approaches $-j\infty$, as expected, suggesting the absence of the metasurface. As can be easily inferred, the same result is obtained also in the case $\varepsilon_1 = \varepsilon_2 = 1$ (*i.e.*, in the absence of both the cylinders).

An analogous expression can be easily obtained also for the case of conducting cylinders, by calculating the limit of Eq. (14) as the cylinder permittivity approaches $-j\infty$. Similar analytical results can be also obtained for other canonical geometries, such as the spherical or the ellipsoidal one. For non-canonical shapes for which the closed-form solution of the scattering problem does not exist, numerical approximations [58] can be used for achieving a semi-analytical design.

Finally, it is worth noticing that the approximations that lead from Eq. (11) to Eq. (12) are rigorously valid only if the arguments of the Bessel functions

approach to zero, *i.e.*, for $a_1 k_0, a_c k_0, a_2 k_0 \sqrt{\varepsilon_2} \to 0$. This is a stronger condition compared to the assumption of electrically small object (*i.e.*, $a_1 k_0, a_c k_0, a_2 k_0 \sqrt{\varepsilon_2} << 1$) that we employed to derive Eq. (11). However, we point out that it is possible to derive the camouflage impedance $Z_s$ even without the small arguments approximation. In this case, of course, the closed-form expression is more cumbersome and reads as:

$$\begin{aligned} Z_s &= jX_s = j\frac{\pi a_c \mu_0 \omega C_0}{2\left(\Delta_1 - \Delta_2\right)} \\ \Delta_{k=1,2} &= \frac{\sqrt{\varepsilon_k} B_{0,k} A_{1,k} - B_{1,k} A_{0,k}}{B_{1,k} F_0 A_{0,k} + \sqrt{\varepsilon_k} A_{1,k}\left(G_{0,k} C_0 - A_{0,1} F_0\right) - G_{1,k} C_0 A_{0,k}} \end{aligned} \tag{15}$$

having $A_{n,k}$, $B_{n,k}$ the same expressions as in Eq. (10) but replacing the parameters $a_2$, $\varepsilon_2$ with $a_k$, $\varepsilon_k$ (*e.g.*, $A_{n,k} = J_n\left(a_k k_0 \sqrt{\varepsilon_k}\right)$), and being $F_n = Y_n\left(a_c k_0\right)$ and $G_{n,k} = Y_n\left(a_k k_0\right)$, where $Y(\cdot)$ are the cylindrical Bessel functions of the second kind.

Interestingly, the availability of an analytical expression for the camouflage surface impedance allows the analysis of its frequency behaviour. From a physical point of view, the mechanism behind the camouflage effect is similar to the one of mantle cloaking: the surface currents supported by the metasurface are engineered to interfere properly with the fields naturally induced by the bare object, giving rise to the altered scattered fields. The important difference is that, in the case of camouflage, the goal is more challenging than the simple minimization of the first-order scattering coefficient since the aim is to achieve a given level of the total scattering. As known in [59], the intrinsic bandwidth limitations of the cloaking effect are due to the Foster's reactance theorem [60] and an increase of the operational bandwidth necessarily requires active loads. We expect the same bandwidth behaviour in case of camouflage, at least for the cases of reduction of the scattering amplitude of the coated object. This is

confirmed by Figure 1.3, where some significant cases of the frequency behaviour of Eq. (14) are reported. It is interesting noticing that there are some scenarios where the camouflaging surface reactance exhibits a Foster response, *i.e.,* the surface reactance *increases* as the frequency increases. Specifically, these scenarios appear when $a_1 > a_2$ or $\varepsilon_1 > \varepsilon_2$, *i.e.,* when we desire to increase the scattering of the bare object to make it appearing as it were larger or realized with electromagnetically denser materials. In the following Sections, we will provide more physical insights about the camouflage possibilities by showing the analytical and full-wave results of some significant examples.

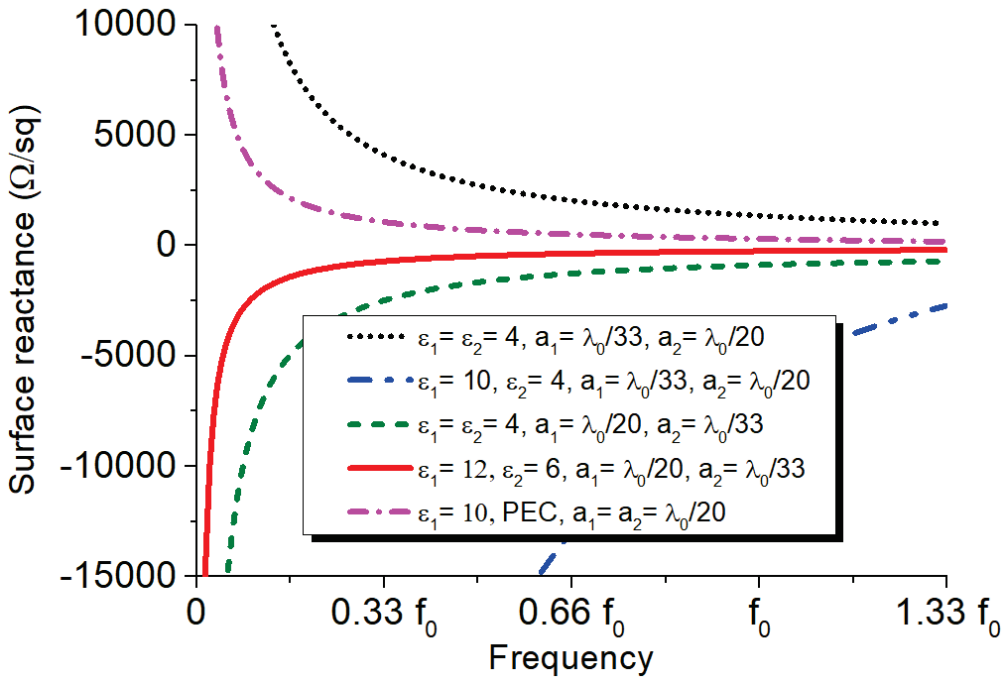


Figure 1.3 Frequency behaviour of the camouflage condition (6) for some significant cases.

# CHAPTER 2

# CAMOUFLAGING DEVICES THROUGH METASURFACES

In this Chapter it is shown that metasurfaces can be used for camouflaging purposes. In particular it is shown how it is possible to modify the scattering properties of object with a cylindrical geometry to make it appears as it were either larger or thinner or composed by a different material. To demonstrate the versatility of the general scattering manipulating approach discussed in Chapter 1, several applications of manipulation of the scattering characteristics of metallic and dielectric cylinders are presented. This Chapter is organized as follow.

In Section 2.1 we present the analytical and numerical results of a cylindrical object made of an electric conductor whose scattering is made equal to the one of a dielectric cylinder, *i.e.*, the possibility to reduce the scattering properties of a cylindrical object to achieve a specific level of the total scattering cross section is presented. On the contrary, in Section 2.2 to opposite case of enchantment of the scattering response of a cylindrical object is discussed showing how exploiting a properly designed metasurface is possible to make the starting object appearing

as it were a stronger scatterer. Finally, in Section 2.3 a potential solution to improve the frequency response of the camouflaging devices exploiting lossy metasurface is discussed with the aid of a relevant example.

My contributions to this topic are available in the publications [J3],[C4],[C9].

## 2.1 Scattering reduction for camouflaging and cloaking

In this Section, starting from the formulas derived in Chapter 1, we show how it is possible to reduce the scattering signature of a metasurface-coated cylinder to achieve a camouflaging or cloaking effect. As a first case, we consider a coated infinite conducting cylinder designed to behave as an infinite dielectric cylinder with the same physical size. This case is somehow similar to the invisibility one, where it is desirable to minimize the scattering signature of the object. However, in our case, we want to achieve a specific level of the scattering signature of the coated object and not its generic minimization.

We consider a cylinder made of a perfect electric conductor (PEC) with radius $a_2 = \lambda_0 / 20$ and a targeted dielectric cylinder with the same radius $a_1 = \lambda_0 / 20$ and $\varepsilon_1 = 4$, being $\lambda_0$ the wavelength at the camouflage frequency $f_0$. By using an ideal ultrathin metasurface, the camouflage effect can be achieved with a metasurface that has a radius $a_c = 1.5 a_2$ and surface impedance equal to $-j65\ \Omega/\mathrm{sq}$, according to Eq.(14). Please note that the radius of the coating metasurface has been chosen in order to still satisfy the quasi-static condition we used in Chapter 1 for deriving Eq. (14).

In Figure 2.1, we report the SCS of the targeted, coated and bare cylinders as the frequency changes. These curves have been evaluated by solving the analytical problem discussed in Chapter 1. As can be appreciated, an ideal non-

dispersive metasurface with surface impedance $Z_s = -j65\ \Omega/\mathrm{sq}$ allows achieving the camouflage condition at the design frequency $f_0$.

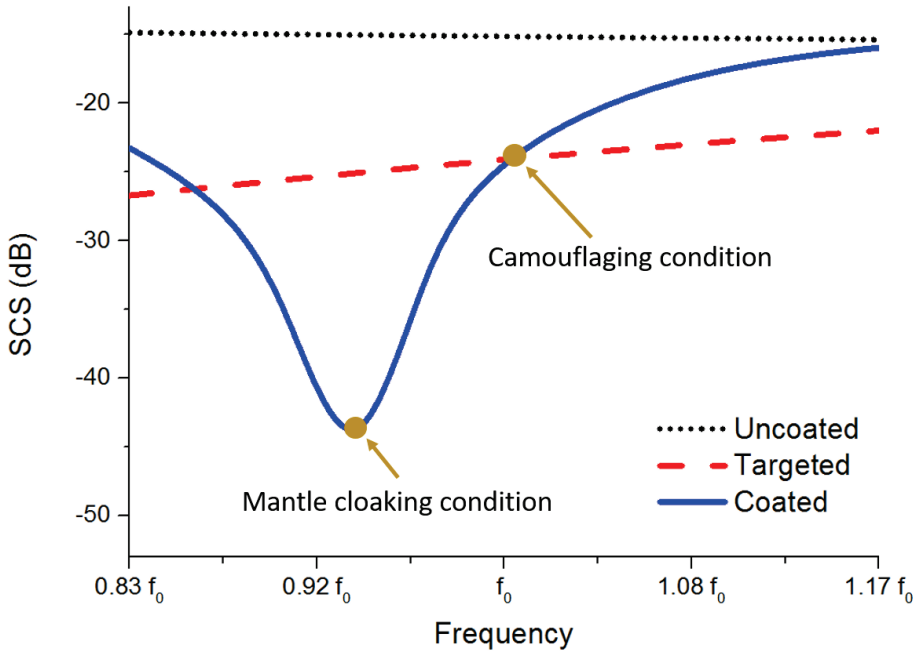


Figure 2.1 Analytical SCS of a PEC (bare), dielectric (targeted) and camouflaged cylinder. The geometrical and electrical characteristics used for this example are: $a_1 = a_2 = \lambda_0/20$, $a_c = 1.5a$ and $\varepsilon_r = 4$.

It is interesting to note that, apparently, a second camouflage condition seems to exist around $0.86 f_0$ This solution, that is not predicted by Eq. (14) and could give the mistaken impression that a second camouflage solution also exists, arises from the fact that the SCS is directly related to the magnitude of the scattering coefficients and that there are two distinct value of $Z_S$ for which the equation $|b_0| = |b_0'|$ applies. However, the second solution only implies an equivalence of the magnitude but not of the phase of the scattered waves and, therefore, does not yield to cylinders with identical scattering response $\left(b_0 \neq b_0'\right)$.

To better understand this point, we invite the reader to have look at Figure 2.2, where the values of the fundamental scattering coefficient of the targeted

cylinder $\left(b_0\right)$ and of the coated cylinder $\left(b_0^{'}\right)$ are reported in both real and imaginary part as a function of the frequency (Figure 2.2 (a)) and as a function of the surface impedance of the cover (Figure 2.2 (b)).

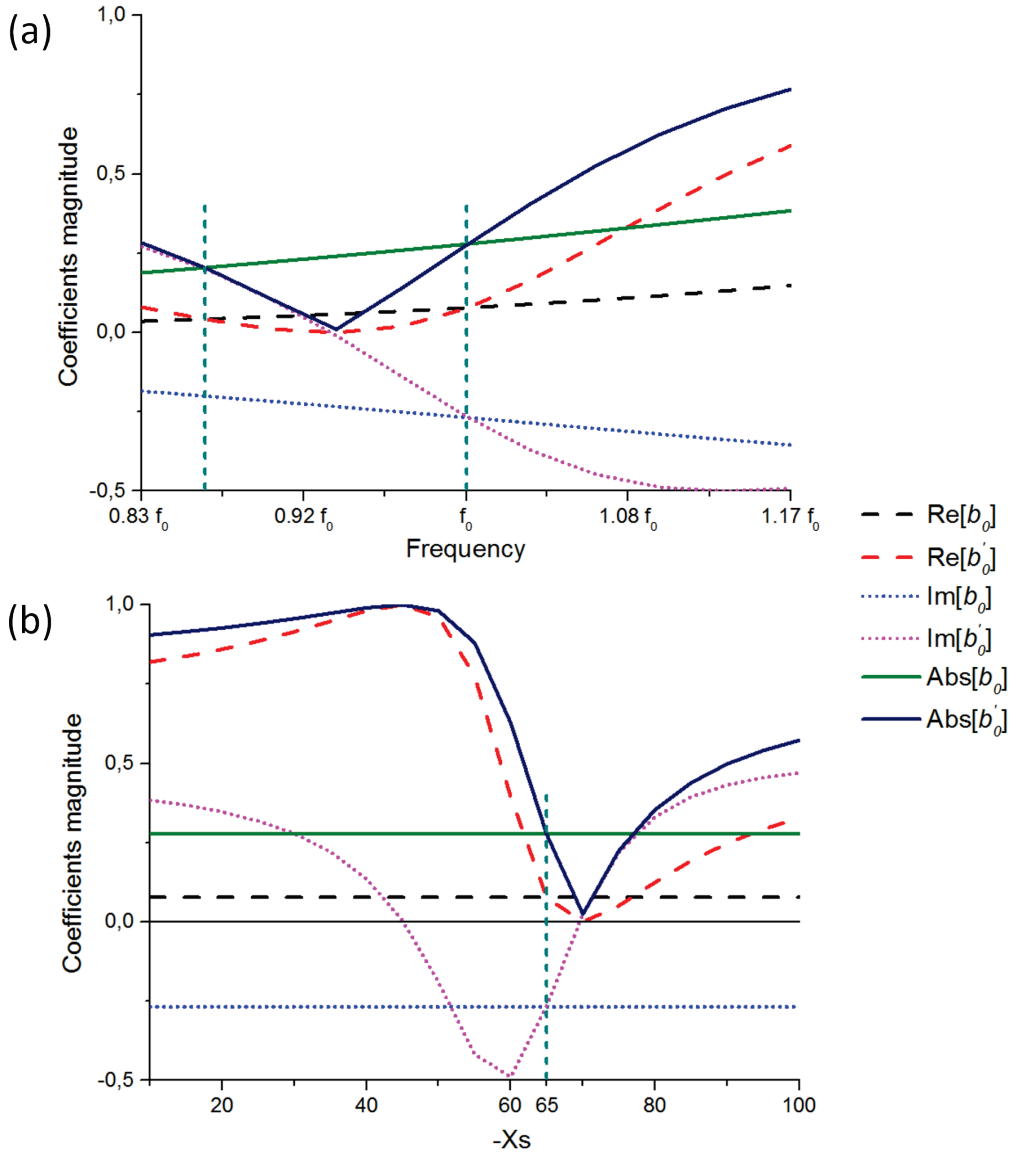


Figure 2.2 Comparison between the fundamental scattering coefficient of the coated ($b_0'$) and targeted ($b_0$) cylinder as (a) the frequency and as (b) the surface impedance $X_s$ of the cover changes.

As clarified in the theoretical part of the dissertation, a camouflage condition is achieved when both the real and the imaginary part of the two scattering coefficients are equal. As it should be clear in Figure 2.2, this condition is only met at the designed frequency $f_0$, *i.e.*, for the value of the surface impedance returned by Eq. (14): $X_s = X_{s1} = -65\ \Omega/\mathrm{sq}$.

The other solution that seems appearing in Figure 2.1 is due to the fact that exists also a different frequency (around 0.86 $f_0$) for which only the absolute value of the two scattering coefficients is the same. For this solution, however, the phase of the scattering coefficient is opposite. Therefore, this second apparent solution is not interesting for camouflage applications because the camouflaged object could be still detectable from the phase distribution of the scattered electromagnetic field that is different than the expected one.

Finally, it is also worth noticing that, analysing Figure 2.1 and as predicted from the analysis on the physical phenomena at the basis of the camouflage effect, the coated cylinder also exhibits a minimum scattering condition (in particular, for this specific case, it occurs around $0.94 f_0$).

To confirm the analytical results, in Figure 2.3 we compare the near-field electric field distributions of the (a) bare, (b) targeted, and (c) camouflaged infinite cylinder for a normally-incident plane wave excitation obtained through full-wave simulations [61]. As expected, the designed metasurface is able to produce almost the same field distribution of the targeted cylinder in terms of magnitude and spatial distribution. It is also interesting to observe that the field is able to penetrate the area between the metasurface and the PEC cylinder, indicating that the conductor is not electromagnetically isolated from the external world.

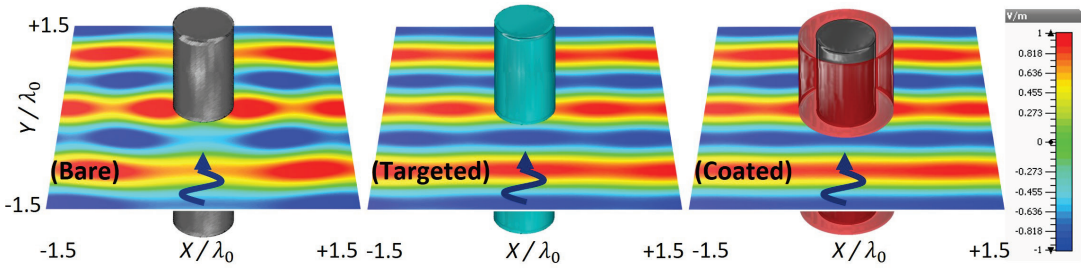


Figure 2.3 Magnitude of the electric field distribution at $f_0$ on a plane perpendicular to the cylinder axis of the (a) bare, (b) targeted and (c) camouflaged cylinder evaluated using full-wave simulations.

As remarked in the theoretical analysis, the intrinsic frequency-dependence of the SCS also allows achieving a mantle cloaking condition at a slightly different frequency than $f_0$. This is shown in Figure 2.4, where it is possible to appreciate the restoration of the plane wave phase front in the cloaked case.

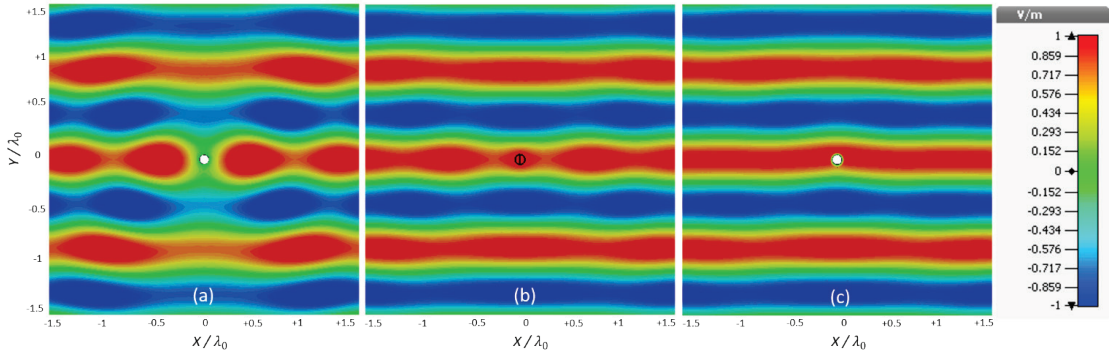


Figure 2.4 Magnitude of the electric field distribution at $0.94f_0$ on a plane perpendicular to the cylinder axis of the (a) bare, (b) targeted and (c) cloaked cylinder evaluated using full-wave simulations.

To conclude this Section, in Figure 2.5, we show the E-field distributions for several frequencies close to the camouflage one. As expected, the illusion effect is quite narrowband due to the intrinsic Foster behaviour of the passive camouflaging metasurface that are able to meet the camouflaging condition (*i.e.*, satisfy Eq. (14)) only at one frequency.

In Section 2.3, we will discuss a possible solution for increasing the bandwidth of the camouflaging effect based on the use of lossy metasurfaces.

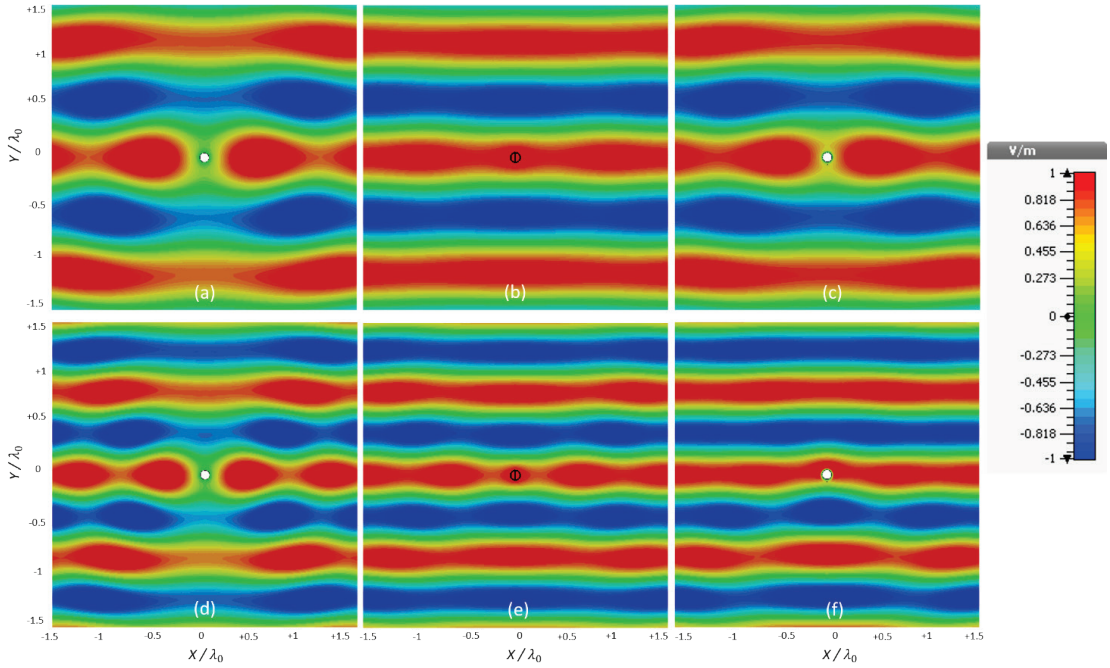


Figure 2.5 Magnitude of the electric field distribution on a plane perpendicular to the cylinder axis of the (a; d) bare, (b; e) targeted and (c; f) camouflaged cylinder evaluated using full-wave simulations at (a-b-c) $0.83f_0$ and at (d-e-f) $1.17f_0$.

## 2.2 Scattering enhancement for camouflaging

To further emphasize the more versatility of the camouflage approach compared to cloaking, in this Section we show how a metasurface can be designed to enhance a weak scattering response and make an object appearing as it were a stronger scatterer. In this case, the targeted object is a dielectric cylinder with relative permittivity $\varepsilon_1 = 12$ and radius $a_1 = \lambda_0 / 20$ whereas the coated cylinder has relative permittivity $\varepsilon_2 = 6$ and radii $a_2 = \lambda_0 / 33.3$ and $a_c = 1.5a_2$. Please note that the overall radius of the coated structure is smaller than the targeted one, even considering the presence of the coating metasurface.

Moreover, to demonstrate the flexibility of the proposed method, we consider here finite-length cylinders with length equal to $4\lambda_0$, which is a reasonable length to consider still valid the analytical formulas derived above. The value of the surface impedance needed to achieve the camouflage effect has been first calculated using Eq. (14) $\left(Z_s = -j210.33\ \Omega/\mathrm{sq}\right)$ and, then, slightly optimized with a full-wave simulator [61] in order to take into account the finite size of the objects $\left(Z_s = -j200\ \Omega/\mathrm{sq}\right)$.

Figure 2.6 compares the 3D scattering cross section in the three cases under a normally-incident TM-plane wave excitation. It can be seen that the coated cylinder exhibits a scattered field distribution very similar to the one of the targeted cylinder. This additional case confirms that a properly engineered single-layer metasurface can be designed to effectively transform the scattering signature of an object into that of another that can be either a weaker or a stronger scatterer.

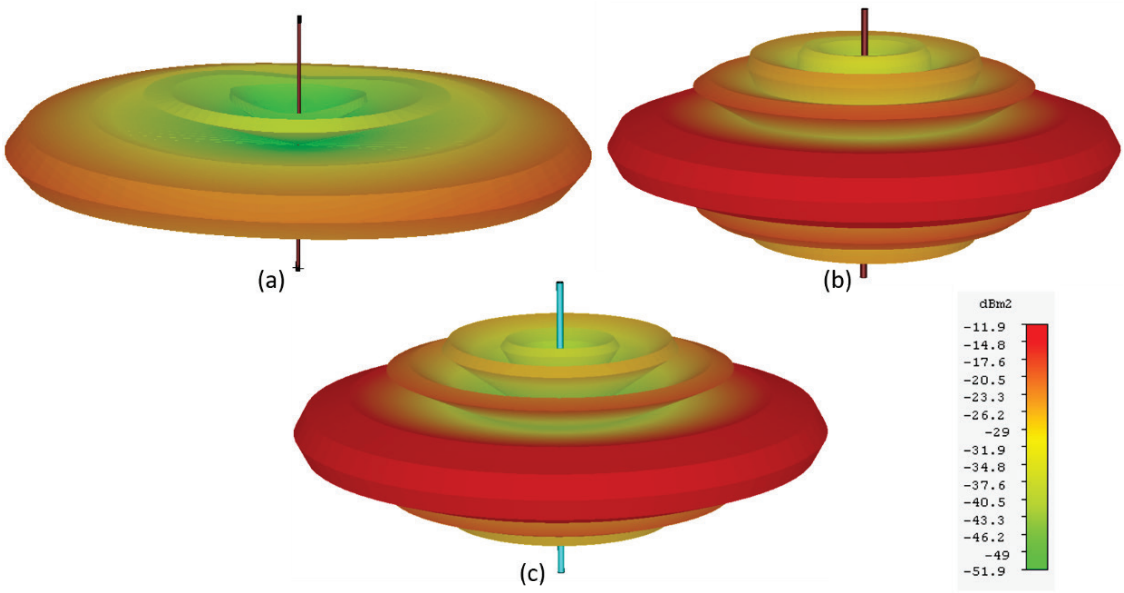


Figure 2.6 3D scattering cross section at $f_0$ of the (a) uncoated, (b) targeted and (c) camouflaged cylinder evaluated through full-wave simulations.

To analyse the frequency behaviour of the scattering enhancement metasurface, we have decided to implement a real metasurface having the specific value of the surface impedance needed to achieve the camouflage behaviour at the design central frequency, *i.e.*, $Z_s = -j200\ \Omega/\mathrm{sq}$. The required metasurface is capacitive, and, therefore, it can be implemented using a horizontal-strip metasurface. Using the design formulas available in [45], we can easily obtain the geometrical values of the metasurface that have a gap $g$ = 18 mm and a period $D$ = 50 mm. The metasurface, shown in Figure 2.7 (b), is composed of 8 copper metallic rings placed around the cylinder to be coated and has been designed to operate at $f_0 = 3$ GHz.

The full-wave SCS as the frequency changes is reported in Figure 2.7 (a) for the cases of bare, targeted, analytically-coated and realistically-coated cylinders. The analytical metasurface used for the comparison is a mathematical sheet whose surface impedance is equal, frequency by frequency, to the camouflaging conditions expressed by Eq. (14). As can be appreciated, and differently from the scattering reduction case analysed in the previous Section, the coated object is able to achieve the scattering level of the targeted one in a very broad frequency range. As predicted at the end of Section 1.2, this is due to the Foster-like frequency behaviour of the camouflaging metasurface required in the scattering enhancement scenario that is well-matched by the designed metasurface [45]. Moreover, we also observe an excellent agreement between the SCS of the real and of the analytical metasurface. At higher frequency, an increasing mismatch between the two curves can be observed. This is an expected effect and it is due to the fact that the analytical formulation is based on the assumption of small arguments of the Bessel functions, that it is progressively violated as the frequency increases.

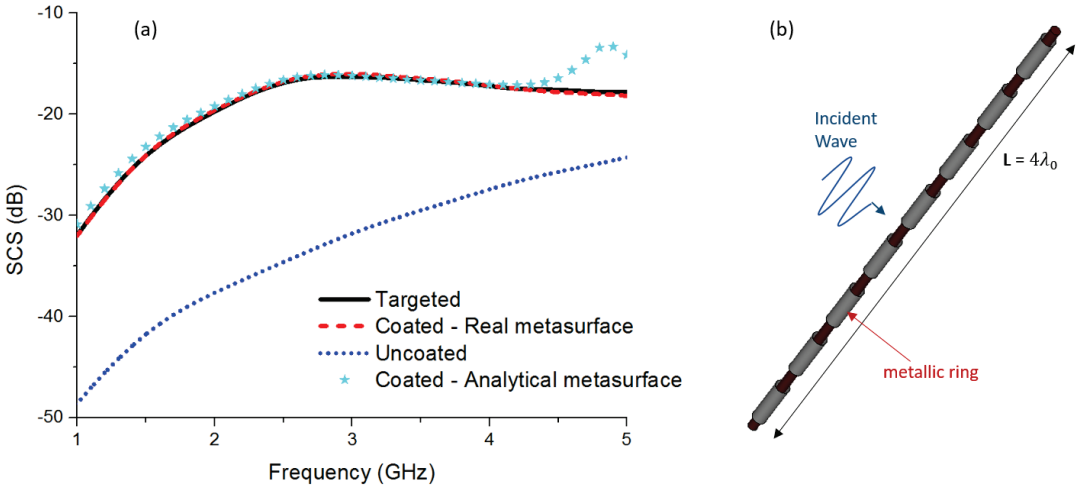


Figure 2.7 SCS of the bare, targeted, analytically-coated and realistically-coated cylinder. The electrical and geometrical parameters used for this example are: $a_1 = \lambda_0/20$, $a_2 = \lambda_0/33.3$, $a_c = 1.5a_2$, $\varepsilon_r = 12$ and $\varepsilon_r = 6$.

## 2.3 Broadband camouflaging through lossy metasurfaces

In this Section, we investigate a possible solution that can be used to improve the frequency performances of the scattering reduction approach analysed in Section 2.1. As discussed in [30], the minimization of the absolute value of the scattering coefficient requires the use of lossless metasurface whose surface impedance is a purely imaginary quantity. In other terms, the presence of Ohmic losses severely limits the performance of an invisibility device.

As stressed above, in the camouflage approach we do not aim to a total reduction of the visibility of an object but to its manipulation. In this situation, we can force the minimization of the fundamental Mie coefficient of the covered object by properly tailoring both the imaginary and the real part of the surface impedance in order to achieve the desired level of the scattering coefficient. Such a new degree of freedom allows flattening the invisibility resonance or, from a

different point of view, increasing the operative bandwidth of the camouflage effect.

In order to analytically determine the required lossy surface impedance, we need to slightly modify the analytical procedure used so far. The first step is to derive the cloaking surface reactance needed to achieve a *minimum scattering condition* in the response of the coated cylinder. To do so, it is possible to use Eq. (14) with $\varepsilon_1 = 1$. Once the optimal cloaking surface reactance ( $X_s^{Cloaking}$ ) has been derived, we need to introduce a real part $R_s$ in the surface impedance $\left(Z_s = R_s + jX_s^{Cloaking}\right)$ and determine the value of $R_s$ which allows to achieve the desired level of the scattering coefficient at the operation frequency $f_0$. To do so, it is possible to equate the two scattering coefficients, $b_0$ and $b_0^{'}$ in a similar way to what we have done to derive Eq. (14) but with the important difference that the surface impedance now also includes a real part.

To better explain this concept, let us consider, as an example, a coated and a targeted dielectric cylinders with relative permittivity $\varepsilon_1 = \varepsilon_2 = 10$ and radius $a_1 = \lambda_0 / 33.3$, $a_2 = \lambda_0 / 20$ and $a_c = 1.5a_2$, respectively. First, we have to analytically determine the lossless surface impedance required to achieve a cloaking condition. We obtain $jX_s^{Cloaking} = j253\ \Omega/\mathrm{sq}$. Then, we need to determine the real part of the surface impedance needed to achieve the desired level of scattering. Equating the two scattering coefficients and imposing $Z_s = R_s + j253\ \Omega/\mathrm{sq}$, we obtain $R_s = 137\Omega/\mathrm{sq}$. In Figure 2.8, we report the analytical scattering cross sections at $f_0$ of the targeted, bare and cloaked cylinder as a function of the real part $R_s$ of the coating surface impedance. As can be appreciated, the introduction of a specific amount of losses allows flattening the invisibility condition, transforming, thus, the cloaking cover into a broadband camouflaging one.

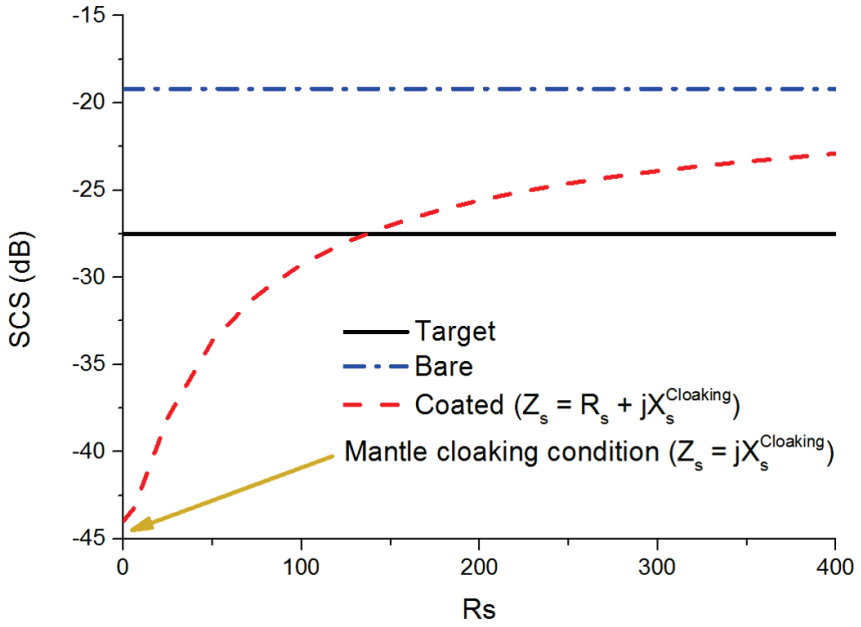


Figure 2.8 Basic principle of lossy camouflaging. Analytically evaluated SCS of a bare, targeted and coated with a tailored lossy metasurface cylinder. The electrical and geometrical parameters used for this example are: $a_1 = \lambda_0/33.3$, $a_2 = \lambda_0/20$, $a_c = 1.5a_2$, $\varepsilon_1 = \varepsilon_2 = 10$ and $\varepsilon_r = 6$.

In Figure 2.9, we report some full-wave simulations confirming the bandwidth improvement returned by this technique. The coated cylinder has been surrounded with both an optimal lossless camouflaging metasurface with surface reactance $Z_s = j369\ \Omega/\text{sq}$, designed using Eq. (15), and different lossy metasurfaces $\left(Z_s = R_s + jX_s^{Cloaking} = Z_s = R_s + j253\ \Omega/\text{sq}\right)$. The optimal lossy metasurface, whose performance are depicted with the dot-dashed line, corresponds to a surface impedance equal to $Z_s = 137 + j253\ \Omega/\text{sq}$.

As can be appreciated in Figure 2.9 (b), the optimal lossless metasurface $\left(Z_s = j369\ \Omega/\text{sq}\right)$ is able to meet the camouflage condition only in a single frequency point. Conversely, in the lossy case $\left(Z_s = R_s + j253\ \Omega/\text{sq}\right)$, shown in Figure 2.9 (a), a broadband camouflage effect is obtained.

It is worth noticing that the introduction of losses in the metasurface increases the extinction cross section (*i.e.*, the sum of the scattering and of the absorption cross section) of the coated object. This means that, while lossy metasurfaces allow achieving the camouflage effect for the scattering cross section in a broader bandwidth, the extinction cross sections of the targeted object and of the coated one are different. Consequently, the object coated with a lossy metasurface cannot be considered perfectly "camouflaged" since its absorption is different from the expected one. However, there are many applications, as for example many radars at microwave frequencies or dark-field microscopies at optical frequencies [62], where the detectability of the object it is related only to its scattering. For these scenarios, lossy metasurface may provide excellent camouflage performances in a broad frequency range.

We conclude this Section by observing that the realization of a lossy metasurface is a quite straightforward task since it can be achieved exploiting the traditional metasurface designs but replacing metals with lossy materials. Some examples for microwave and optical frequencies are available in [63] and [64], respectively.

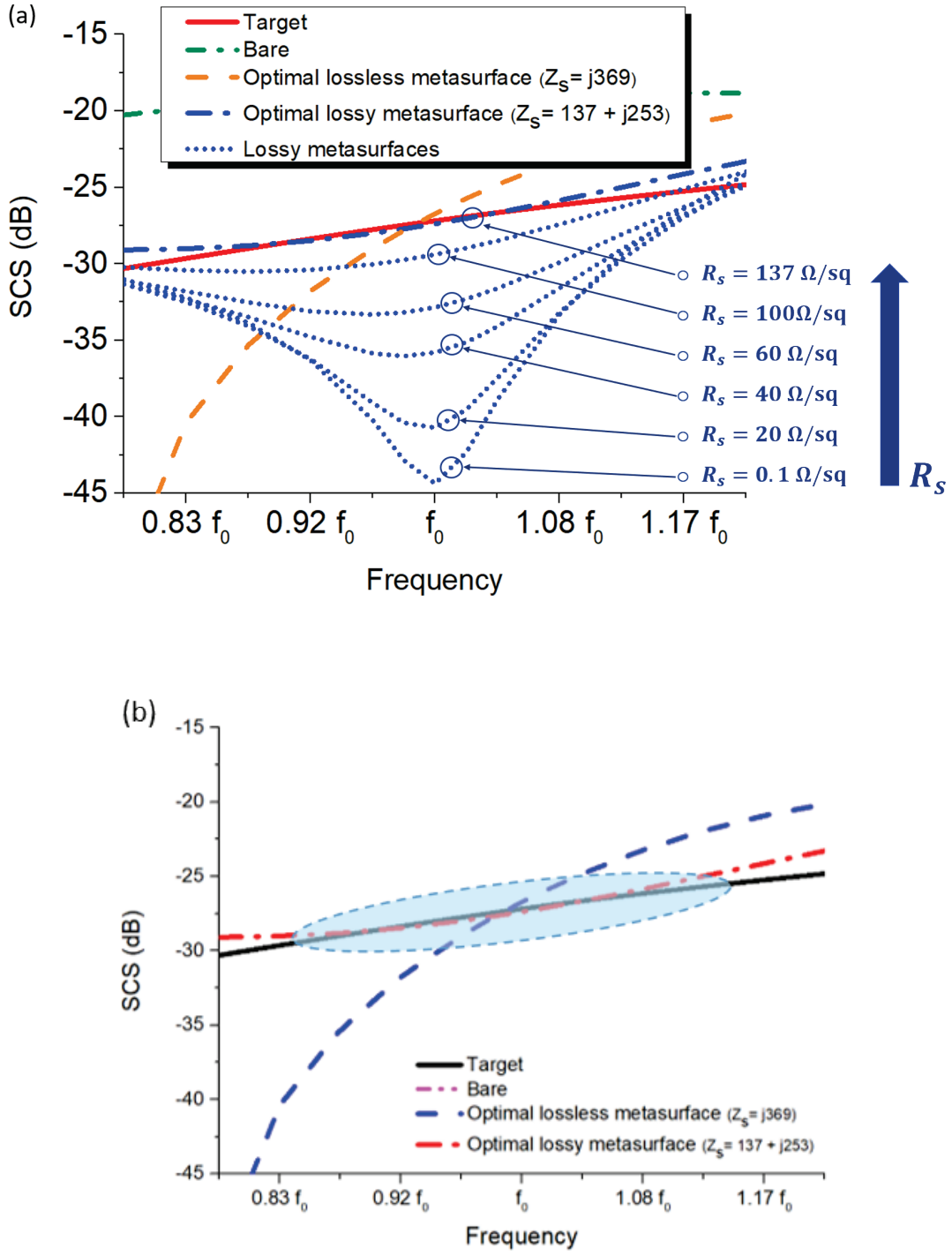


Figure 2.9 Camouflage performances of lossless and lossy metasurfaces evaluated through full-wave simulations ($a_1 = \lambda_0/20$, $a_2 = \lambda_0/33.3$, $a_c = 1.5a_1$, $\varepsilon_1 = \varepsilon_2 = 10$). In the panel (a) the performance of lossy metasurfaces is reported for different value of the surface resistance $R_s$ (from 0.1 Ω/sq to 137 Ω/sq); in the panel (b) a comparison between the performances of the optimal lossless ($Z_s$ = j177 Ω/sq) and optimal lossy ($Z_s$ = 137 + j253 Ω/sq) metasurfaces it is shown.

# CHAPTER 3

# CLOAKING DEVICES THROUGH METASURFACES FOR ANTENNA APPLICATIONS

In this Chapter innovative applications of the mantle cloaking technique for antennas are presented. In particular, it is discussed the possibility of designing mantle cloaking devices to enhance the performance and characteristics of wire antennas, enabling the design of telecommunication systems enriched with unusual functionalities. Two main applications are discussed: mantle cloaks to enhance the performances of nanosatellite telecommunication systems which enable new configurations of the telecommunication system mounted on board, and waveform-selective mantle cloaking devices for antennas able to make an antenna either invisible or visible, depending on the waveform of the impinging signal, exploiting circuit-loaded metasurfaces.

The Chapter is organized as follow.

In Section 3.1 it is shown how electromagnetic cloaking may be used to enhance the performances of the telecommunication systems in miniaturized satellites. In particular, in Subsection 3.1.1 the problem of the possible

interference effects arising between the antennas mounted on nanosatellites and the on-board equipment it is presented. In Subsection 3.1.2 it is shown how the mantle cloaking allows minimizing the impact of the passive structures of the satellite on the antenna's performance. Then, in Subsection 3.1.3 some new configurations of nanosatellites' antenna subsystem enabled by the mantle cloaking technique are discussed presenting innovative nanosatellite systems equipped with multi quasi-isotropic and multi-band antennas.

In Section 3.1.3 the design of an unconventional mantle cloaking device loaded with a lumped-elements circuit able to either hide or restore the visibility of a wire antenna depending on the waveform of the impinging signal is discussed. In particular, in Subsection 803.2.1 the possibility of designing a waveform-selective cloaking metasurface for a wire dipole antenna able to achieve waveform-selective invisibility at the operational frequency of the antenna if illuminated by a short-pulsed or a continuous signal is discussed. Then, in Subsection 3.2.2 the design of the waveform-selective lumped-elements circuit loading the metasurface is discussed and its time-domain response characterized. Finally, in Subsection 3.2.3 the waveform-selective cloaking metasurface is designed and its performance evaluated in term of transmitting properties in the time- and frequency- domains.

My contributions to this topic are available in the publications [J1],[J2],[C1],[C2],[C3].

## 3.1 Mantle cloaks to enhance the performances of satellite telecommunication systems

In the last decade, there has been an increasing interest in the development of cloaking techniques able to make an object completely undetectable, not only

to electromagnetic fields [25],[27],[29] but also to thermal and mechanical fields [65],[66]. Among the different approaches proposed so far, mantle cloaking [30] has emerged as an effective technique characterized by remarkable overall performances, straightforward implementation and ease of fabrication. Moreover, since this technique is based on metasurfaces, the corresponding cloaking devices are lightweight, thin and conformal, especially at radiofrequencies and microwaves, since the cloaking metasurfaces can be realized through patterned metallic sheets able to synthesize the surface impedance required to cancel the scattering from the object to hide.

One of the main advantages of mantle cloaking over other cloaking approaches based, for instance, on transformation electromagnetics [25] lies in the possibility to preserve the electromagnetic functionalities of the covered objects. This peculiar aspect makes this technique particularly appropriate to cloak antennas and sensors as it has been recently proven in [35],[36],[37],[38],[39],[40],[41],[42] for the case of dipoles and monopoles. The possibility to make an antenna invisible to other radiating systems placed nearby is an important new degree of freedom that can be exploited in highly-dense telecommunication platforms where an ever-increasing number of antennas are packaged together within a limited space.

Satellite platforms represent a significant example where electromagnetic interferences and coupling dramatically limit the functionalities of the on-board communication systems.

Due to the low weight and conformal requirements, the space systems are generally equipped with wire antennas that have the advantage to be deployable after the launch. Other radiator solutions based, for example, on patch antennas would restrict the satellite surface available for energy

harvesting with important consequences on the energy autonomy of the entire platform [67].

Moreover, wire antennas are also preferred for their quasi-isotropic radiation pattern [68]. Depending on the type of application, nanosatellites are not always equipped with an alignment control system, due to the low available energy on board, and their spatial orientation in a given moment is totally arbitrary [69]. For this reason, the satellite antenna should exhibit an isotropic gain pattern to minimize the average free-space path loss between the space platform and the ground station. However, the presence of deployable equipment on the satellite, such as external sensors or solar panels, may affect the antenna radiation pattern, severely reducing its degree of isotropy. The metallic passive structures available on the satellite, in fact, can behave either as passive reflectors or directors, causing an unwanted shaping of the radiated beam [70]. This effect makes the link budget between the satellite and the ground station strongly dependent on the satellite orientation. In this context, we emphasize that, due to the limited energy available on the nanosatellite and the significant distance between it and the ground station, even a small reduction in the antenna directivity could affect the telecommunication link.

In this Section, we present a possible solution to this issue based on the use of electromagnetic cloaking to overcome the perturbing effects of deployable objects on the performances of satellite wire antennas. The proposed solution will be also exploited to overcome the mutual coupling between different antennas placed on the same space platform [40] introducing, thus, an unprecedented degree of freedom in the design of the communication systems of small satellites. These are the first studies where electromagnetic cloaking is employed in a space application and the potential impact of the proposed solution is remarkable due to the challenging telecommunication issues that still

affect the small satellites. This new field of application could pave the way to a wide industrial diffusion of cloaking devices.

### 3.1.1 Case study of the CubeSat-class spacecraft

As a reference scenario to check the effectiveness of the proposed idea, we consider a realistic nanosatellite system based on the CubeSats technology [71].

A CubeSat is a particular type of miniaturized satellite used for space research and made of one or more 10×10×10 $cm^3$ cubic units (1U). The CubeSats technology provides a standard for the design of low-cost nanosatellites with the aim to increase the accessibility to space and sustain frequent launches. An example of a CubeSat satellite is the so-called CubeSTAR [72], depicted in Figure 3.1.

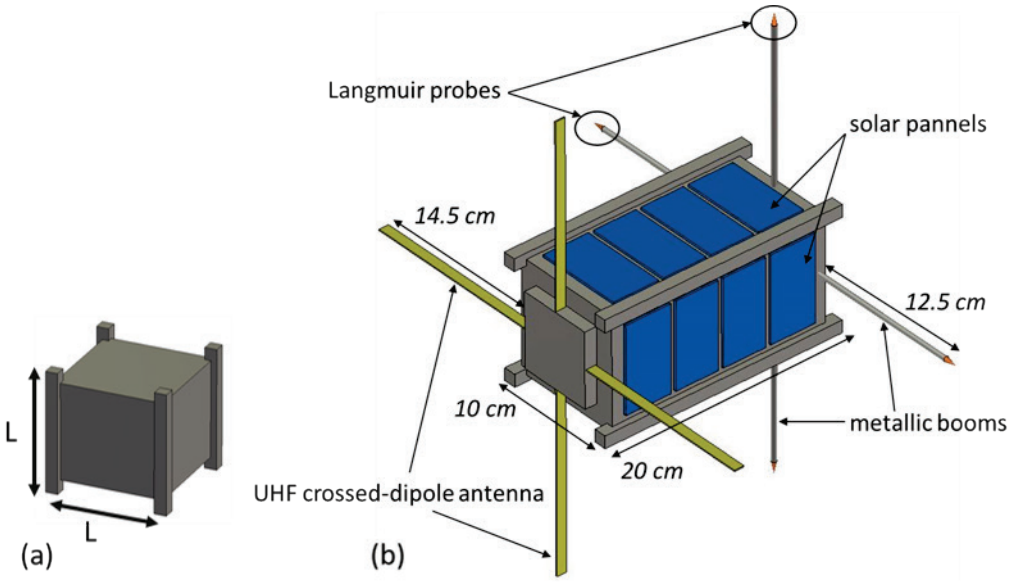


Figure 3.1 Sketch of (a) a one unit (1U) CubeSat and (b) a two units (2U) CubeSTAR. The nanosatellite edge is equal to $L$ = 10 cm.

Defined as a 2U structure, a CubeSTAR is a space weather nanosatellite whose aim is to measure the absolute electron density in the ionosphere. For this purpose, the satellite exploits deployable metallic sensor booms terminated by

Langmuir probes. The radiation system used to communicate with the ground station (for telemetry, tracking, and command) consists of a turnstile crossed-dipoles antenna operating in the UHF amateur satellite band (435-438 MHz) with a central frequency $f_0$ = 436.5 MHz and a channel bandwidth of 25 kHz. As discussed above, this antenna solution is preferred for its quasi-isotropic radiation pattern that guarantees a link budget almost independent on the satellite space orientation. Moreover, a turnstile antenna can be easily designed to radiate the circularly-polarized field required by satellite communications [73].

The 3D radiation diagram of such a turnstile antenna placed on the nanosatellite, obtained through full-wave simulations [61], is illustrated in Figure 3.2 (a). It is worth noticing that the radiation diagram is slightly different than the one expected by a free-space turnstile antenna due to the presence of the metallic frame of the satellite that behaves as a director. However, this effect does not compromise the link budget since a quasi-isotropic pattern without any radiation null can be still observed.

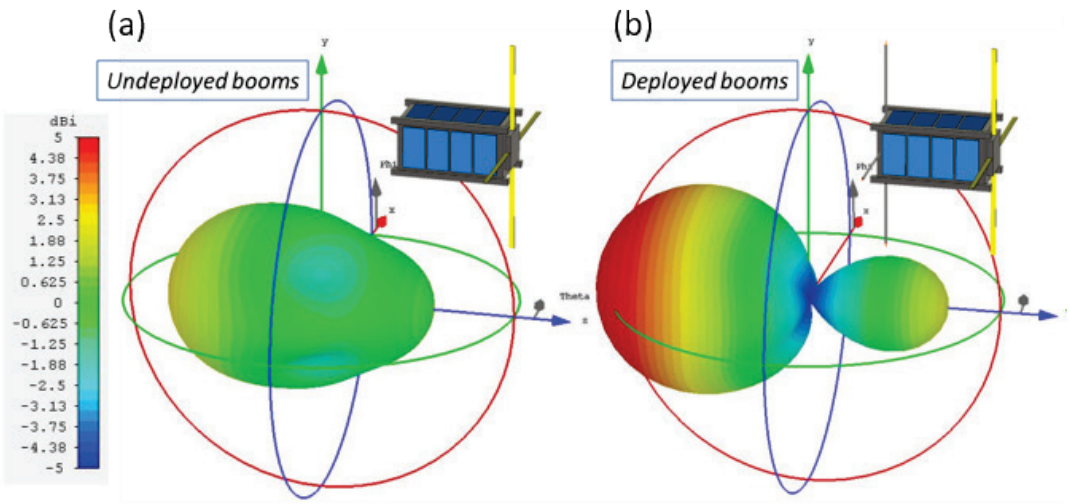


Figure 3.2 3-D gain patterns at $f_0$ in the case of (a) undeployed and (b) deployed booms.

Due to the relatively small electrical dimensions of the nanosatellite at the antenna operation frequency, the deployable metallic cylindrical booms (whose radius is $a$ = 2 mm) used to measure the ionosphere electron density are placed within the near field of the antenna system. As illustrated in Figure 3.2 (b), their presence strongly perturbs the radiation diagram of the antenna and dramatically affects its near-field distribution with a consequent change of the antenna input reactance. In particular, being the payload booms slightly shorter than the dipoles, these structures behave as passive directors for the antenna system, sharpening the radiation diagram and introducing radiation nulls (at ± 60° ca.). Hence, the link budget is strongly dependent on the satellite orientation and the communication with the ground station is not always guaranteed.

It is important to underline that the communication system of a nanosatellite is a critical aspect that requires a particular attention. In fact, even a small drop in the maximum theoretical achievable gain of the antenna mounted on board can easily compromise the communication link between the nanosatellite and the ground station.

This point can be better explained analytically studding the link-budget between a nanosatellite equipped with an ideal isotropic antenna and its ground station, in order to evaluate the typical power levels characterizing these scenarios and highlight the importance of the potential maximum gain drop. The first step of our analysis involves the use of an analytical model for the evaluation of the link-budget between the nanosatellite and its ground station. Here, we assume that the CubeSat is equipped with an ideal perfectly-isotropic antenna. By using Friis transmission equation, a simplified model of the CubeSat-to-ground station communication link can be written as follows:

$$P_r\left[dBm\right] = P_t\left[dBm\right] + G_r\left[dB\right] + G_t\left[dB\right] - 20\log_{10}\left(4\pi R/\lambda\right) \tag{16}$$

where $P_r$ is the received power at the ground station, $Pt$ is the transmitted power by the antenna on the CubeSat, $G_r$ and $Gt$ are the gain of the ground station and of the on-board antenna, respectively, $R$ is the length of the communication channel, and $\lambda$ is the operation wavelength.

Typically, CubeSats are launched into a circular low-earth orbit at 500-600 km and, thus, the free space loss, which is the last term in Eq. (1), is around -140.8 dB. The omnidirectional communication system placed on-board is designed to operate in the VHF or UHF bands. If we consider a central frequency equal to 436 MHz, a transmitted power of 1 W, and assume to use a circularly-polarized commercial parabolic dish (maximum gain 18 dBc) as for the ground station antenna, the maximum received power in the downlink scenario is around -92.8 dB, *i.e.*, 5.25 $10^{-7}$ μW. Please note that Friis transmission formula employed above is a simplified model that does not include the effective noise temperature of the antennas, losses for polarization mismatch and cable losses. However, this simple equation offers a clear idea of the typical power levels in a CubeSat communication channel and, thus, shows how the link budget is strongly dependent on the ability of the on-board antenna to guarantee a radiation pattern almost independent from the space orientation of the satellite.

### 3.1.2 Mantle cloak design and numerical results

In order to significantly reduce the influence of the deployable booms on the antenna performances, we covered each of the four booms with a mantle cloak capable of highly reducing its scattering in the antenna operation bandwidth.

A sketch of a CubeSTAR with cloaked booms is shown in Figure 3.3. The design of the cloaking devices applied to the booms has been conducted with the formulas available in [36],[45] with the aim to achieve the required surface

reactance at the central frequency of the antenna. Please note that, since the metallic booms are metallic cylinders slightly shorter than the crossed dipoles, the surface reactance $X_s$ required to reduce their scattering contribution at the central frequency of the CubeSTAR antenna is inductive [74]. Hence, vertical metallic strips are the most suitable geometry to achieve such an average surface reactance [30].

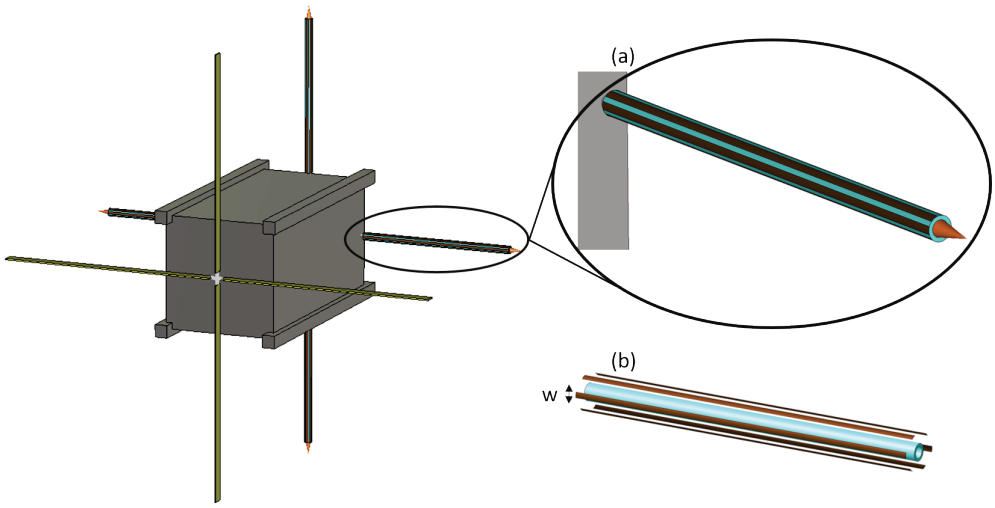


Figure 3.3 CubeSTAR with cloaked booms. (a) Detail of the metasurfaces used to achieve cloaking effect and (b) "exploded" components view.

Please note that, since the scattering of electrically thin cylinders is dominated by the TM contribution (*i.e.*, electric field parallel to the cylinder axis) [56], a single-polarized mantle cloak is an effective solution for reducing the booms total scattering [30].

After a quick numerical optimization, needed to take into account the finite length of the cylinder and its curvature, the cloaks adopted in our setup, shown in Figure 3.3, consist of six electrically thin metallic strips ($w$ = 1.9 mm) patterned on a hollow dielectric cylinder ($\varepsilon_r = 8$, outer radius $a_c = 1.5a$, inner radius $a$). The simple and conformal pattern of the metasurface and the high robustness of

the design towards fabrication tolerances [40] allow satisfying all the specific requirements of satellite applications. As can be appreciated in Figure 3.4, this design drastically reduces the scattering cross section (SCS) of the metallic booms.

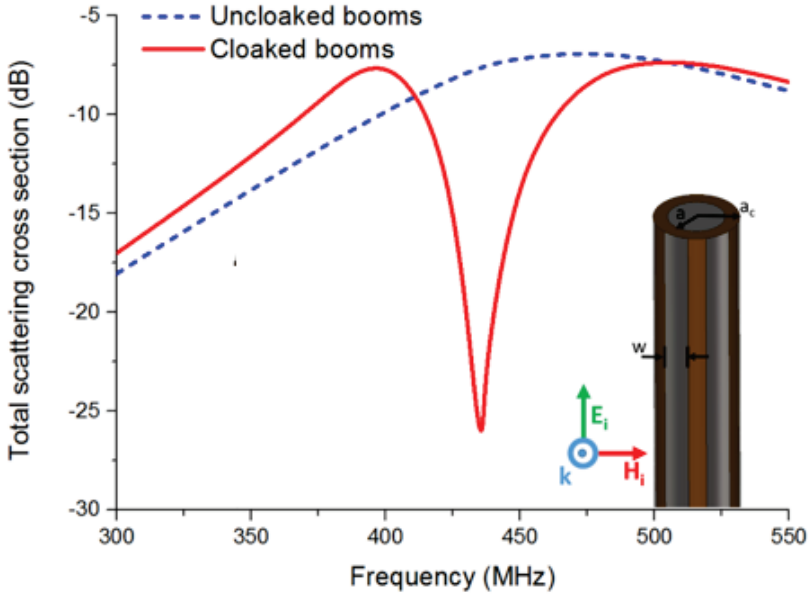


Figure 3.4 SCS *vs*. frequency of the CubeSat booms in the uncloaked and cloaked scenario. In the inset, a detail of the metasurface is shown.

Moreover, for the numerical simulations, particular attention has been put in satisfying these specific requirements. Thus, we have considered real properties of ECCOSTOCK® HIK substrates ($\varepsilon_r = 8$ and $\tan\delta = 0.002$), which are a series of dielectric materials with low water absorption and low outgassing suitable for space applications.

The radiation and matching properties of the crossed dipoles in presence of the cloaked booms are shown in Figure 3.5, Figure 3.6 and Figure 3.7.

Specifically, in Figure 3.5 we compare the far-field gain distribution of the crossed dipoles antenna at the central frequency $f_0$ = 436.5 MHz in the two cases of (a) undeployed sensors booms and (b) deployed cloaked sensor booms. As it can be appreciated, the two 3D distributions are almost equal, and the benefits

of the cloaks are clearly evident if compared with the 3D distribution in the uncloaked case shown in Figure 3.2 (b).

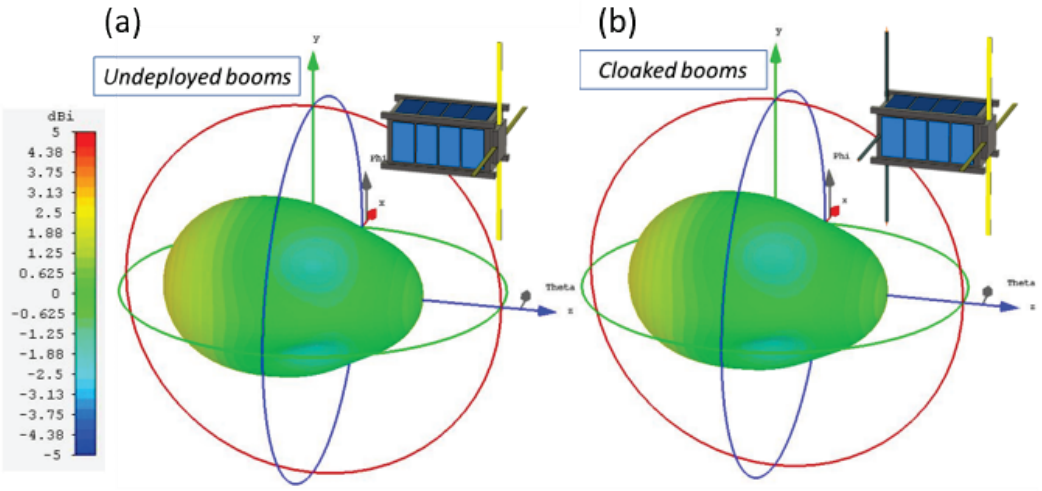


Figure 3.5 3-D gain patterns in the case of (a) undeployed booms, and (b) deployed cloaked booms. The radiation patterns are evaluated at $f_0$.

The cloaking effect is confirmed in Figure 3.6, where we show the gain patterns of the antenna on the $\Phi = 0$ plane in the undeployed, deployed, and deployed cloaked booms at the central operative frequency and at the lower and upper frequency limits of the antenna operational bandwidth. The patterns are compared with the one of an ideal isotropic antenna. As can be appreciated, the cloaks properly operate within all the antenna bandwidth due to the non-resonant nature of mantle cloaking.

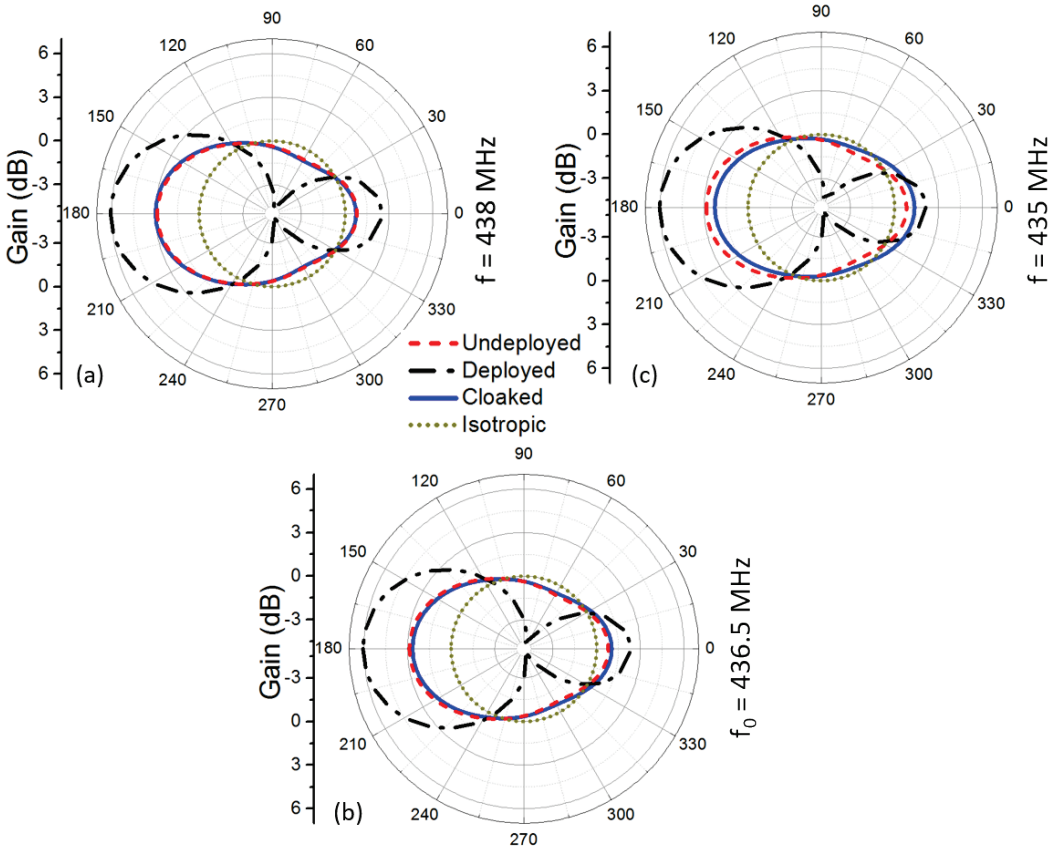


Figure 3.6 Gain patterns on the Φ = 0° plane for the case of undeployed (dashed line), deployed (dash-dotted line), and deployed cloaked booms (continuous line) compared to the one of an ideal isotropic antenna (dotted line). Three frequencies are considered: (a) $f_{max}$ = 438 MHz, (b) $f_0$ = 436.5 MHz and (c) $f_{min}$ = 435 MHz.

Analogous considerations can be made observing Figure 3.7 where we report the magnitude of the reflection coefficient of the antenna in the three cases discussed so far. Note that, due to the inductive reactance introduced by the mantle cloaks, the impedance at the input port of the antenna is restored in the whole operational bandwidth.

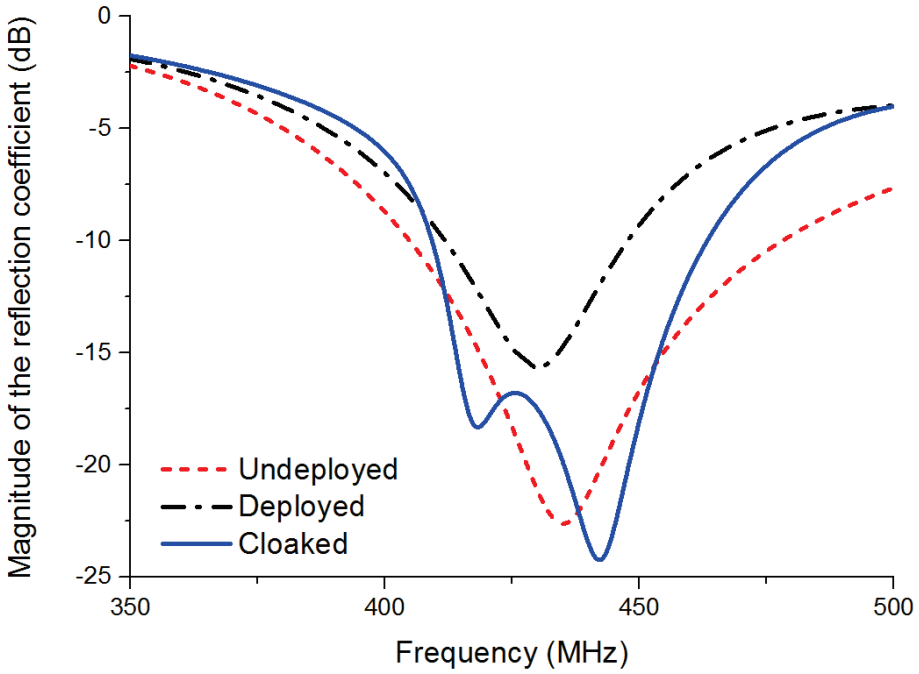


Figure 3.7 Magnitude of the reflection coefficient at the input port of the crossed dipoles in the undeployed, deployed, and deployed cloaked booms scenarios.

We emphasize that the improvements returned by the cloaks in terms of gain pattern and impedance matching would also allow installing supplemental equipment on the nanosatellite, thanks to the lower energy required by the entire system to maintain the communication link with the ground station.

Moreover, we emphasize that the cloaks placed around each metallic boom do not cover the Langmuir sensors (please, see the detail of Figure 3.3 (a)). Therefore, also considering the typical materials composing the cloak (traditional dielectrics and metals), no interaction between the cloaks and the sensors is expected. Moreover, it is worth mentioning that the proposed setup also ensures an easy deployability. In fact, since their length is shorter than the satellite main body size, the coated booms can be easily folded along the face of the CubeSTAR during the launch and, then, deployed with the help of torsion-spring hinges.

Finally, we analyse the robustness and versatility of the cloaking solution discussed above towards the variations of the geometry of both the antenna and the deployable sensors. In Figure 3.8 (a), we illustrate the first geometry analyzed to evaluate the robustness of the cloaks towards an angular rotation of 35° of the antennas system. As can be noticed, the cloaks are able to perfectly restore the original radiation diagram of the antenna in the undeployed case. The same considerations apply for the shift of the metallic booms towards the nanosatellite edges, as shown in Figure 3.8 (b).

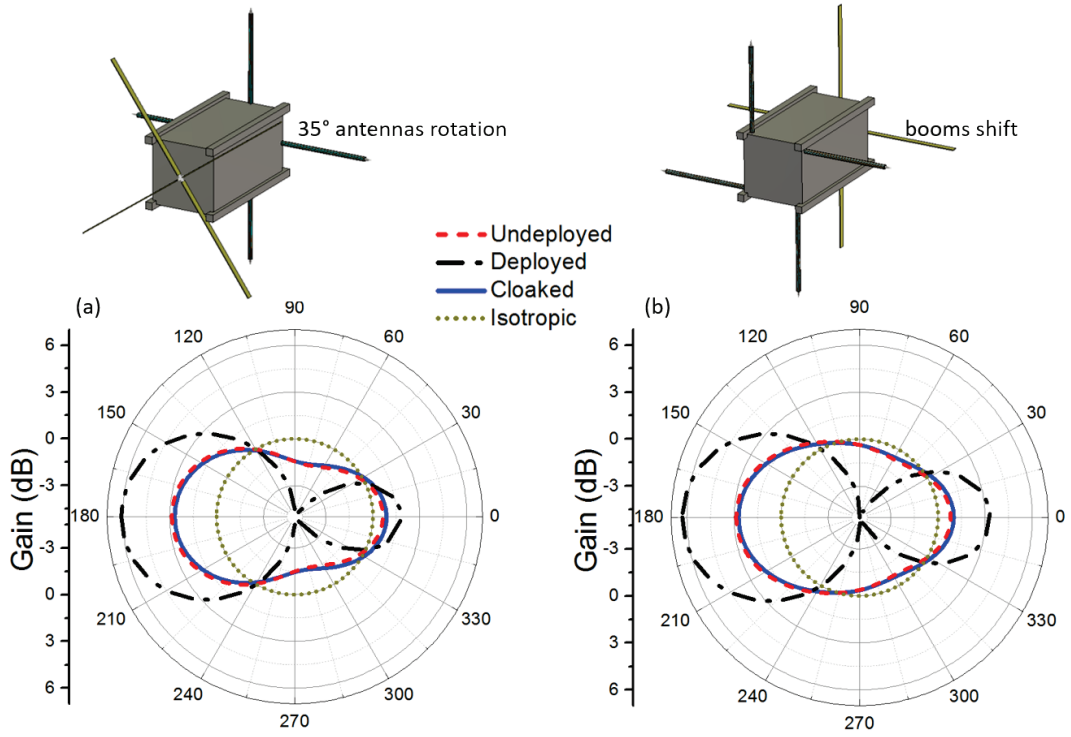


Figure 3.8 Gain patterns on the Φ = 0° plane for the case of undeployed (dashed line), deployed (dash-dotted line), and deployed cloaked booms (continuous line) compared to the one of an ideal isotropic antenna (dotted line). (a) 35° antenna rotation; (b) shift of the booms towards the nanosatellite edges.

### 3.1.3 New configurations enabled by mantle cloaking

The possibility to minimize the possible interference effects arising between the nanosatellite's antenna system and the deployable equipment mounted on board, introduce a completely new degree of freedom in the design of the satellite. In fact, the introduction of the mantle cloaking technique in the design process enables completely new configurations, which would be otherwise impossible to achieve. Here, we propose and discuss some of these unprecedented configurations enabled by the cloaking technology, which may pave the way to a new paradigm in the design of miniaturized space platforms. In particular, we show how exploiting properly designed cloaking devices is possible to design even more compact solution based on the use of a 1U nanosatellite instead of the 2U CubeSTAR, and also how similar cloaking solutions can be employed for multiple-antenna scenarios enabling, thus, unprecedented multi-band solutions in nanosatellite systems.

#### *Compact nanosatellite systems*

The same designed cloak discussed for the CubeSTAR scenario can be employed to reduce the overall dimension of the nanosatellite [4]. Specifically, here we have considered a slightly different scenario compared to the CubeSTAR case discussed so far, reducing the dimension of the nanosatellite to the one of a 1U nanosatellite, instead of the 2U CubeSTAR, with the same scientific goal of measuring the electron density in the ionosphere using Langmuir probes. In fact, since the booms can be made invisible to the antenna, they can be placed in extremely close proximity to the dipoles, *i.e.*, the 2U satellite can be reduce to a 1U.

The sketch of the compact CubeSTAR system is reported Figure 3.9. As can be appreciated, compared to the previous solution, this one has the advantage to

be more compact, lighter and, consequently, less expensive. Also in this case, the communication link with the ground station is guaranteed by a deployable crossed-dipole antenna operating at the central frequency of $f_0$ = 436 MHz.

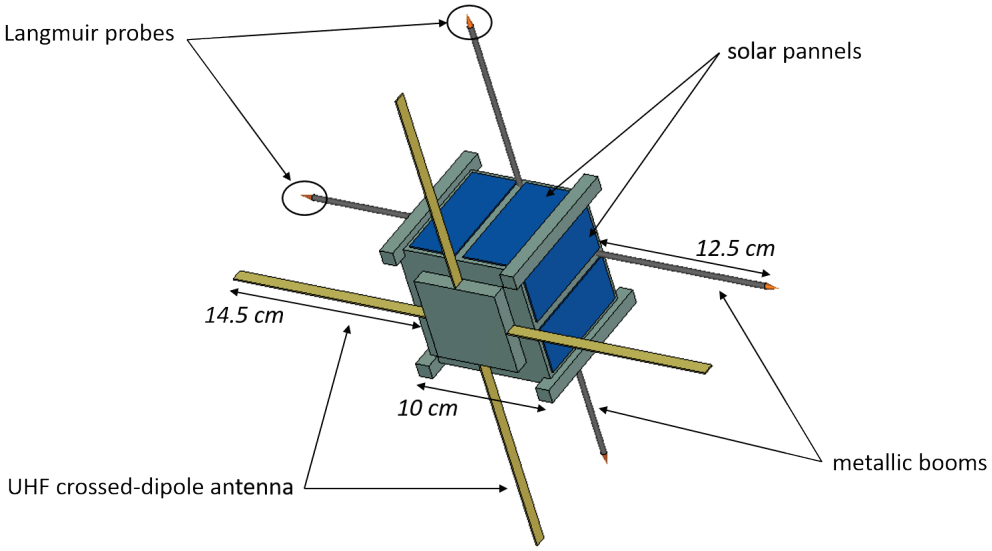


Figure 3.9 Sketch of the 1U CubeSTAR.

In Figure 3.10 are reported the radiative characteristics of such antenna in the case of undeployed and deployed payload sensors at the central frequency of operation (*i.e.*, $f_0$ = 436 MHz), respectively. Observing the radiative characteristic of the undeployed booms' case (Figure 3.10 (a)), can be appreciated another advantage of the discussed solution compared to the previous 2U configuration. Due to the smaller dimension of the metallic frame of the nanosatellite, in this case, the radiation diagram is less perturbed and more similar to the symmetrical one characterizing an ideal cross- dipole antenna. However, as can be appreciated in Figure 3.10 (b), the radiative performance of the antenna are completely deteriorated once the booms are deployed. The booms act like directors of the antenna and, due to the sharpening of the radiation diagram the antenna's radiation diagram point just to one side *i.e.*, there is almost a 50%

possibility of a drop in the communication link with the ground station depending on the spatial orientation of the satellite.

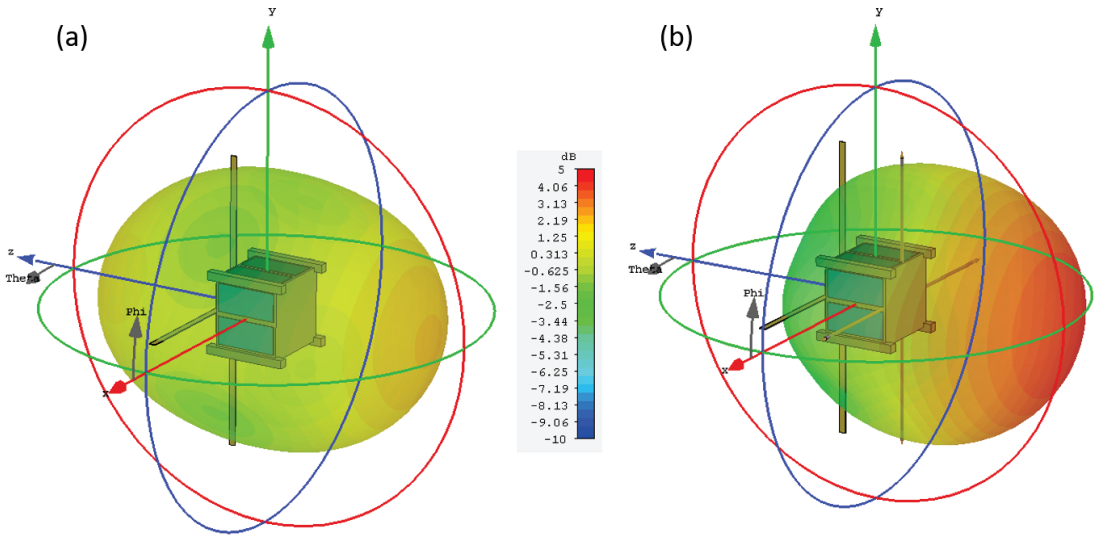


Figure 3.10 3-D gain patterns at $f_0$ in the case of (b) undeployed and (a) deployed booms.

In Figure 3.11 the behaviour of the reflection coefficient at the input port of the antenna in the undeployed and deployed scenarios are reported. It is possible to observe that even in the deployed case the antenna has acceptable performance.

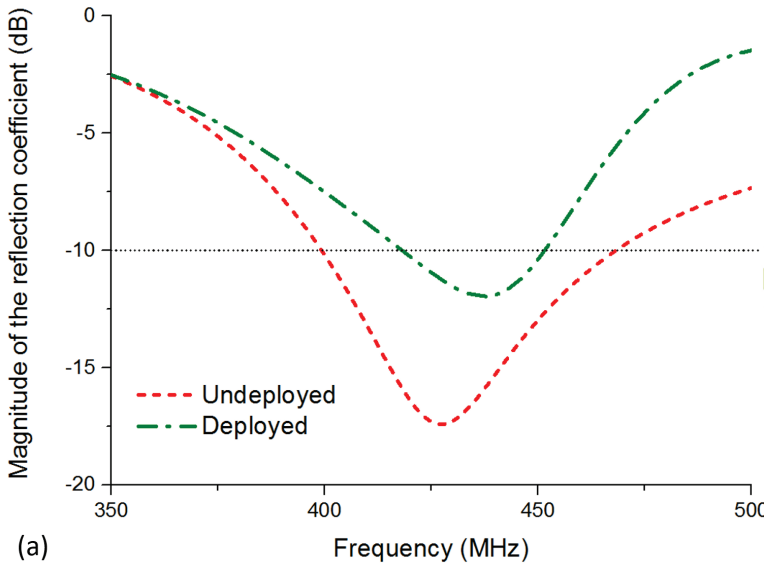


Figure 3.11 Magnitude of the reflection coefficient of the crossed-dipoles in the undeployed.

Exploiting the same conformal cloaking device designed in the 2U CubeSTAR scenario, with the same geometrical and material characteristics, it is possible to completely restore the radiative characteristics of the nanosatellite and the radiation and matching properties of the antenna in presence of the cloaked booms are shown in Figure 3.12 and Figure 3.13.

In particular, in Figure 3.12 (a) the far-field gain distribution of the crossed dipoles antenna operating at the central frequency $f_0$ = 436 MHz is reported. The benefits of the cloaks are evident if compared with the 3D distribution in the undeployed case shown in Figure 3.10 (a), since the two diagrams are almost equal. Thus, the quasi-isotropic radiation pattern of the antenna and the reliability of the communication link with the ground station is ensured. The cloaking effect is confirmed in Figure 3.12 (b), where the gain patterns of the antenna on the $\Phi = 0$ plane in the undeployed, deployed, and deployed cloaked booms at $f_0$ = 436 MHz are shown. The patterns are compared with the one of an ideal isotropic antenna. As can be appreciated, the cloak is able to restore the radiation pattern as if the booms were undeployed.

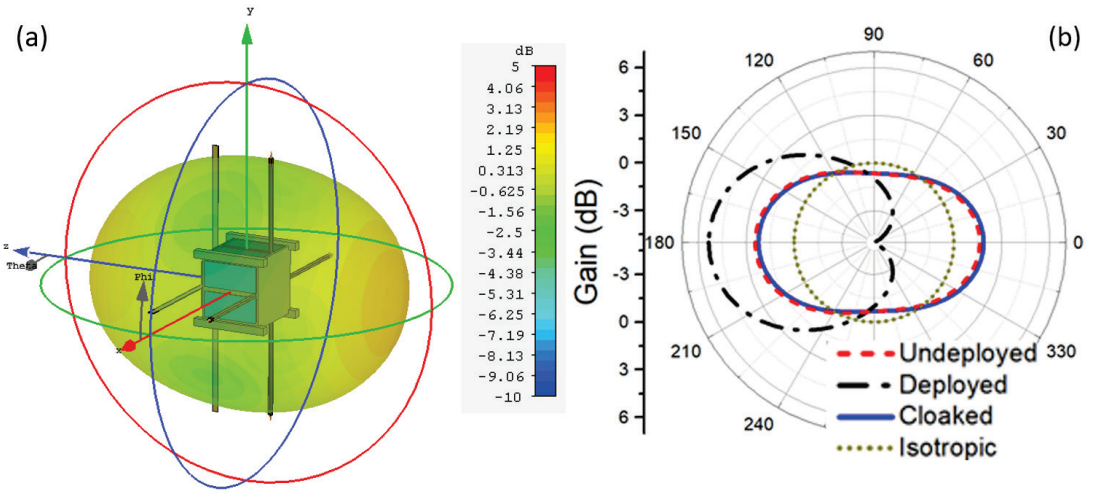


Figure 3.12 (a) 3-D gain patterns at $f_0$ in the case of deployed cloaked booms. (b) Gain patterns for the undeployed, deployed, and deployed cloaked booms scenarios compared to an ideal isotropic antenna.

In Figure 3.13 we report the magnitude of the reflection coefficient of the antenna in the cloaked case. Note that, even if a small frequency of the resonance is present compared to the behaviour in the undeployed case, the impedance at the input port of the antenna is not perturbed at the frequency of operation $f_0$.

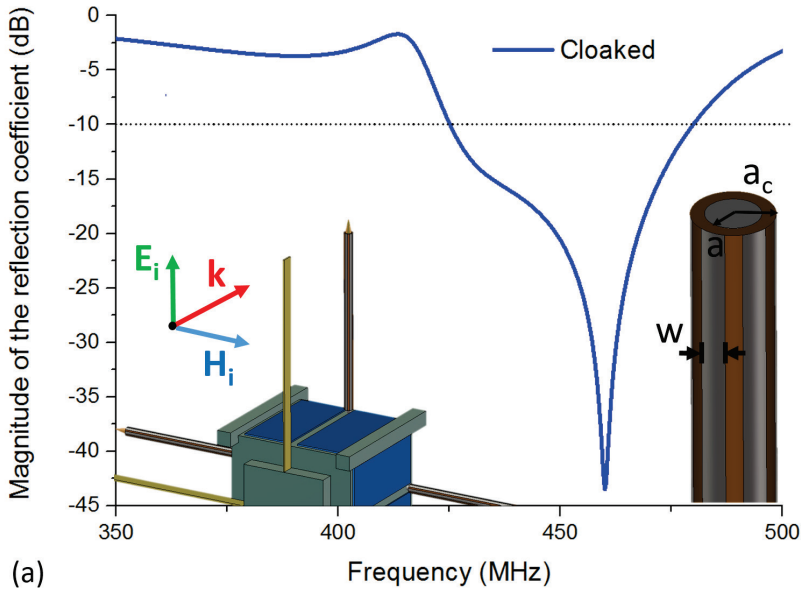


Figure 3.13 Magnitude of the reflection coefficient of the crossed-dipoles in deployed cloaked booms scenarios and details of the metasurface.

In order to verify the ability of the designed mantle cloak to reduce the interference effects on the radiation performance of the antenna and, thus, increase reliability of the overall system, we have, in this case, also analysed the behaviour of the communication link between the 1U CubeSTAR and the ground station *vs*. the rotation angle of the orbiting nanosatellite. To do so, due to the electrically large dimension of the problem, it was not possible to use the same full-wave numerical solver used for the cloak design. Such method, in fact, would require huge computational resources and a dramatic simulation time. The numerical algorithm adopted here relies on the discretization of the

calculation area limited to the object boundaries that leads to a linear equation system with less unknowns with respect to a volumetric method. The obtained equation system is solved through the Multi-Level Fast Multipole Method (MLFMM) integrated in the same commercial 3D electromagnetic simulator we used before that, being particularly suited for electrically large models, allows significant computation time reduction.

In Figure 3.14, we illustrate a sketch of the full-wave simulation setup. The ground-station antenna is a parabolic dish antenna (with a diameter of 2.4 m) placed at a distance $L$ = 600 km from the nanosatellite. This antenna has been excited by the far-field gain of the 1U CubeSTAR at $f_0$ in three different scenarios: (a) deployed cloaked booms, (b) deployed uncloaked booms, and (c) undeployed booms.

These three gain patterns, shown in Figure 3.14, have been computed with FEM-simulations and imported in the MLFMM solver. As a result, we have evaluated the magnitude of the electric field received by a probe placed in the focus of the ground-station antenna, while rotating the far-field source with respect to the 1U CubeSTAR rotation angle $\theta$.

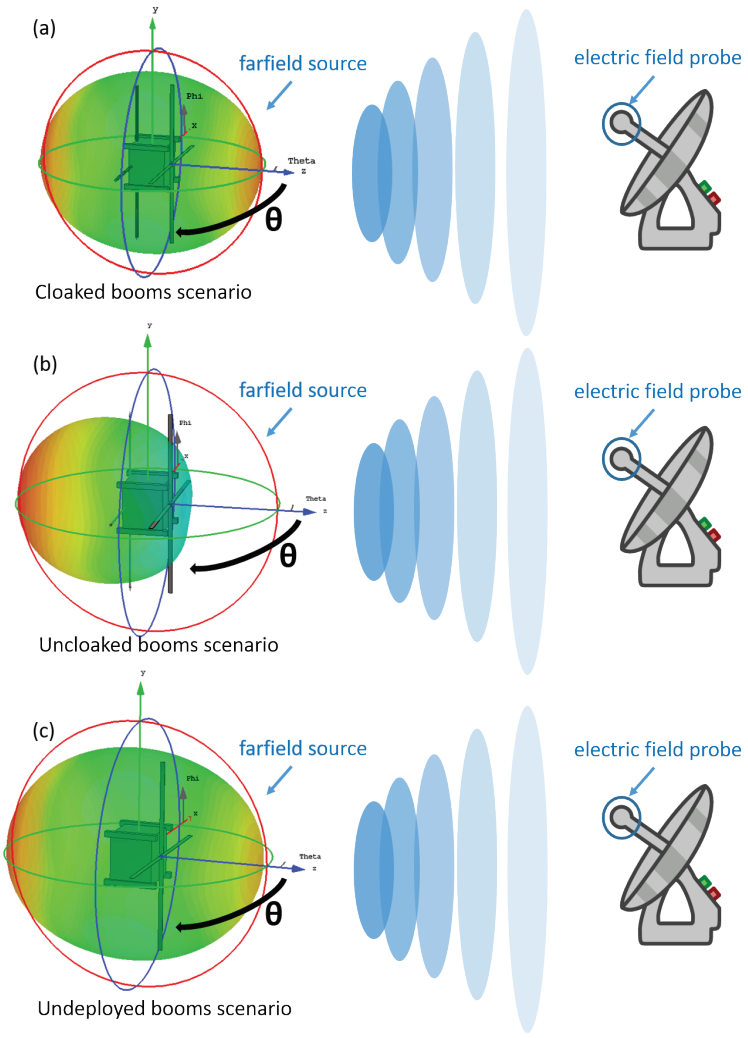


Figure 3.14 Sketch of the full-wave simulation setup used to evaluate the nanosatellite-to-ground link-budget in (a) the cloaked, (b) uncloaked and (c) undeployed booms scenarios. The power received by the electric filed probe has been computed by varying the rotation angle $\theta$ in order to evaluate the reliability of the communication link with respect to a spatial rotation of the CubeSat.

In particular, in Figure 3.15, we report the magnitude of the received electric field normalized to the value received by the parabolic antenna when illuminated by an isotropic source. Two different cases are considered (Figure 3.15 (a) and Figure 3.15 (b), respectively): CubeSTAR oriented along the y-axis (as the ones in Figure 3.14) and CubeSTAR 45° rotated with respect to the y-axis.

As expected, in the case of uncloaked deployed booms, the received power is maximum when the highly directive radiation pattern is aligned toward the ground station ($\theta$ = 180°). However, for 0° < $\theta$ < 90° and 270° < $\theta$ < 360°, the received power is significantly less compared to the undeployed booms case and could compromise a proper communication link. On the contrary, the designed claok leads to a restoration of the level of the received power, as if the booms were undeployed, confirming the beneficial effect of the cloak. Specifically, it is possible to appreciate how the value of the received electric field slightly oscillates around the required value of an ideal isotropic antenna.

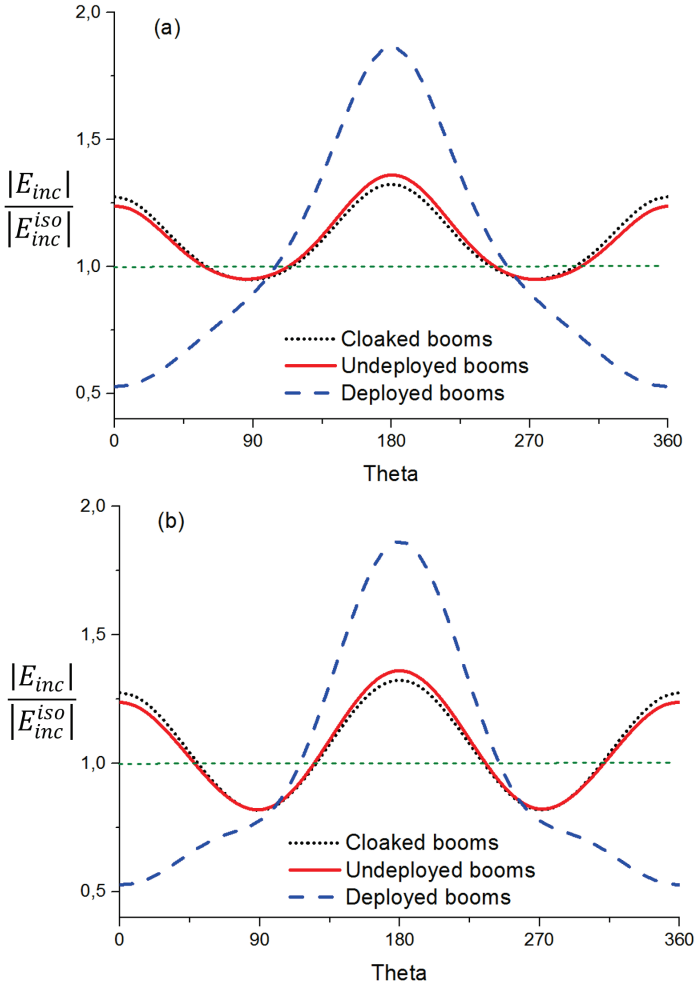


Figure 3.15 Comparison between the normalized magnitude of the electric field received by the ground station vs. the CubeSat rotation angle. Two cases are considered: (a) CubeSat parallel to the $y$ axis and (b) shifted by 45°.

Finally, for sake of completeness, we briefly analyze the effect of the proposed cloak on the polarization of the radiated field of the crossed dipole antenna. As well known, in satellite communication the polarization of the radiated field can be a critical factor. For this kind of communications, a circularly polarized field is preferred, in order to limit the absorption effect by the atmosphere and the effect of potential polarization conversions. In our case, however, due to the presence of the frame of the 1U CubeSTAR, a reduction of the polarization purity of the crossed-dipole placed on-board is expected.

In Figure 3.16, we show the performance in terms of the axial ratio evaluated in the *xy* plane, with reference to the coordinate system of Figure 3.14 (*i.e.*, $\theta = 0$), in the cases of cloaked deployed, undeployed, and uncloaked deployed booms.

As it is possible to appreciate, the designed cloak is also able to completely restore the original polarization performance of the antenna, ensuring a polarization purity as if the booms were undeployed. Moreover, it is worth mentioning that the axial ratio in the forward direction is not perturbed by the presence of the booms due to their rotational symmetry with respect to the crossed dipoles. These results further confirm that the designed mantle cloaks allow an important restoration of the expected radiation diagram of the nanosatellite antenna with a consequent improvement of the satellite-to-ground link budget.

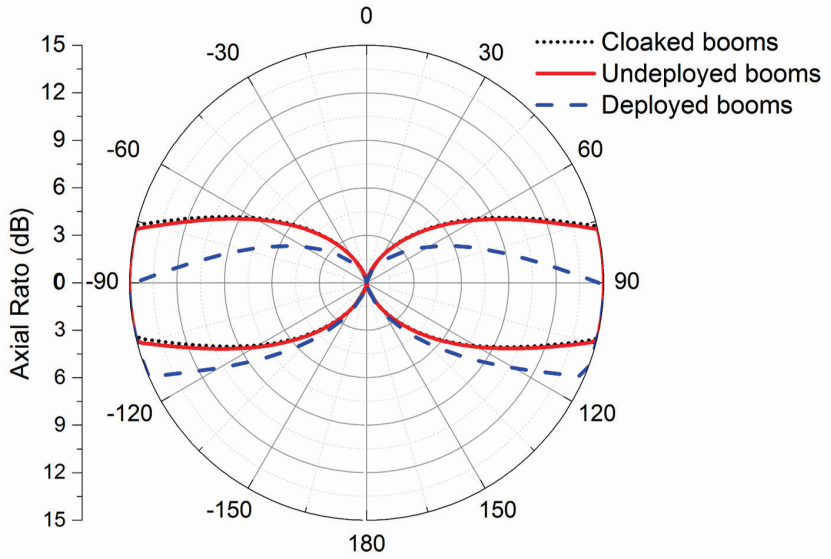


Figure 3.16 Axial Ratio of the CubeSat crossed-dipole antenna in the cases of cloaked deployed booms (dotted line), undeployed booms (continuous line), and uncloaked deployed booms (dashed line).

## *Nanosatellite systems equipped with multifunctional antennas*

Here, we show that, notably, electromagnetic cloaking can be exploited also to design multi-band nanosatellites. Conventionally, the limited size of the satellite does not allow to install more than one quasi-isotropic antenna, *e.g.*, operating either in the UHF ($f_1$ = 436 MHz) or in the VHF ($f_2$ = 144 MHz). Multi-band nanosatellites are usually equipped with highly directive antennas in order to avoid any possible destructive interference effect [75], since equipping the nanosatellite with more than one quasi-isotropic antenna will strongly affect their radiative performances due to the arising interference effects. However, the possibility to equip small nanosatellite with more than one quasi-isotropic antenna operating at different frequencies would represent a great opportunity to increase the overall operative frequency bandwidth of the platform and, thus, the number of information exchanged with the ground station.

Moreover, it would represent a new interesting design opportunity in the growing field of small nanosatellite constellation [76],[77], *i.e.*, networks of nanosatellites that present the advantages to have satellite systems reconfigurable and more flexible space mission. One main challenge for this satellite networks is the antenna system used on board which would require to be able to communicate at the same time with the ground station and the other satellite of the network without a drop of the communicant link. Thus, this critical aspect could easily be overcome designing more than one quasi-isotropic antenna operating at different frequencies, *i.e.*, one able to communicate with the ground station and the other one with the other satellites of the constellation.

To check the effectiveness of the proposed idea, as a reference scenario we consider a CubeSat system equipped with two cross dipole antennas at the opposite side of the nanosatellite and operating in the UHF ($f_1$ = 436 MHz) and in the VHF ($f_2$ = 144 MHz) frequency spectrums. These represent the most common frequency spectrum used for this amateur system. A sketch of the proposed CubeSat system is reported in Figure 3.17. It is possible to distinguish the two crossed dipole antennas: the larger one operates in the VHF frequency spectrum while the smaller one operates in the UHF frequency spectrum.

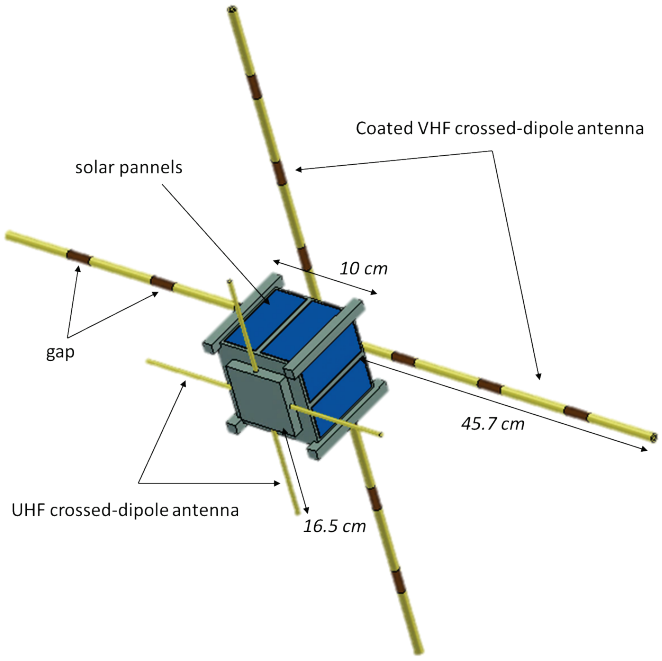


Figure 3.17 Sketch of the multifunctional antennas' CubeSat.

Similar to the equivalent terrestrial scenario [40], we expect a strong interaction between the two antennas placed in such a close proximity ($\lambda_1/6$ with $\lambda_1$ free space wavelength at $f_1$) due to the arising blockage effect. In particular, from Figure 3.18 we can appreciate the reflective effect off the larger antenna to the smaller one. Specifically, Figure 3.18 are reported the radiative characteristics of the UHF antenna in the case of undeployed and deployed VHF antenna at the central frequency of operation (*i.e.*, $f_0$ = 436 MHz), respectively. As can be appreciated, the larger antenna (VHF antenna) act like a reflector for the smaller one (UHF antenna), making unreliable its corresponding link with the ground.

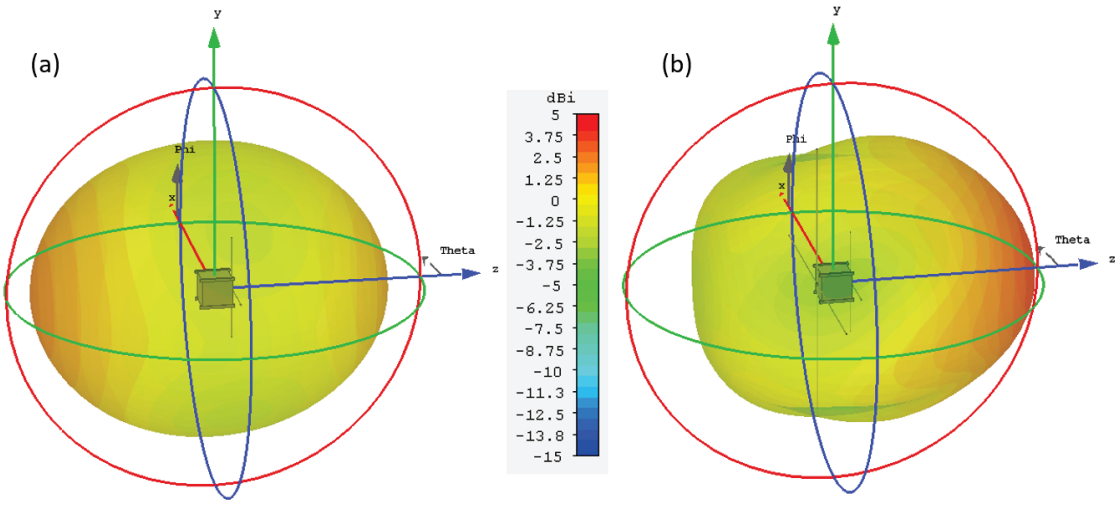


Figure 3.18 3-D gain patterns at $f_1$ = 436 MHz (UHF) in the case of (a) undeployed and (b) deployed VHF antenna.

However, a properly engineered mantle cloak to be put around the crossed-dipole VHF antenna is able to minimize the mutual blockage between them without affecting the performance of the antenna onto which it is applied. The design of the cloaking devices has been conducted with the formulas available in [36],[45] with the aim to achieve the required surface reactance able to minimize the scattering signature of the VHF antenna ($f_2$ = 144 MHz) at the central frequency of the UHF antenna ($f_1$ = 436 MHz). It is worth noticing that differently from the cases discussed in previous Sections, the surface reactance $X_s$ required to reduce the scattering signature of the VHF antenna at $f_1$ = 436 MHz is capacitive [74], since the VHF dipoles are metallic cylinders longer than the UHF dipoles. Hence, horizontal metallic strips are the most suitable geometry to achieve such an average surface reactance [30]. The final cloak adopted in the setup, shown in Figure 3.17, consist of eight electrically thin metallic horizontal strips spaced by $g$ = 30 mm, and patterned on a hollow dielectric cylinder ($\varepsilon_r = 15$, outer radius $a_c = 1.5a$, inner radius $a$ = 2 mm).

As shown in Figure 3.19, the designed mantle cloak once placed all around the crossed-dipole antenna operating in the VHF is able to restore the original

radiation diagram of the UHF antenna. In particular, Figure 3.19 (a) the far-field gain distribution of the crossed dipoles antenna operating at the central frequency $f_1$ = 436 MHz (UHF) is reported. The benefits of the cloaks are evident if compared with the 3D distribution in the undeployed VHF antenna case shown in Figure 3.18 (b). Thus, the quasi-isotropic radiation pattern of the antenna and the reliability of the communication link with the ground station is ensured. The cloaking effect is also confirmed by Figure 3.19Figure 3.12 (b), where the gain patterns of the antenna on the $\Phi = 0$ plane in the undeployed, deployed, and deployed cloaked VHF antenna at $f_1$ = 436 MHz are shown. The patterns are compared with the one of an ideal isotropic antenna. As can be appreciated, the cloak is able to restore the radiation pattern as if the VHF antenna was undeployed.

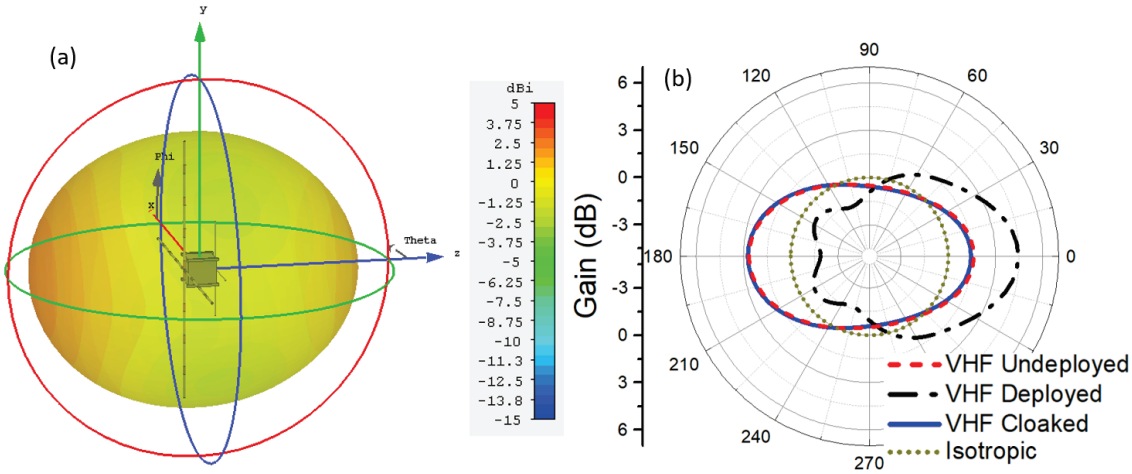


Figure 3.19 (a) 3-D gain patterns at $f_1$ = 436 MHz (UHF) in the case of deployed cloaked VHF antenna. (b) Gain patterns for the undeployed, deployed, and deployed cloaked VHF antenna scenarios compared to an ideal isotropic antenna.

In Figure 3.20 we also report the magnitude of the reflection coefficient of the UHF antenna in the undeployed, deployed, and cloaked VHF antenna cases. Note that in this configuration, even in the deployed VHF antenna case, a good

impedance matching at the input port of the UHF antenna is present, however, as discussed, still the radiation diagram is perturbed without the cloak.

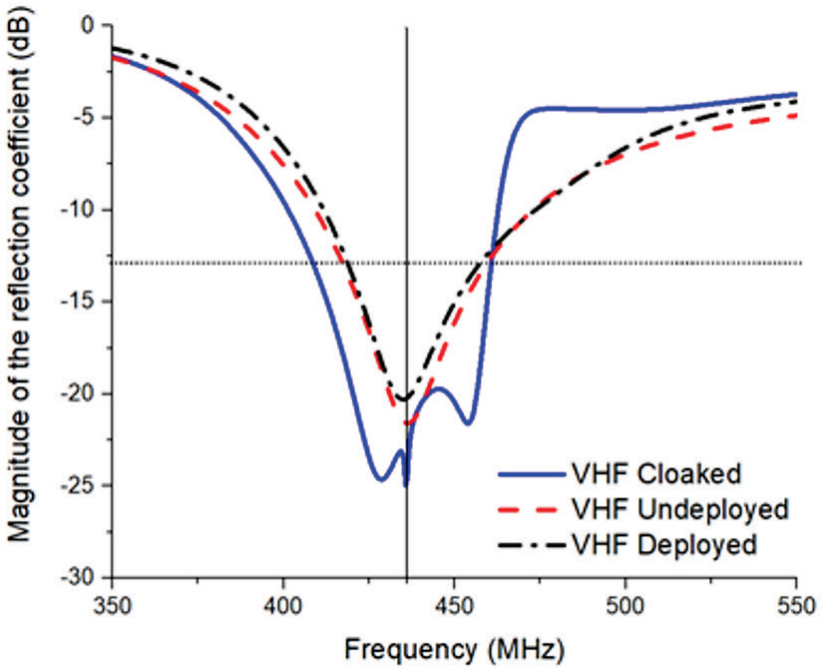


Figure 3.20 Magnitude of the reflection coefficient at the input port of the UHF crossed dipole antenna in the undeployed, deployed, and deployed cloaked VHF antenna scenarios.

We finally discussed the radiative and electrical characteristics of the VHF antenna.

Since the UHF antenna is electrically small compared to the VHF antenna, we do not expect any negative interfering effect arising on the VHF antenna performance due to the presence of the UHF antenna. This is confirmed by Figure 3.21 where are reported the radiative characteristics of the VHF antenna in the case of undeployed and deployed UHF antenna at the central frequency of operation (*i.e.*, $f_2$ = 144 MHz), respectively. It can be notice that, the UHF antenna does not perturb the radiative performance of the VHF antenna, since the 3D gain distribution are almost equal.

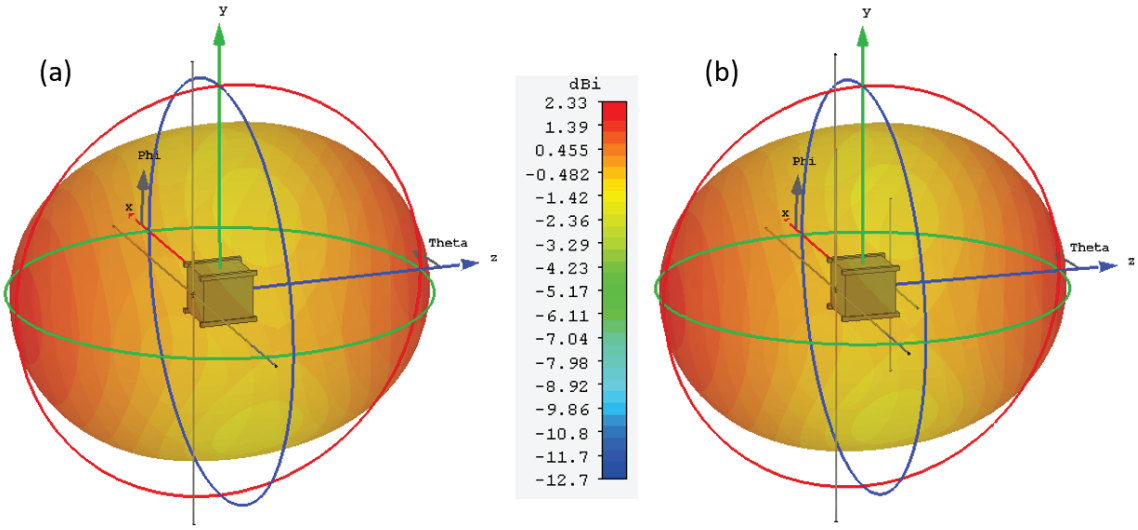


Figure 3.21 3-D gain patterns at $f_2$ = 144 MHz (VHF) in the case of (a) undeployed and (b) deployed UHF antenna.

However, it is important underline that it is crucial to verify that the radiative performance of the VHF antenna are still not deteriorated by the presence of the cloak, once applied all around. As can be appreciated in Figure 2.23 (a), the cloak does not perturb the gain distribution of the antenna, compared to the undeployed UHF antenna case shown in Figure 2.22 (a). This is due to the fact that the cloaking metasurface is able to minimize the scattering signature of the VHF antenna at the frequency of operation of the UHF antenna (*i.e.*, $f_1$ = 436 MHz). Specifically, the metasurface is characterized by a capacitive value of the surface reactance $Xs(f)$ able to minimize the scattering contribution of the metallic cylinders of the crossed-dipole antenna at the specific frequency $f_1$ = 436 MHz, while at the lower frequency $f_2$ = 144 MHz (VHF), the metasurface is almost transparent [4] since the metasurface is passive and exhibits, thus, a Foster frequency behaviour [33], i.e., the value of the $Xs(f)$ is very high.

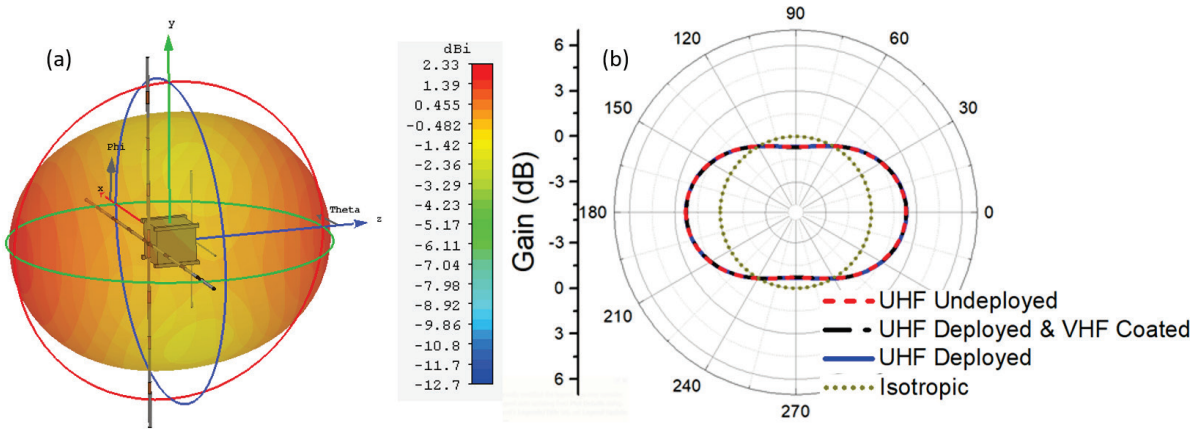


Figure 3.22 (a) 3-D gain patterns at $f_2$ = 144 MHz (VHF) in the case of deployed cloaked UHF antenna. (b) Gain patterns for the undeployed UHF antenna, deployed UHF antenna, and deployed UHF with the coated VHF antenna scenarios compared to an ideal isotropic antenna.

To conclude, in Figure 3.23 we also report the magnitude of the reflection coefficient of the VHF antenna in the undeployed UHF antenna, deployed UHF antenna, and deployed UHF with the coated VHF antenna scenarios. Please note that due to the presence of the dense dielectric substrate with high value of the permittivity ($\varepsilon_r = 15$) placed all around the VHF antenna, we can observe a slightly shift at lower frequency of the resonance of the VHF antenna once coated with the mantle cloak. However, this shift can be easily compensated and taken in to account during the design process of the VHF antenna slightly shortening the dipoles height.

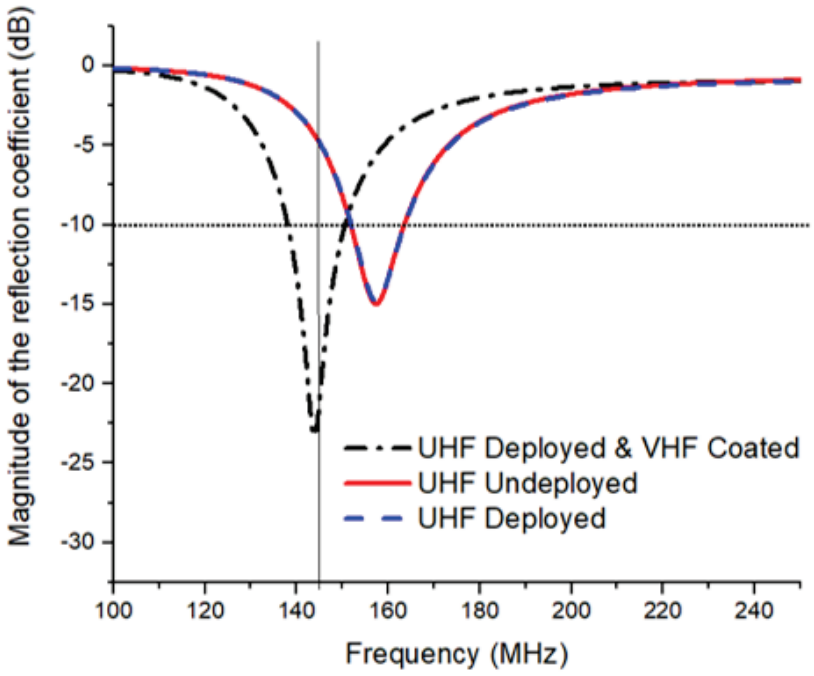


Figure 3.23 Magnitude of the reflection coefficient at the input port of the VHF crossed dipole antenna in the undeployed UHF antenna, deployed UHF antenna, and deployed UHF with the coated VHF antenna scenarios.

## 3.2 Waveform-selective mantle cloaks for antennas applications through circuit-loaded metasurfaces

In the previous Sections, has been proved that, for antenna applications, the mantle cloaking technique [30] can be of particular interest, because it exploits conformal and easily manufacturable metasurfaces and it does not electromagnetically isolate the hidden object from the surrounding environment. This technique has allowed designing invisible wire sensors [42] and minimizing the interference effects between antennas and passive objects in both terrestrial and satellite applications [40],[80].

It is worth noticing that, in these works, the employed metasurfaces are passive, reciprocal, and linear, leading to a cloaking behaviour that depends

neither on the power level nor on the waveform of the incident field. However, recently, there has been a growing interest in the development of metasurfaces enriched with advanced electromagnetic functionalities through the use of linear or nonlinear lumped electronic circuits.

For instance, in [81] nonlinear circuits have been used to design a metasurface able to absorb high-power pulsed surface currents while maintaining minimum disturbance to low-power pulsed RF illumination and, thus, providing a shielding from high-power external interfering sources. The same similar approach based on the use of nonlinear elements like diodes have been used in [82] to control the reflective and transitive properties of mushroom-type high-impedance surfaces, by a tuning of the working states of the integrated diodes.

In the field of electromagnetic cloaking, some efforts to exploit nonlinear elements for cloaking applications have been introduced at both optical [83] and microwave frequencies [84],[85]. In particular, in [84] a tunable transmission-line cloak has been discussed exploiting varactor diodes to achieve ideally an on/off switching invisibility effect. Instead, in [85], exploiting the nonlinearity of diode pairs, a power-dependent mantle cloak for antenna applications has been proposed. Specifically, it has been shown that the cloaking behaviour of a capacitive metasurface could be switched on/off by loading the gaps of the capacitive horizontal metallic strips metasurface with a few diode pairs. This advanced functionality of the metasurface has been then exploited to design new power-dependent antennas able to modify their radiative characteristics depending on the input power level.

Finally, in [86] waveform-selective metasurfaces able to distinguish between different waveforms of the propagating surface waves were presented. In this case, waveform selective properties have been used to design an absorber

capable of storing high-power pulse energy and dissipating it between consecutive pulses, exploiting properly designed lumped elements circuits. In particular, the waveform-selective absorbing characteristics have been achieved storing the energy of the high-power pulse in capacitors during the illumination, while between pulses discharging the energy into resistors.

In this Section, following the approach exploited in the aforementioned works, we discuss the possibility of designing unconventional mantle cloaking devices able to either hide or restore the visibility of a wire antenna at its own operational frequency if illuminated by a short-pulsed or a continuous signal, respectively. The waveform selective behavior is achieved exploiting circuit-loaded metasurfaces made of lumped elements such as diodes, inductors and resistors. The proposed configuration could pave the way to a new generation of invisibility devices characterized by advanced and unconventional functionalities.

### 3.2.1 Waveform-selective cloaking

The waveform-selective cloak we propose here is a device whose invisibility behaviour depends on the impinging waveform. In particular, the waveform-selective cloak we deal with is able to suppress the scattering signature of an object when excited by a pulse wave (PW) without affecting the scattering characteristics of the coated object when illuminated by a continuous wave (CW). A sketch of the working principle of such a waveform-selective mantle cloak when applied to a wire antenna is illustrated in Figure 3.24. As it can be appreciated, when a PW illuminates the coated antenna, the cloaking behavior is turned on forbidding any electromagnetic interaction between the external waves and the antenna. Differently, when a CW signal impinges onto the coated antenna, the cloaking effect is turned off allowing the reception of a useful signal

by the antenna itself. The described unconventional behavior obtained through waveform-selective cloaking could be of particular interest for defense applications since, in this way, the coated antenna would be invisible to an external enemy radar that emits PW, while keeping its operation for a CW emitted by a base station.

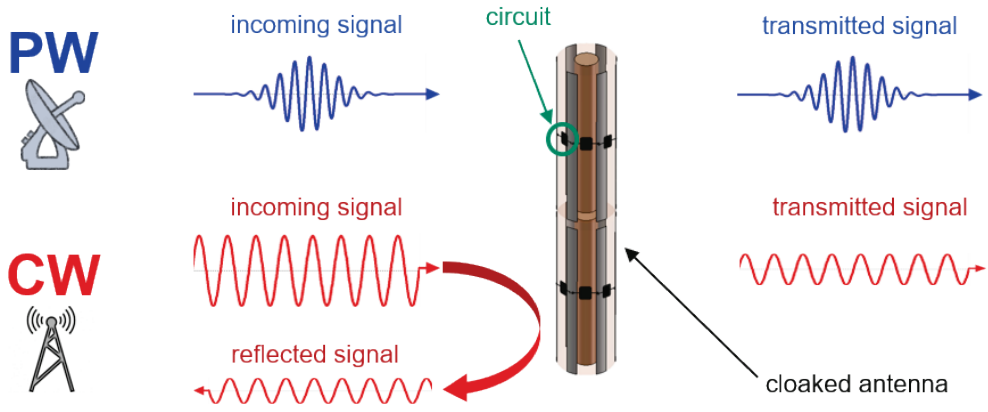


Figure 3.24 Sketch of the waveform-selective cloaking concept when applied to a wire antenna. The cloak works if illuminated by a pulse wave (PW) while it is switched off if illuminated by a continuous wave (CW).

Moreover, the waveform-selective cloak allows to overcome a fundamental limitation of cloaking for antennas. In fact, as known from the fundamental theory of passive cloaking [42], an antenna cannot be cloaked at its own operational frequency and, at the same time, efficiently operates in transmission/reception. As can be appreciated from Figure 3.25, without loss of generality for the case of a resonant dipole wire antenna, an antenna cloaked at its own resonant frequency would be strongly mismatched to the load, *i.e.*, the magnitude of the reflection coefficient would be almost equal to 0 (dB scale). Therefore, the antenna would be unable to efficiently receive or transmit. From a physical point of view, this is essentially due to the optical theorem [78] and, consequentially, to the energy conservation principle. In fact, for the optical theorem it is possible to write that:

$$\sigma_{ext} = \sigma_{abs} + \sigma_{scat} = \lambda_0 / \pi \, \mathrm{Im}\left[ s_\theta(0,0) \right] \tag{17}$$

where $\sigma_{ext}$ is the total extinction cross section of the object, $\sigma_{abs}$ is the absorption cross section, $\sigma_{scat}$ is the scattering cross section, $\lambda_0 / \pi \, \mathrm{Im}\left[ s_\theta(0,0) \right]$ is the normalized scattering amplitude parallel to the impinging filed in the forward direction ($s_\theta(0,0)$). Eq. (17) means that an object with zero or weak total scattering (*e.g.*, $\sigma_{scat} = 0$ and, thus, $s_\theta(0,0) = 0$) must has zero or weak total absorption (*e.g.*, $\sigma_{abs} = 0$), *i.e.*, some absorption is always required in order to have nonzero scattering. Since the optical theorem apply to the scattering of any object illuminated by a plane wave linearly polarized, in the specific case of wire antenna, it implies that an antenna characterized by zero scattering (*e.g.*, cloaked at its own resonant frequency) is unable to receive/transmit since it would be characterized by zero absorption. This statement is also consistent with the limit of absorption from receiving antenna discussed in the antenna theory field [79].

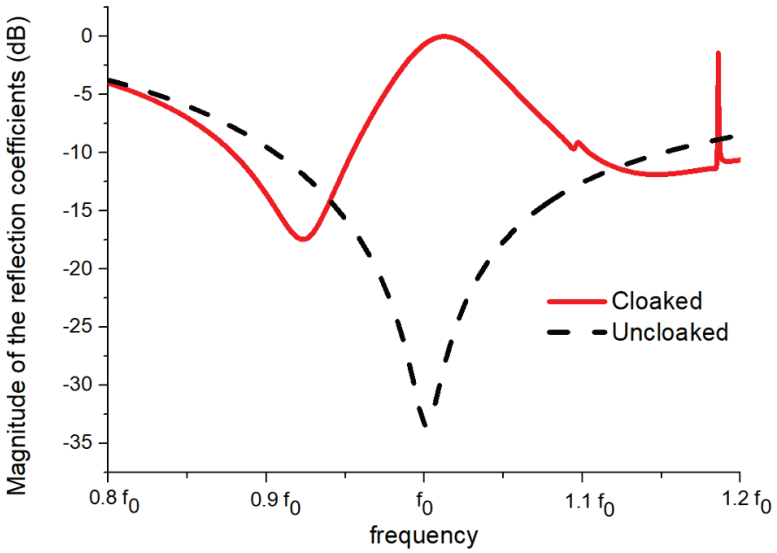


Figure 3.25 Magnitude of the reflection coefficient at the input port of a dipole antenna cloaked at its own resonant frequency.

The proposed waveform-selective cloak allows to overcome this fundamental limitation since enable to design an antenna invisible to a radar emitting short-pulsed signal, while keeping its proper behavior for the continuous signals needed for communication purposes. However, it is worth noticing that, the PW should have at least a pulse duration of 10 ns, since the frequency bandwidth of a PW characterized by a shorter pulse duration, would overcome the maximum frequency bandwidth achievable by the mantle cloaking technique [40], in the current status of the technology .

### 3.2.2 Design of the loading circuit

A waveform-dependent cloaking device for wire antenna can be designed exploiting a metallic strips metasurface loaded with a lumped-element circuit connected to the strips' gaps (Figure 3.26). In this scenario, the metallic-strip metasurface is designed to suppress the scattering signature of the antenna at its own resonance frequency (*e.g.*, 1 MHz) accordingly with the mantle cloaking approach [30]. Such a metasurface is then loaded with the circuit shown in Figure 3.26 (a). It consists of a 4 diodes full-bridge rectifier and a series combination of an inductance ($L$) and a resistor ($R$) in parallel to the input ports ($P_1$ and $P_2$) connecting two separate metallic strips. When the metasurface is illuminated by an external filed, the fundamental frequency of the signal is converted by the full-bridge rectifier to an infinite set of frequency components, with the main one at zero frequency. Therefore, a main DC component appears. Here, due to the presence of the inductance $L$, initially the flow of the induced current is initially opposed, and the two ports of the circuit ($P_1$ and $P_2$) are in an open circuit condition. However, gradually, the opposing effect of the inductance weakens, and current starts flowing between the two ports trough the resistance $R$. Consequently, the two ports of the circuit are short-circuited,

*i.e.*, the two strips of the metasurface are short-circuited and the cloaking metasurface becomes a perfect electric conductor (PEC) and loses its cloaking behavior. Therefore, thanks to the loading circuit, the metasurface behaves as a cloaking device for PW and as a PEC layer for CW.

It is worth noticing, that the presence of the ratification process due to the diodes is essential to the correct behaviour of the circuit. The non-linear characteristics of the diodes allows to exploit the transient characteristic of the inductance $L$ generating an opposing electromotive force that weakens after some time. Without the DC conversion, the circuit would behave in a similar way for both the PW and CW signals.

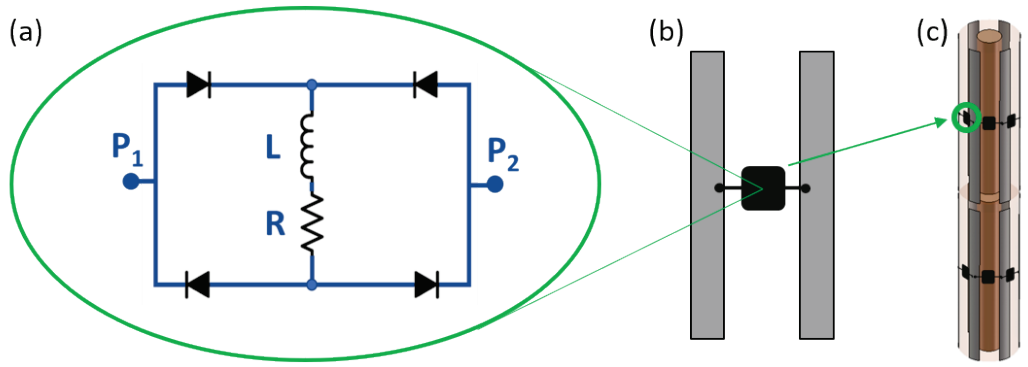


Figure 3.26 (a) Detail of the waveform-selective circuit, (b) detail of the circuit loaded on to the metasurface unit cell and (c) overview of the waveform-selective cloak coating the dipole antenna.

In order to confirm the expected behavior, numerical simulations exploiting the commercial software for circuit simulations Advanced Design System (ADS) have been carried out. The schematic of the analysed waveform-selective circuit is reported in Figure 3.27. The lumped elements have the following values: $L$ = 1 mH, $R$ = 1 Ω, and the behavior of the circuit has been analyzed in term of the currents flowing between $P_1$ and $P_2$. In particular, currents probes have been placed in the point named *Probe A* and *Probe B* to evaluate the performance of the circuit. A voltage source has been exploited to excite the circuit, and the

waveforms of the exciting signals are reported in Figure 3.28. As can be appreciated, in case of PW a damped sign function at a frequency $f_0$ = 1 MHz has been exploited, while in the case of CW a sign function at the same frequency $f_0$ has been used. Both the signals have the same amplitude of 10 V.

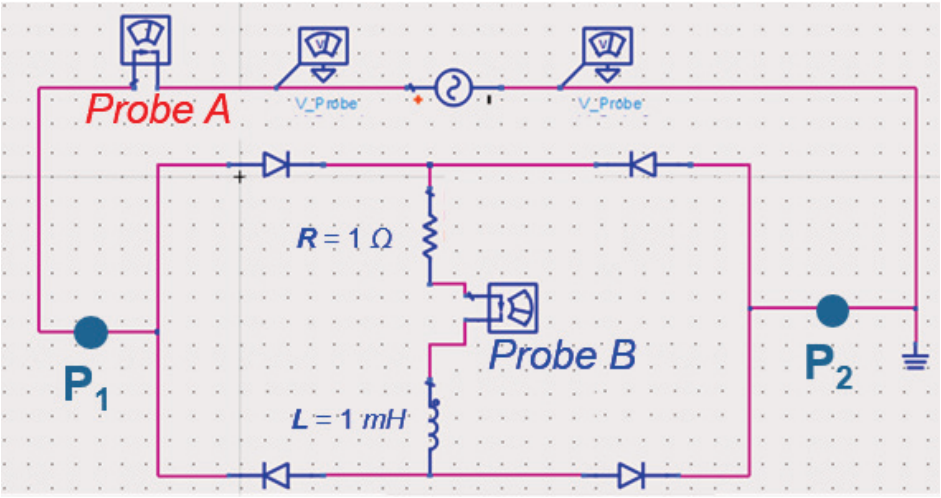


Figure 3.27 Schematic of the waveform-selective circuit. The circuit consists of a 4 diodes full-bridge rectifier and a series combination of an inductance (L = 1 mH) and a resistor (R = 1 Ω). Probe A is used to evaluate the input current. Probe B is used to evaluate the current flowing between the $P_1$ and $P_2$.

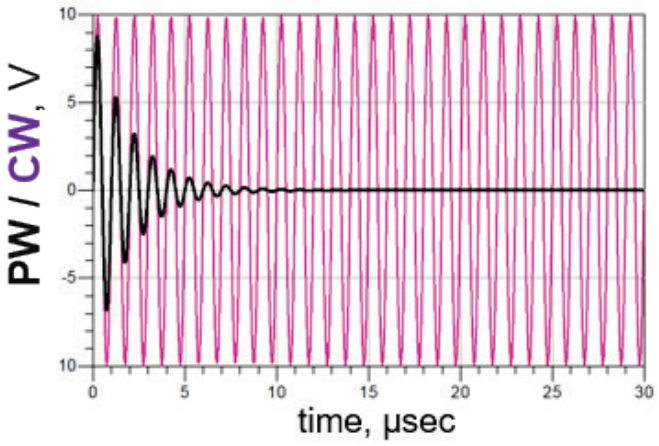


Figure 3.28 Voltage signal waveforms exciting the lumped-elements circuit.

The results of the simulations are showed in Figure 3.29. As can be appreciated, when the PW is excited (Figure 3.29 (a)) weak currents (around 6 mA) flowing through the circuit can be measured, indicating the open circuit condition of the two ports $P_1$ and $P_2$. On the contrary, in case of the CW (Figure 3.29 (b)), after an initial rise time, a steady state of conduction between the two ports is achieved and a strong current (around 6 A) is induced, thus, ports $P_1$ and $P_2$ are short circuited. Please, pay attention to the different scale of the graphs between the PW and CW cases. From Figure 3.29 it is also possible to appreciate that, due to the rectification process enabled by the diode, we observe the envelope curve signature of the currents.

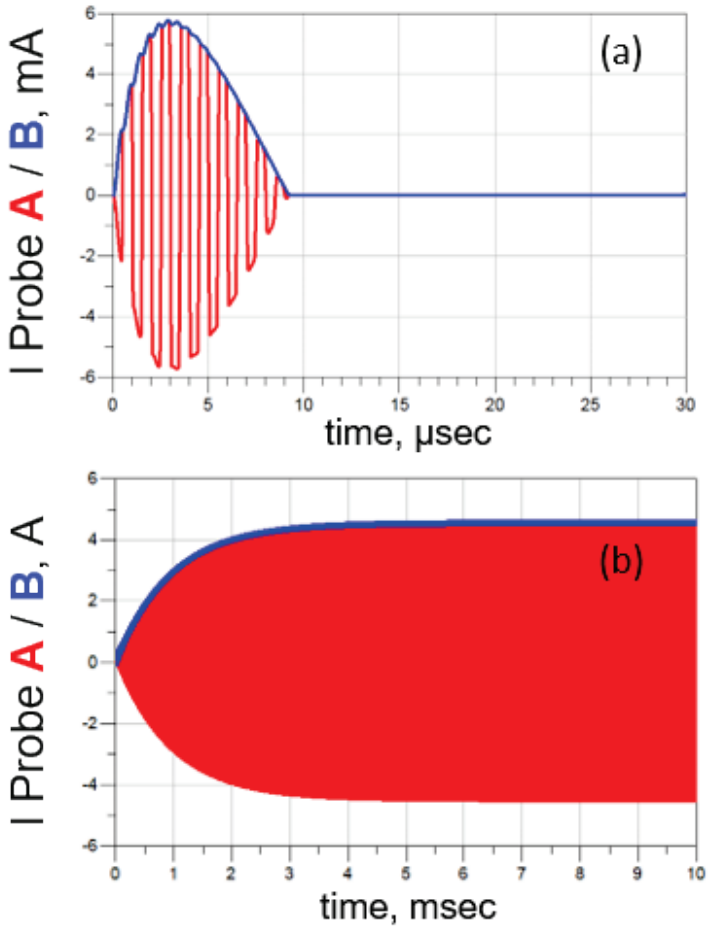


Figure 3.29 Time domain response of the circuit given in terms of the currents measured in $P_1$ and $P_2$ for (a) a PW signal and (b) a CW signal.

Moreover, it is worth noticing, that the different response of the circuit depending on the waveform of the signal, strictly relates to the relationship between the time constant of the circuit ($\Delta\tau = L/R$) and the time period of the PW signal ($\Delta t$). In particular, the response of the circuit behaves differently only if $\Delta\tau > \Delta t$ and in fact, in the case analysed so far, it can be easily verified that $(\Delta\tau = 1ms) > (\Delta t = 1\mu s)$.

The dependence of the circuit response from the relationship between $\Delta\tau$ and the $\Delta t$ of the PW is confirmed in Figure 3.30. Here, we report the behaviour of the currents flowing in the circuit between $P_1$ and $P_2$, in the case of $\Delta\tau > \Delta t$. In this case, thus, the value of the inductance $L$ has been reduced to 1 nH, such that $\Delta\tau = 1\,\text{ns}$ (*i.e.*, $\Delta\tau < \Delta t$).

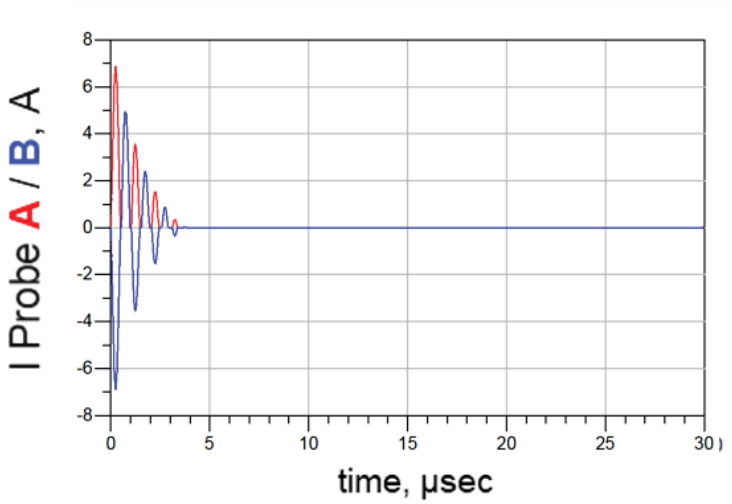


Figure 3.30 Time domain response of the circuit given in terms of the currents measured in $P_1$ and $P_2$ for a PW signal, when $\Delta t > \Delta\Gamma$ (*i.e.*, for L = 1 nH and R = 1 Ω).

Finally, in order to highlight the importance of the rectification process, we report the response of the circuit when the diodes are not present. As can be appreciated from Figure 3.31, without the 4 diodes full bridge rectifier, the circuit would behave in the same way, independently from the waveform of the exciting signal. In fact, the currents flowing through the circuit would be

extremely weak (around 3 mA) for both the PW and CW cases, indicating the open circuit condition of the two ports P1 and P2.

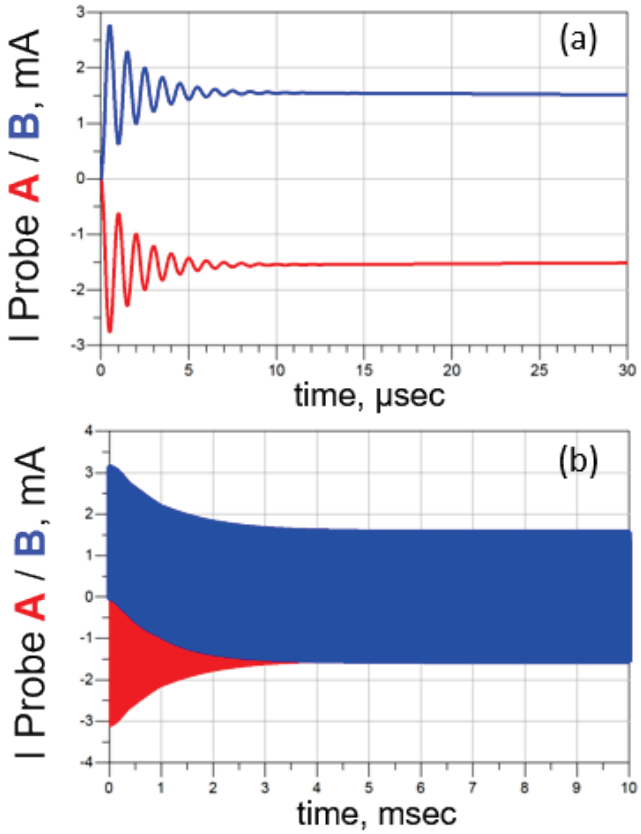


Figure 3.31 Time domain response of the circuit without the 4 diodes full-bridge rectifier given in terms of the currents measured in $P_1$ and $P_2$ for (a) a PW signal and (b) a CW signal.

### 3.2.3 Waveform-selective cloaking metasurface design and numerical results

To confirm the waveform-selective characteristic of the cloaking metasurface, a full-wave [61] and circuit [87] co-simulation analysis has been conducted. First, we have designed a dipole wire antenna operating at $f_0$ = 1 MHz with a radius $a = \lambda_0 / 50$. Then, a proper cloaking device able to cloak the antenna at its own resonant frequency has been designed, following the mantle cloaking technique

approach [30]. Has known form the fundamental theory of mantel cloaking [30] and cloaking for antennas [35],[36],[40],[42], the required cloaking reactance $X_s$ to cloak a wire dipole antenna at its resonant frequency is inductive. Hence, vertical metallic strips are the most suitable geometry to achieve such an average $X_s$ [36],[45]. Following the design formulas in [36],[45] and after a numerical full-wave optimization needed to take into account the finite length of the cylinder and its curvature, the cloaks adopted in our setup, shown in the insert of Figure 3.32, consist of twelve electrically thin metallic strips of width $w = \lambda_0/100$, patterned on a hollow dielectric cylinder with a permittivity of $\varepsilon_r = 6.5$, outer radius $a_c = 1.2a$ and inner radius equal to the radius of the dipole antenna $a = \lambda_0/50$. In Figure 3.32, it is also reported the frequency behaviour of the total scattering cross section of the antenna in the uncoated and coated cases. As can be appreciated, mantle cloak drastically reduces the scattering cross section of the antenna at its own resonant frequency at $f_0$ = 1 MHz.

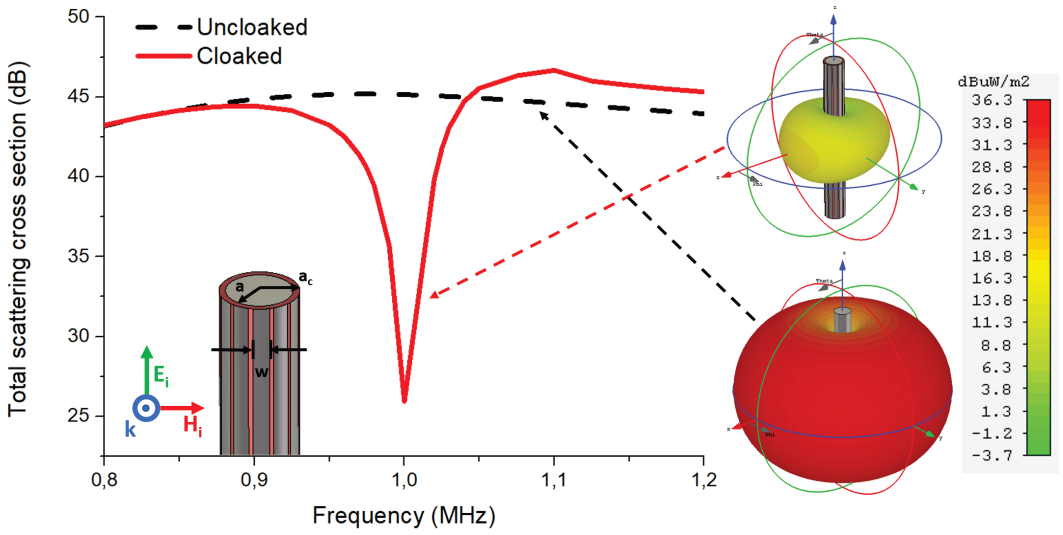


Figure 3.32 SCS vs. frequency of the dipole antenna in the uncloaked and cloaked scenario. In the inset, detail of the cloaking device coating the dipole (geometrical parameters: $w = \lambda_0/100$, $a_c = 1.2a$, $a = \lambda_0/50$) and 3-D radiated power patterns in the uncloaked and cloaked cases.

Once the cloaking metasurface has been design, it has been loaded with the waveform-selective circuit described in the previous Section. In order to confirm the waveform-selectivity cloaking behaviour, a co-simulation between the full wave numerical simulator CST Microwave Studio [61] and the circuit simulator Advanced Design System - ADS [87] has been adopted. Exploiting the full-wave numerical simulator and its frequency domain solver, the scattering matrix of the unit cell of the cloaking metasurface has been derived. To retrieve the scattering matrix to be imported after into the circuit simulator as touchstone file, in CST Microwave Studio the unit cell of the metasurface has been modelled. The details of the simulated setup are reported in Figure 3.33 (a). Here, it is shown the metasurface unit cell realized by two vertical metallic steeps with a width of $w/2$, separated by a gap loaded by a discrete port, which will be used in the circuit simulator to load the waveform-selective lumped-elements circuit. It is worth noticing that the input and output port of the simulation have been separated from the unit cell by two $\lambda_0/2$ transmission line segments. In Figure 3.33 (b) the equivalent circuit representation of the setup is reported. The characteristics of the structure have been evaluated in term of the S-parameters and the 3x3 scattering matrix has been computed. Please, note that the length of the transmission-line segments has been tuned frequency by frequency to be precisely $\lambda_0/2$ at every frequency sample of the simulation.

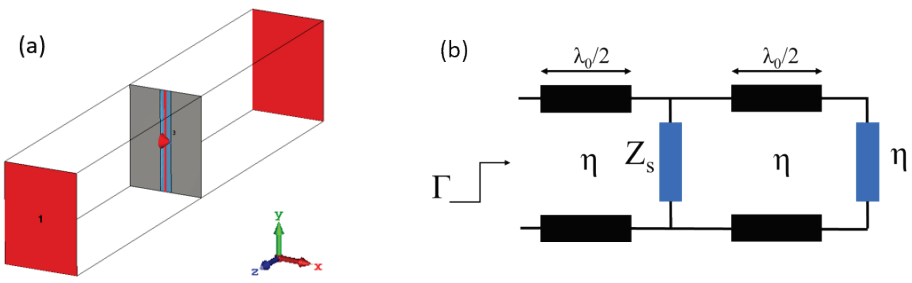


Figure 3.33 (a) Unit cell of the metasurface implemented in a full-wave simulator with the loading port (the red pin between the metasurface's strips) for the extraction of the S-matrix. (b) Equivalent circuit model of the structure.

The 3x3 scattering matrix of the metasurface unit cell has been then imported as a touchstone file into the circuit simulator ADS. The final simulation setups are shown in Figure 3.34. Two different simulation setups have been set. One without the waveform-selective circuit (Figure 3.34 (a)), and one with the loading waveform-selective circuit designed in the previous Section (Figure 3.34 (b)). The performance of the waveform-selective cloaking metasurface has been evaluated in term of output voltage, *i.e.*, in term of transmitted by the metasurface field, when exciting with a PW or a CW with the main frequency component at $f_0$ = 1 MHz (the same waveforms reported in Figure 3.28 have been exploited). Please, note that the 184 Ω resistances at the input and at the output of the circuit represents the line impedance $\eta$ in full-wave simulation setup (Figure 3.33 (b)).

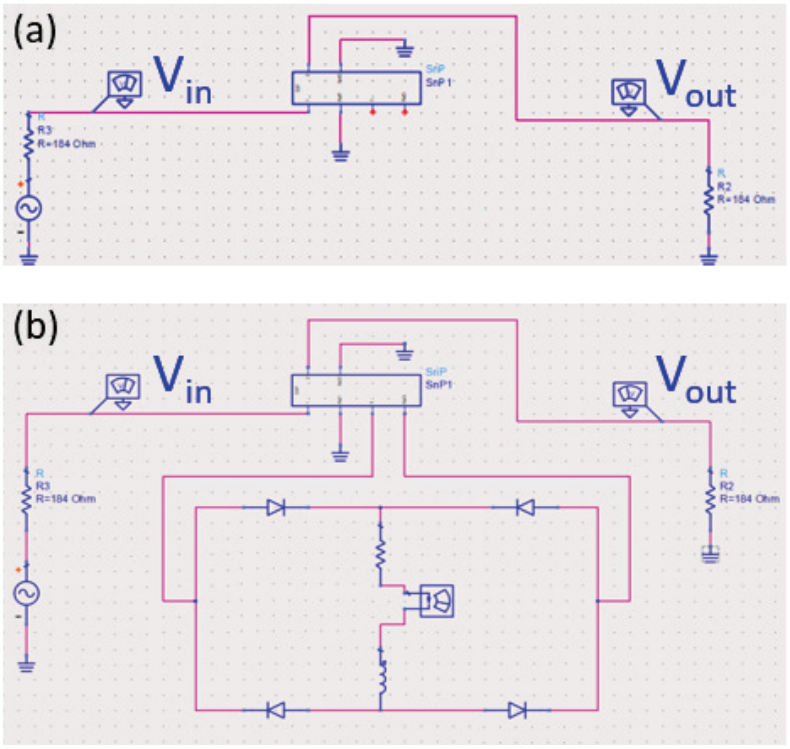


Figure 3.34 The setup used in the full-wave and circuit co-simulation, in case of (a) circuit - unloaded and (b) -loaded metasurface.

In Figure 3.35 the performance of the circuit-unloaded metasurface in term of the normalized voltages measured at the input and output port of the setup, shown in Figure 3.34 (a), in case of CW is reported. In particular, the time domain (on the left) and the frequency domain (on the right) responses are shown. In the insert, for the sake of clarity, the equivalent unit cell of the metasurface implemented in the full-wave simulator is reported.

As can be appreciated, for a CW, in the circuit unloaded configuration, the signal at the input is equal to the output signal.

The same analysis has been performed in the case of PW when exciting the same circuit-unloaded metasurface. The results are reported in Figure 3.36. As can be appreciated, also in this case, the input and output voltages are equal, indicating that the cloaking metasurface behave in the same way, independently from the waveform of the impinging signal.

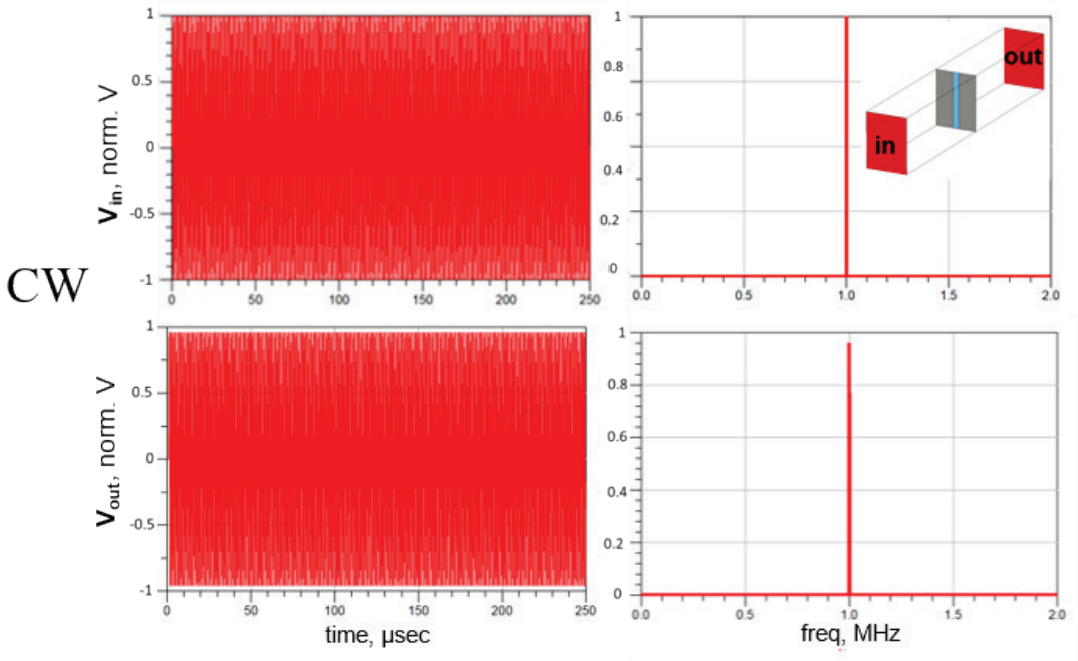


Figure 3.35 Performance of the circuit -unloaded metasurface evaluated through full-wave and circuit co-simulation, when exciting the structure with a CW signal, evaluated in term of the normalized input and output voltages.

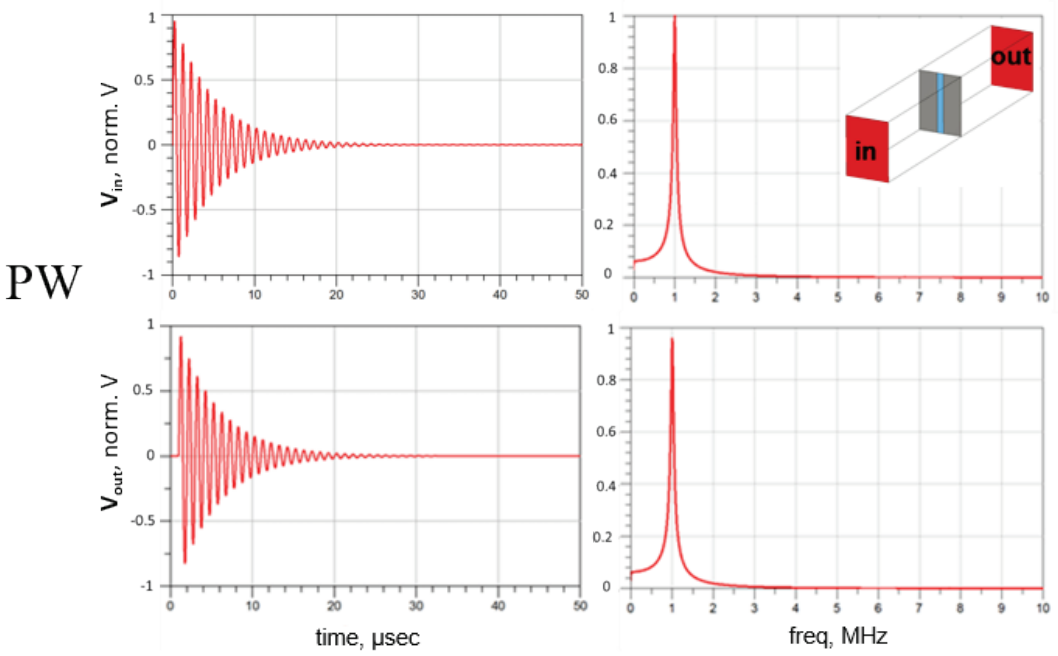


Figure 3.36 Performance of the circuit -unloaded metasurface evaluated through full-wave and circuit co-simulation, when exciting the structure with a PW signal, evaluated in term of the normalized input and output voltages.

Finally, the performances of the circuit-loaded cloaking metasurface in term of normalized measured voltages at the input and output ports of the setup reported in Figure 3.34 (b) have been evaluated. In Figure 3.38 and Figure 3.37 the time domain (on the left) and the frequency domain (on the right) responses of the circuit when excited by a CW and a PW are shown, respectively. In the insert, the equivalent unit cell of the metasurface implemented in the full-wave simulator when loaded with the circuit element is reported.

In particular, in Figure 3.38 the response of the waveform-selective cloaking metasurface to a CW can be appreciated. Here, can be observed that the input and output voltages are significantly different. From the time domain response of the structure (on the left) it is possible to appreciate the opposing effect of the inductance L of the loading circuit. After some time, the voltage at the output (i.e., transmitted by the metasurface) is almost zero, indicating the short circuit

condition of the strips of the cloaking metasurface. Thus, the metasurface behave as a perfect electric conductor. This is confirmed by the frequency domain response of the loaded metasurface. The main frequency component of the input signal at f0 = 1 MHz approaches the zero. It is worth noticing that, comparing the frequency domain response shown in Figure 3.38 to the one reported in Figure 3.37, high order odd harmonics are generated, due to the ratification process of the diodes. However, characterized by a very small magnitude.

In Figure 3.38, instead, the response of the waveform-selective cloaking metasurface to a PW is reported. As can be appreciated, the voltages at the input and output are almost equal. In particular, from the frequency domain response, a slight reduction of the magnate of the main component at $f_0$ = 1 MHz can be noticed. This is due to the rectification process of the diodes and their non-ideal response. In fact, a triggering voltage of 0.8 V can be measured across the diodes and this voltage drops reduce inevitably the amplitude of the measured output voltage. Moreover, it is worth noticing that, compared to the CW case of Figure 3.37, the reduction of the frequency component at $f_0$ it is one order of magnitude lower. This means that the waveform-selective cloaking metasurface behave differently depending on the waveform of the input signal, *i.e.*, the value of the surface reactance $X_s$ of the metasurface changes if illuminated by a PW or CW. Therefore, it is possible to tune the surface reactance of the waveform-depending metasurface in such a way that for a PW it assumes the required value to achieve a cloaking effect, while for a CW it changes assuming a different value for witch the cloaking effect is turned off.

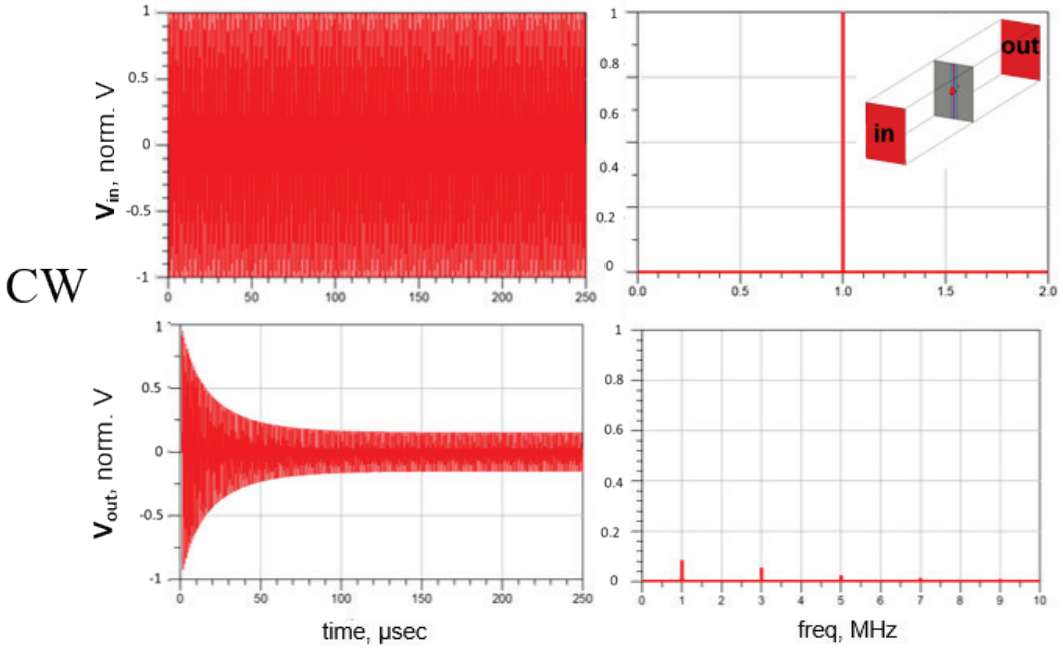


Figure 3.37 Performance of the circuit -loaded metasurface evaluated through full-wave and circuit co-simulation, when exciting the structure with a PW signal, evaluated in term of the normalized input and output voltages.

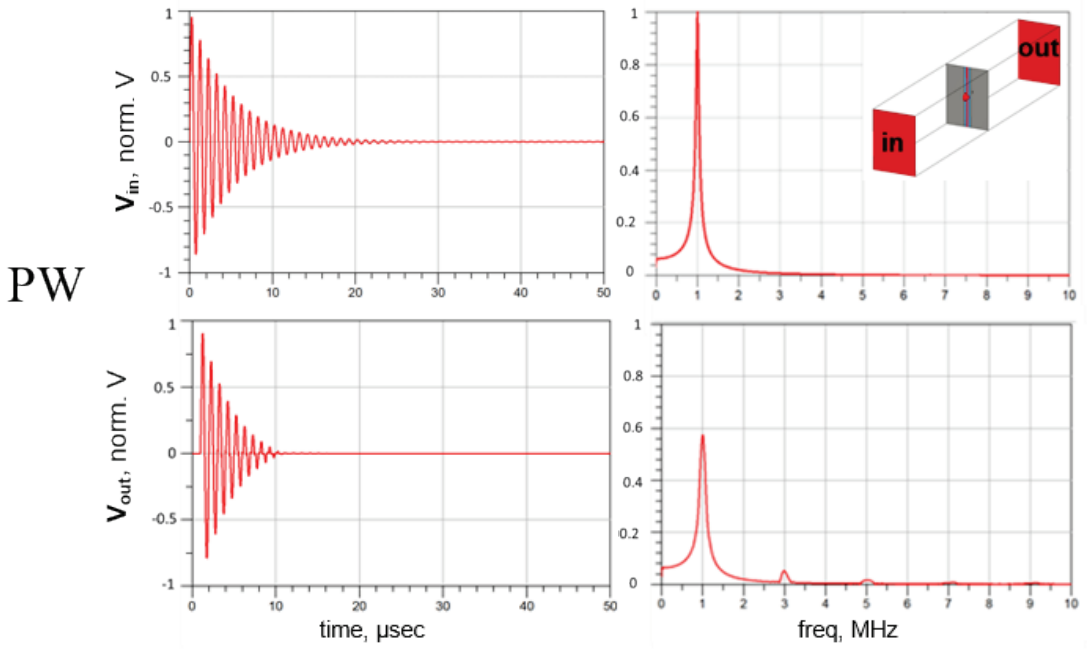


Figure 3.38 Performance of the circuit -loaded metasurface evaluated through full-wave and circuit co-simulation, when exciting the structure with a PW signal, evaluated in term of the normalized input and output voltages

# CHAPTER 4

# CONCLUSIONS

The present dissertation presents the results of the three years PhD course on Applied Electronics. In particular, the idea of scattering manipulation and control of objects of cylindrical geometry based on metasurfaces has been theoretically and numerically discussed, and some applications in antenna scenarios have been presented.

First, the intriguing possibility of tailoring the scattering response of an electrically-small object using metasurfaces has been discussed, and a theoretical approach has been presented in view of camouflaging or cloaking applications. More specifically, the analytical solution to the scattering problem of a metasurface coated cylindrical object has been presented, and a closed form expression of the surface impedance of the metasurface needed to tailor at will the scattering response of the cylinder has been developed. Thanks to this close form expression, the theoretical frequency behaviour of the surface impedance has been shown and analysed.

Moreover, some significant examples of the camouflaging effects that it is possible to achieve exploiting the developed theory have been presented,

splitting them into the general cases of scattering reduction and scattering enhancement transformation.

In particular, as an example of scattering reduction, the relevant case of camouflage of a metallic cylinder into a dielectric one exploiting a metasurface designed using the developed formulas has been discussed. As significant example of scattering enhancement instead, the case of tailoring of a weak scatterer into a stronger scatterer has been presented, validated by full-wave simulations. Finally, a technique to increase the frequency performance of the camouflage effect has been shown. Exploiting metasurfaces characterized by a controllable amount of losses it has been shown that it is possible to increase the frequency bandwidth of the camouflaging effect, in particular for the case of scattering reduction.

In the last part of this thesis, two different applications of the cloaking approach have been presented.

In the first one, an innovative solution for satellite communications able to dramatically reduce the interference effects arising between the antennas mounted on the platform and its deployable equipment has been discussed. By analysing a typical CubeSat satellite, it has been shown how it is possible to make the deployable objects effectively invisible to the antennas within the entire operation bandwidth. This result has been achieved using a simple, conformal and low-cost metasurface cover, characterized by a straightforward implementation and ease of fabrication that make this solution particularly suitable for satellite applications.

Finally, the versatility of the cloaking solution on the design of the nanosatellite has been discussed. In particular, it has been highlighted how the cloak functionality allow to place the deployable equipment in the very near field of the antenna, and how it allows to design unprecedent miniaturized

satellite equipped with multi-functional antenna system operating at very different frequencies. The proposed setups prove that cloaking technology can be particularly useful in satellite applications, enabling new degrees of freedom in the design of miniaturized space platforms.

In the second application, the idea of a waveform-dependent cloaking device has been discussed. The cloak behaves as an invisibility device if illuminated by a PW while it is disabled for a CW. This behaviour is achieved exploiting a metasurface made of metallic strips and loaded with a circuit able to switch its behaviour depending on the impinging waveform. In particular, the circuit is designed exploiting simple and cheap circuit lumped elements like diodes, resistors and inductors. In particular, a possible application for making a dipole antenna invisible to a radar while keeping its operation for a communication link has been discussed.

In conclusion, the scattering manipulating approach, validated by analytical and full-wave simulations, provides a general methodology for manipulating the scattering signature of an object, as has been proved by the relevant examples of cloaking trough metasurfaces for antenna applications.

# References


[1] G.V. Eleftheriades, and K.G. Balmain, *Negative Refraction Metamaterials: Fundamental Principles and Applications*. Hoboken, NJ: Wiley-IEEE Press, 2005.

[2] N. Engheta, and R.W. Ziolkowski, *Electromagnetic Metamaterials: Physics and Engineering Explorations*. Hoboken, NJ: Wiley-IEEE Press, 2006.

[3] R. Marqués, F. Martín, M. Sorolla, and F. Capolino, *Metamaterials with Negative Parameters: Theory, Design and Microwave Applications*. Hoboken, NJ: Wiley-Interscience, 2008.

[4] S. Zouhdi, A. Sihvola, and A. P. Vinogradov, *Metamaterials and Plasmonics: Fundamentals, Modelling, Applications*. Dordrecht, NL: Springer-Verlag GmbH, 2008.

[5] P.B. Johnson, R. W. Christy, "Optical constants of the noble metals," *Phys. Rev. B*, Vol. 6, pp. 4370-4379, 1972.

[6] E.D. Palik, *Handbook of Optical Constants of Solids*, Boston, NE: Academic Press, 1998.

[7] L.D. Landau, L.P. Pitaevskii, and E.M. Lifshitz, *Electrodynamics of Continuous Media, Second Edition*: Volume 8. Oxford, EN: Pergamon Press, 1984.

[8] V.G. Veselago, "The electrodynamics of substances with simultaneously negative values of ε and μ,", *Sov. Phys. Uspekhi*, Vol. 10, pp. 509–514, 1968.

[9] D.R. Smith, W.J. Padilla, D.C. Vier, S.C. Nemat-Nasser, and S. Schultz, "Composite medium with simultaneously negative permeability and permittivity," *Phys. Rev. Lett*., Vol. 84, pp. 4184-4187, 2000.

[10] J. B. Pendry, A. J. Holden, D. J. Robbins and W. J. Stewart, "Magnetism from conductors and enhanced nonlinear phenomena," in *IEEE Transactions on Microwave Theory and Techniques*, vol. 47, no. 11, pp. 2075-2084, Nov. 1999.

[11] N. Fang, H. Lee, C. Sun, and X. Zhang, "Sub–diffraction-limited optical imaging with a silver superlens," *Sci*., Vol. 308, pp. 534-537, 2005.

[12] A. Salandrino, and N. Engheta, "Far-field subdiffraction optical microscopy using metamaterial crystals: Theory and simulations," *Phys. Rev. B*, Vol. 74, 075103, 2006.

[13] Z. Liu, H. Lee, Y. Xiong, C. Sun, and X. Zhang, "Far-field optical hyperlens magnify-ing sub-diffraction-limited objects," *Sci*., Vol. 315, pp. 1686, 2007.

[14] M. Silveirinha, A. Alu and N. Engheta, "Infrared and optical invisibility cloak with plasmonic implants based on scattering cancellation," Phys. Rev. B, 78, 075107, 2008.

[15] N. Engheta, "Circuits with light at nanoscales: Optical nanocircuits inspired by metamaterials," Sci., Vol. 317, pp. 1698-1702, 2007.

[16] Cummer, S. A., Christensen, J. & Alù, A. Controlling sound with acoustic metamaterials. *Nat. Rev. Mater.* **1**, 16001 (2016).

[17] Schittny, R., Kadic, M., Guenneau, S. & Wegener, M.Experiments on transformation thermodynamics: molding the flow of heat. *Phys. Rev. Lett.* **110**, 195901 (2013).

[18] Kadic, M., Bückmann, T., Schittny, R. & Wegener, M.Metamaterials beyond electromagnetism. *Rep. Prog. Phys.***76**, 126501 (2013).

[19]S.A. Tretyakov, and S.I. Maslovski, "Veselago materials: What is possible and impossible about the dispersion of the constitutive parameters," *IEEE Antennas Propag. Mag*., Vol. 49, pp. 37-43, 2007.

[20]J. S. Toll, "Causality and the Dispersion Relation: Logical Foundations", *Physical Review*. **104**: 1760–1770, 1956.

[21]S. A. Tretyakov, Metasurfaces for general transformations of electromagnetic fields, Phil. Trans. R. Soc. A 2015 373 20140362, 2015.

[22]C. L. Holloway, E. F. Kuester, J. A. Gordon, J. O'Hara, J. Booth and D. R. Smith, "An Overview of the Theory and Applications of Metasurfaces: The Two-Dimensional Equivalents of Metamaterials," in *IEEE Antennas and Propagation Magazine*, vol. 54, no. 2, pp. 10-35, April 2012.

[23]N. Yu, F. Capasso, "Flat optics with designer metasurfaces". *Nat. Mater*. **13**: 139–150, 2014.

[24]E. Knott M.T. Tuley and J.F. Shaeffer, *Radar Cross Section Second Edition*, Boston, United State of America, Artech House Publishers, 1993.

[25]J. B. Pendry, D. Schurig, and D. R. Smith, Controlling electromagnetic fields, Science **312**, 1780 (2006).

[26]U. Leonhard, "Optical conformal mapping," Sci., vol. 312, pp. 1777-1780, 2006.

[27]P. Alitalo, O. Luukkonen, L. Jylha, J. Venermo, and S.A. Tretyakov, Transmission-Line Networks Cloaking Objects From Electromagnetic Fields, IEEE Trans. Antennas Propag. **56**, 416 (2008).

[28]P.-S. Kildal, A. A. Kishk, and A. Tengs, "Reduction of forward scattering from cylindrical objects using hard surfaces," IEEE Trans. Antennas Propag., vol. 44, no. 11, pp. 1509–1520, Nov. 1996.

[29]A. Alù and N. Engheta, Achieving transparency with plasmonic and metamaterial coatings, Phys. Rev. E **72**, 016623 (2005).

[30] A. Alù, Mantle cloak: Invisibility induced by a surface, Phys. Rev. B **80**, 245115 (2009).

[31] F. Monticone, and A. Alù, Invisibility exposed: physical bounds on passive cloaking, Optica **3**, 718 (2016).

[32] D. Schurig, J. J. Mock, B. J. Justice, S. A. Cummer, J. B. Pendry, A. F. Starr, D. R. Smith, Metamaterial Electromagnetic Cloak at Microwave Frequencies, Science **314**, 977 (2006).

[33] D Rainwater, A Kerkhoff, K Melin, J C Soric, G Moreno and A Alù, Experimental verification of three-dimensional plasmonic cloaking in free-space, New J. Phys. **14**, 013054 (2012).

[34] P. Alitalo, F. Bongard, J.-F. Zürcher, J. Mosig, and S. Tretyakov, Experimental verification of broadband cloaking using a volumetric cloak composed of periodically stacked cylindrical transmission-line networks, Appl. Phys. Lett. **94**, 014103 (2009).

[35] A. Monti, J. Soric, A. Alù, F. Bilotti, A. Toscano, and L. Vegni, Overcoming mutual blockage between neighboring dipole antennas using a low-profile patterned metasurface, IEEE Antenn. Wireless Propag. Lett. 11, 1414 (2012).

[36] A. Monti, J. Soric, A. Alù, A. Toscano, and F. Bilotti, Anisotropic Mantle Cloaks for TM and TE Scattering Reduction, IEEE Trans. Antennas Propag. 63, 1775 (2015).

[37] H. M. Bernety and A. B. Yakovlev, Reduction of Mutual Coupling Between Neighboring Strip Dipole Antennas Using Confocal Elliptical Metasurface Cloaks, IEEE Trans. Antennas Propag. 63, 1554 (2015).

[38] Z. H. Jiang, P. E. Sieber, L. Kang, and D. H. Werner, Restoring Intrinsic Properties of Electromagnetic Radiators Using Ultralightweight Integrated Metasurface Cloaks , Adv. Funct. Mater. **25**, 4708 (2015.

[39]J. C. Soric, A. Monti, A. Toscano, F. Bilotti, and A. Alù, Dual-Polarized Reduction of Dipole Antenna Blockage Using Mantle Cloaks, IEEE Trans. Antennas Propag. **63**, 4827 (2015).

[40]A. Monti, J. Soric, M. Barbuto, D. Ramaccia, S. Vellucci, F. Trotta, A. Alù, A. Toscano, and F. Bilotti, Mantle cloaking for co-site radio-frequency antennas, Applied Phys. Lett. **108**, 113502 (2016).

[41]A. Alù and N. Engheta, Cloaking a Sensor, Phys. Rev. Lett. **102**, 233901 (2009).

[42]J. C. Soric, R. Fleury, A. Monti, A. Toscano, F. Bilotti and A. Alù, "Controlling Scattering and Absorption With Metamaterial Covers," IEEE Trans. Antennas Propag., vol. 62, no. 8, pp. 4220-4229, Aug. 2014.

[43]M. Fruhnert, A. Monti, I. Fernandez-Corbaton, A. Alù, A. Toscano, F. Bilotti, and C. Rockstuhl, Tunable scattering cancellation cloak with plasmonic ellipsoids in the visible, Phys. Rev. B **93**, 245127 (2016).

[44]R. Fleury, F. Monticone, and A. Alù, Invisibility and Cloaking: Origins, Present, and Future Perspectives, Phys. Rev. Applied **4**, 037001 (2015).

[45]Y. R. Padooru, A. B. Yakovlev, P. Y. Chen, and A. Alù, Analytical modeling of conformal mantle cloaks for cylindrical objects using sub-wavelength printed and slotted arrays, J. Appl. Phys. **112**, 034907 (2012).

[46]J. C. Soric, A. Monti, A. Toscano, F. Bilotti, and A. Alù, Multiband and wideband bilayer mantle cloaks, IEEE Trans. Antennas Propag. **63**, 3235 (2015).

[47]P. Y. Chen, M. Farhat, S. Guenneau, S. Enoch, and A. Alù, Acoustic scattering cancellation via ultrathin pseudo-surface, Appl. Phys. Lett. **99**, 191913 (2011).

[48]M. D. Guild, A. Alù, and M. R. Haberman, Cloaking of an acoustic sensor using scattering cancellation, Appl. Phys. Lett. **105**, 023510 (2014).

[49] Y. Lai, J. Ng, H. Y. Chen, D. Z. Han, J. J. Xiao, Z. Q. Zhang, and C. T. Chan, Illusion Optics: The Optical Transformation of an Object into Another Object, Phys. Rev. Lett. **102**, 253902 (2009).

[50] F. Yang, Z. L. Mei, W. X. Jiang and T. J. Cui, Electromagnetic illusion with isotropic and homogeneous materials through scattering manipulation, J. Opt. **17**, 105610 (2015).

[51] Z. H. Jiang and D. H. Werner, Metasurface-enabled electromagnetic cloaking and illusion coatings beyond the quasi-static limit, Proc. 2014 IEEE AP-S Int. Symp, Memphis, TN, (2014).

[52] N. Xiang, Q. Cheng, H. B. Chen, J. Zhao, W. X. Jiang, H. F. Ma and T. J. Cui, Bifunctional metasurface for electromagnetic cloaking and illusion, Appl. Phys. Express, **8** (2015).

[53] Z. H. Jiang and D. H. Werner, Quasi-Three-Dimensional Angle-Tolerant Electromagnetic Illusion Using Ultrathin Metasurface Coatings, Adv. Funct. Mater. **24**, 7728 (2014).

[54] M. Selvanayagam and G. V. Eleftheriades, Experimental Demonstration of Active Electromagnetic Cloaking, Phys. Rev. X **3**, 041011 (2013).

[55] M. Alaoui, K. Rustomji, T. M. Chang, G. Tayeb, P. Sabouroux, R. Quidant, S. Enoch, S. Guenneau and R. Abdeddaim, Cyclic concentrator, carpet cloaks and fisheye lens via transformation plasmonics, J. Opt., **18**, 044023 (2016).

[56] C. F. Bohren and D.R. Huffman, *Absorption and Scattering of Light by Small Particles* (John Wiley & Sons, New York, 2008).

[57] Milton Abramowitz and Irene A.Stegun, *Handbook of Mathematical Functions* (Dover Publications Inc., New York, 1998).

[58] A. Sihvola, P. Yla-Oijala, S. Jarvenpaa and J. Avelin, Polarizabilities of Platonic Solids, IEEE Trans. Antenn. Propag. **52**, 2226 (2004).

[59]P. Y. Chen, C. Argyropoulos, and A. Alù, Broadening the Cloaking Bandwidth with Non-Foster Metasurfaces, Phys. Rev. Lett. **111**, 233001 (2013).

[60]R. M. Foster, " A reactance theorem", Bell System Technical Journal, vol.3, no. 2, pp. 259–267, 1924.

[61]CST - Computer Simulation Technology. *CST Microwave Studio*. Available: http://www.cst.com.

[62]S. Mühlig, A. Cunningham, J. Dintinger, M. Farhat, S. Bin Hasan, T. Scharf, T. Bürgi, F. Lederer, and C. Rockstuhl, Reply on the Comment on "A self-assembled three-dimensional cloak in the visible" in Scientific Reports **3**, 2328 (2013).

[63]H. Mosallaei and K. Sarabandi, A one-layer ultra-thin meta-surface absorber, Proc. 2005 IEEE AP-S Int. Symp, Washington, DC, (2005).

[64]A. Monti, A. Toscano, and F. Bilotti, Exploiting the surface dispersion of nanoparticles to design optical-resistive sheets and Salisbury absorbers, Opt. Lett. **41**, 3383 (2016).

[65]L. Shen, B. Zheng, Z. Liu, Z. Wang, S. Lin, S. Dehdashti, E. Li, H. Chen, "Large-Scale Far-Infrared Invisibility Cloak Hiding Object from Thermal Detection," Adv. Opt. Mater., vol. 3, pp. 1738-1742, 2015.

[66]Y Yang, H Wang, F Yu, Z Xu, H Chen, "A metasurface carpet cloak for electromagnetic, acoustic and water waves," Sci. Rep., 6, 20219, 2016.

[67]A. Nascetti, E. Pittella, P. Teofilatto, and S. Pisa, "High-Gain S-band Patch Antenna System for Earth-Observation CubeSat Satellites," IEEE Antenn. Wireless Propag. Lett., vol. 14, pp. 434-437, 2015.

[68]C. Balanis, Antenna Theory: Analysis and Design. Wiley & Sons, Hoboken, 2005.

[69]J. Li, M. Post, T. Wright, and R. Lee, “Design of Attitude Control Systems for CubeSat-Class Nanosatellite,” J. Control Sci. Eng, 657182, 2013.

[70]J. Tresvig and T. Lindem, "Investigating the Coupling Effects Between CubeSTAR's Communication Antenna and Deployable Payload Sensors," in IEEE Antennas Propag. Mag, vol. 58, pp. 90-129, 2016.

[71]W. A. Shiroma, L. K. Martin, J. M. Akagi, J. T. Akagi, B. L. Wolfe, B. A. Fewell, and A. T. Ohta, “Cubesats: A bright future for nanosatellites,” Central European J. Eng., vol. 17, no. 1, pp. 24–31, 2011.

[72]J. Tresvig and T. Lindem, “Cubestar—A nanosatellite for space weather monitoring,” in Proc. 1st IAA Conf. University Satellite Mission Cubesat Workshop.

[73]M. Barbuto, F. Trotta, F. Bilotti, A. Toscano, “A Combined Bandpass Filter and Polarization Transformer for Horn Antennas.” IEEE Antenn. Wireless Propag. Lett., vol. 12, pp. 1065-1068, 2013.

[74]J. C. Soric, P. Y. Chen, A. Kerkhoff, D. Rainwater, K. Melin, and A. Alù, “Demonstration of an ultralow profile cloak for scattering suppression of a finite-length rod in free space,” New J. Phys., vol. 15, no. 3, p. 033037, 2013.

[75]B. Klofas and K. Leveque, “A Survey of CubeSat Communication Systems,” SRI International, 2008.

[76]N.H.Crisp, K.Smith and P.Hollingsworth, “Launch and deployment of distributed small satellite systems,” Acta Astronautica, vol. 114, pp. 65–78, 2015.

[77]W. Xiaohui, L. Shuang and S. Yuchen, “Concept design and cluster control of advanced space connectable intelligent microsatellite,” Acta Astronautica, vol. 141, pp. 1-7, 2017.

[78]R. G. Newton, "Optical Theorem and Beyond". Am. J. Phys., vol. 44, pp. 639–642, 1976.

[79] J. B. Andersen and A. Frandsen, "Absorption efficiency of receiving antennas," IEEE Trans. Antenna Propag., vol. 53, no. 9, pp. 2843–2849, Sep. 2005.

[80] S. Vellucci, A. Monti, M. Barbuto, A. Toscano and F. Bilotti, "Satellite Applications of Electromagnetic Cloaking," IEEE Trans. Antennas Propag., vol. 65, no. 9, pp. 4931-4934, Sept. 2017.

[81] D. F. Sievenpiper, "Nonlinear grounded metasurfaces for suppression of high-power pulsed RF currents," IEEE Antennas Wireless Propag. Lett., vol. 10, pp. 1516–1519, 2011.

[82] A. Forouzmand, C. S. R. Kaipa, and A. B. Yakovlev, "Mushroom-type structures with the wires connected through diodes: Theory and applications," J. Appl. Phys., vol. 120, p. 015303, 2016.

[83] C. Argyropoulos, P.Y. Chen, F. Monticone, G. D'Aguanno, and A. Alu, "Nonlinear plasmonic cloaks to realize giant all-optical scattering ` switching," Phys. Rev. Lett., vol. 108, p. 263905, 2012.

[84] E. A. Gurvitz, E. A. Sedykh, and M. K. Khodzitskiy, "Nonlinear cloaking at microwave frequencies," Proc. SPIE, vol. 8455, p. 845532, 2012.

[85] A. Monti, M. Barbuto, A. Toscano and F. Bilotti, "Nonlinear Mantle Cloaking Devices for Power-Dependent Antenna Arrays," IEEE Antenn. Wireless Propag. Lett., vol. 16, pp. 1727-1730, 2017.

[86] H. Wakatsuchi, S. Kim, J. J. Rushton, and D. F. Sievenpiper, "Waveform-Dependent Absorbing Metasurfaces," Phys. Rev. Lett., vol. 111, no. 24, 245501, Dec. 2013.

[87] ADS - Advanced Design System. Available: https://www.keysight.com.

# List of Figures

# List of Publications

## *Journal papers*


[J1] S. Vellucci, A. Monti, M. Barbuto, A. Toscano, F. Bilotti, "Use of Mantle Cloaks to Increase Reliability of Satellite-to-Ground Communication Link," IEEE Journal on Multiscale and Multiphysics Computational Techniques, vol. 2, pp. 168-173, 2017.

[J2] S. Vellucci, A. Monti, M. Barbuto, A. Toscano, F. Bilotti, "Satellite Applications of Electromagnetic Cloaking," IEEE Transaction on Antennas and Propagation, vol. 65, pp. 4931-4934, 2017.

[J3] S. Vellucci, A. Monti, A. Toscano, F. Bilotti, "Scattering Manipulation and Camouflage of Electrically Small Objects through Metasurfaces," Physical Review Applied, 7, 034032, 2017.

[J4] A. Monti, J. Soric, M. Barbuto, D. Ramaccia, S. Vellucci, F. Trotta, A. Alù, A. Toscano, F. Bilotti, "Mantle cloaking for co-site radio-frequency antennas," Applied Physics Letters, 108, 113502, 2016.

[J5] C. Ponti, S. Vellucci, "Scattering by Conducting Cylinders Below a Dielectric Layer With a Fast Noniterative Approach," IEEE Microwave Theory and Techniques, vol. 63, pp. 30-39, 2015.

## *Conference papers*

[C1] S. Vellucci, A. Monti, M. Barbuto, A. Toscano, F. Bilotti, "Recent Developments in the Design of Waveform-Selective Mantle Cloaks for Antenna Applications," Proceedings of the 12th International Congress on Advanced Electromagnetic Materials in Microwaves and Optics – Metamaterials 2018, Espoo, Finland, 27 August – 1 September, 2018.

[C2] S. Vellucci, A. Monti, M. Barbuto, A. Toscano, F. Bilotti, "Towards Waveform-Selective Cloaking Devices Exploiting Circuit-Loaded Metasurfaces," Proceedings of the 2018 IEEE International Symposium on Antennas and Propagation and North American Radio Science Meeting in Boston, MA, July 8 - July 13, 2018.

[C3] S. Vellucci, A. Monti, M. Barbuto, A. Toscano, F. Bilotti, "Exploiting Electromagnetic Cloaking to Design Compact Nanosatellite Systems," Proceedings of the 2018 IEEE International Symposium on Antennas and Propagation and North American Radio Science Meeting in Boston, MA, July 8 - July 13, 2018.

[C4] S. Vellucci, A. Monti, A. Toscano, F. Bilotti, "Scattering Control and Camouflage through Metasurfaces," Proceedings of the 2018 IEEE International Symposium on Antennas and Propagation and North American Radio Science Meeting in Boston, MA, July 8 - July 13, 2018.

[C5] S. Vellucci, A. Monti, M. Barbuto, A. Toscano, F. Bilotti, "Enhancing the performances of satellite telecommunication systems exploiting electromagnetic cloaking," Proceedings of the 11th International Congress on Advanced Electromagnetic Materials in Microwaves and

Optics – Metamaterials 2017, Marseille, France, 27 August – 2 September, 2017.

[C6] M. Barbuto, A. Monti, D. Ramaccia, A. Tobia, S. Vellucci, A. Alù, A. Toscano, F. Bilotti, "Electromagnetic Cloaking for Antennas," Proceedings of the 11th International Congress on Advanced Electromagnetic Materials in Microwaves and Optics – Metamaterials 2017, Marseille, France, 27 August – 2 September, 2017, (invited paper).

[C7] M. Barbuto, A. Monti, A. Alù, D. Ramaccia, A. Tobia, S. Vellucci, A. Toscano, and F. Bilotti, "Invisible Antennas for Crowded Radio Platforms," Proceedings of the IEEE MTT-S International Microwave Workshop Series on Advanced Materials and Processes (IMWS), Pavia, Italy, 2 September, 2017 (invited paper).

[C8] M. Barbuto, A. Monti, D. Ramaccia, A. Tobia, S. Vellucci, F. Bilotti, A. Toscano, "Cloaking and magnet-less non-reciprocity through metamaterials," Proceedings of the DENORMS Action's Workshop on "Modelling of high performance acoustic structures Porous media, metamaterials and sonic crystals", Rome, Italy, 24– 25 Jenuary, 2017.

[C9] S. Vellucci, A. Monti, G. Oliveri, A. Massa, A. Toscano, F. Bilotti, "Scattering camouflage and manipulation using metasurfaces," Proceedings of the 10th International Congress on Advanced Electromagnetic Materials in Microwaves and Optics – Metamaterials 2016, Crete, Greece, 17– 22 September, 2016.

[C10] A. Monti, J. Soric, M. Barbuto, D. Ramaccia, S. Vellucci, F. Trotta, A. Alù, A. Toscano, F. Bilotti, "Cloaking receiving and transmitting antennas: theoretical aspects and applications," Proceedings of the 10th International Congress on Advanced Electromagnetic Materials

in Microwaves and Optics – Metamaterials 2016, Crete, Greece, 17– 22 September, 2016 (invited paper).

[C11] M. Barbuto, A. Monti, D. Ramaccia, A. Tobia, S. Vellucci, F. Bilotti, A. Toscano, "Optimal Design Of Metamaterial-Inspired Devices For Improving The Performances Of Horn Antennas," Proceedings of the 14th Workshop on Optimization and Inverse Problems in Electromagnetism - IEEE OIPE 2016, Rome, Italy, 13– 15 September, 2016.

[C12] G. Guarnieri, G. Mauriello, S. Scafè, M. Barbuto, A. Monti, D. Ramaccia, A. Tobia, S. Vellucci, A. Toscano, F. Bilotti, "Metamaterials Meeting Industrial Products: A Successful Example in Italy," Proceedings of the 2016 IEEE International Symposium on Antennas and Propagation and North American Radio Science Meeting in Fajardo, Puerto Rico, June 26 - July 1, 2016.

[C13] Bilotti, A. Toscano, M. Barbuto, A. Monti, D. Ramaccia, A. Tobia, F. Trotta, S. Vellucci, "Metamaterials and related applications at visible frequencies," Proceedings of GioNa 2016, Rome, Italy, 22-23 June, 2016.

[C14] M. Barbuto, F. Bilotti, A. Monti, D. Ramaccia, A. Tobia, A. Toscano, S. Vellucci, "Applications of numerical methods in metamaterials at microwave frequencies," Proceedings of the 13th International Workshop on Finite Electromagnetic Elements for Microwaves Engineering – FEM 2016, Florence, Italy, 16– 18 May, 2016.

[C15] C. Ponti, S. Vellucci, "Scattering by Conducting Cylinders Below a Dielectric Layer With a Fast Noniterative Approach," Proceedings of the Mini-Special Issue on 2014 IEEE International Conference on Numerical Electromagnetic Modeling and Optimization for RF,

Microwave, and Terahertz Applications – NEMO 2014, Pavia, Italy, 14-16 May, 2014.

## *Other*

[1] S. Vellucci, A. Monti, A. Toscano, F. Bilotti, "Metasurfaces for Low Observable Aircraft," POLARIS Innovation Journal, vol. 25, pp. 24-27, 2016.

# Biographical note

**Stefano Vellucci** received the B.S. and M.S. (*summa cum laude*) degrees in electronic engineering from ROMA TRE University, Rome, Italy, in 2012 and 2015, respectively. In November 2015 he started his Ph.D. research program at the Department of Applied Electronic, ROMA TRE University under the supervision of Prof. Filiberto Bilotti and Prof. Alessandro Toscano.

Before starting his Ph.D., he was an Engineer with Elettronica S.p.A., Rome, Italy, where he was an antenna designer engineer involved in the Eurofighter Typhoon Project. His main research interests include the design of artificially engineered materials and metasurfaces for microwave components, and the design of cloaking devices, especially for antennas applications.

Dr. Vellucci is currently member of the Virtual Institute for Artificial Electromagnetic Materials and Metamaterials (METAMORPHOSE VI, the International Metamaterials Society), and of the Institute of Electrical and Electronics Engineers (IEEE). He has been serving as a Technical Reviewer of many high-level international journals related to electromagnetic field theory and metamaterials. He was the recipient of the *Leonardo-Finmeccanica* Innovation Award for "Young Students", in 2015, of the Outstanding Reviewers Award from the *IEEE Transactions on Antennas and Propagation*, in 2018, and of the *IEEE AP-S Award* of the Central-Southern Italy Chapter, in 2019.